

# Novel pH-responsive hybrid peptide block copolymers for intracellular delivery applications

by

Angela Mu Hsien Leung

A thesis  
presented to the University of Waterloo  
in fulfillment of the  
thesis requirement for the degree of  
Master of Applied Science  
in  
Chemical Engineering

Waterloo, Ontario, Canada, 2010

© Angela Mu Hsien Leung 2010

## **Author's Declaration**

I hereby declare that I am the sole author of this thesis. This is a true copy of the thesis, including any required final revisions, as accepted by my examiners.

I understand that my thesis may be made electronically available to the public.

## Abstract

The creation of novel polymeric materials remains a vital field, particularly for potential applications in drug and gene delivery. The synthesis of these materials is important, as well as a clear understanding of the physical properties of the polymers. Lastly, tests for potential applications are vital in order to improve and optimize the polymeric system.

The polyglutamate-b-poly(N,N-diethylaminoethyl methacrylate) (PLG-b-PDEAEMA) block copolymer was successfully synthesized. The resulting polymer had a defined molecular weight with approximately 18 L-glutamate and 38 DEAEMA units and a low polydispersity index.

The physical properties of the PLG-b-PDEAEMA block copolymer were investigated. As a result of the pH-sensitive groups of the polymer, the solution characteristics changed depending on the charge density of the individual blocks. At low pH, the PDEAEMA block is soluble and positively charged while the PLG block is insoluble. At high pH, the PLG block is negatively charged and hydrophilic, while the PDEAEMA block is hydrophobic. At the mid-range pH values, the polymer chain is partially charge with both positive and negative moieties. The critical micelle concentration, size of the self-assembled structures, surface charge and morphology were found to change with pH.

In order to investigate the potential applications of the PLG-b-PDEAEMA polymer, the interactions between the polymer and plasmid DNA were investigated and characterized. The delivery of the polymer/DNA polyplexes to a neuroblastoma cell culture was investigated, however, no cell transfection was observed.

Another aspect of the project was to understand the physical properties of poly(L-glutamate) dendritic polymers. Well-defined poly(L-glutamate) arborescent polymers from linear to G3 were characterized for their acid-base characteristics and aggregation behaviour at high solution pH. The Gibbs free energy required to abstract a proton was studied using potentiometric titration and it was

found that the  $pK_a$  and the free energy increased at higher generations due to greater electrostatic forces. As a result of the hydrophilic glutamate groups and the hydrophobic hexyl group, the dendritic polymers aggregated to form self-assembled structures. The self-assembled structures possessed similar hydrodynamic radii, ranging from 90 to 110 nm. The radius of gyration, in comparison, decreased from 90 to 30 nm with increasing arborescent polymer generations, indicating more core-dense aggregates at higher generations.

## Acknowledgements

I would not have been able to complete the research for my thesis without the help of my mentor, Professor Michael Tam. I have learned much about research under his supervision and I am very thankful for his support. Furthermore, Professor Tam understood my wanderlust and gave me the opportunity to do research at the National University of Singapore with one of his collaborators, for which I am grateful.

I would also like to thank Professor Mario Gauthier and Gregory Whitton for their help in polymer chemistry and providing me with the samples for one of my projects. I would not have been able to complete my thesis without their support.

During my time in Singapore, I would like to thank Professor Heng-Phon Too for his insight. I owe a lot to Sarah Ho, who taught me everything I know about cell culturing and showed me how to become a better researcher. Furthermore, I am grateful for Lihan Zhou and the rest of the group for teaching and helping me during my time there.

I would not have made it where I am without the support of my labmates. I would like to start with Sahar, for always being there to help me and for making the lab lively. To her, I owe many, many hugs. Additionally, I would not have made it all the late nights in the lab were it not for Sahar, Sara, Neha and Yennan – one of whom was always there with me in the middle of the night. And of course, everyone else in the research group, who were always there to help or amuse me.

I would also like to thank my friends, for ensuring that I maintain a work-life balance. If not for them, I would have long lost my sanity in the lab. And last but not least, I would like to thank my family, for supporting me all the way.

## Table of Contents

Author's Declaration.....	ii
Abstract.....	iii
Acknowledgements.....	v
Table of Contents.....	vi
List of Figures.....	viii
List of Tables.....	xi
Chapter 1 Introduction.....	1
1.1 Project Motivation.....	2
1.2 Project Objectives.....	3
1.3 Organization of Thesis.....	4
Chapter 2 Literature Review: Peptide-Based Block Copolymers.....	5
2.1 Synthesis.....	5
2.1.1 Peptide Synthesis.....	5
2.1.2 Conventional Polymerization.....	9
2.1.3 Click Chemistry.....	14
2.2 Self-Assembly.....	15
2.2.1 Factors affecting self-assembly.....	15
2.2.2 Hybrid peptide block copolymers.....	17
2.2.3 Block copolypeptides.....	20
2.3 Applications.....	25
2.3.1 Gene Therapy.....	26
2.4 Outlook.....	29
Chapter 3 Synthesis of Peptide-based Block Copolymers.....	30
3.1 Introduction.....	30
3.2 Experimental.....	31
3.2.1 Materials.....	31
3.2.2 Instrumentation.....	31
3.2.3 Synthetic Protocols.....	32
3.3 Results and Discussion.....	36
3.3.1 PBLG.....	37
3.3.2 PDEAEMA.....	39

3.3.3 Block Copolymer Synthesis .....	41
3.4 Conclusions .....	42
Chapter 4 Characterization of Poly(L-glutamate) Arborescent Polymers.....	43
4.1 Introduction .....	43
4.2 Experimental .....	44
4.2.1 Polymer Synthesis .....	44
4.2.2 Instrumentation.....	44
4.3 Results and Discussion.....	45
4.3.1 Potentiometric Titration.....	45
4.3.2 Critical aggregation concentration of the PLG arborescent polymers.....	50
4.3.3 Self-Assembled Structures .....	53
4.4 Conclusion.....	58
Chapter 5 Self-Assembly Behaviour and Applications of Poly(L-glutamate)-b- poly(2-(diethylamino)ethyl methacrylate) .....	61
5.1 Introduction .....	61
5.2 Experimental .....	62
5.2.1 Materials .....	62
5.2.2 Instrumentation.....	63
5.2.3 Cell Culture .....	64
5.3 Results and Discussion.....	65
5.3.1 Potentiometric Titration of PLG-b-PDEAEMA.....	65
5.3.2 Critical Micellization Concentration .....	68
5.3.3 pH-Dependent Self-Assembly of PLG-b-PDEAEMA.....	70
5.3.4 Polyplex Formation .....	79
5.3.5 Cell Transfection .....	82
5.4 Conclusions .....	83
References .....	86
Chapter 2 References.....	86
Chapter 3 References.....	93
Chapter 4 References.....	93
Chapter 5 References.....	94

## List of Figures

Figure 2.1: NCA ring opening polymerization .....	6
Figure 2.2: Phosgenation of an amino acid using triphosgene.....	7
Figure 2.3: NCA formation using Leuch's method, shown here for Z <sub>3</sub> -arginine, where Z is a urethane protecting group .....	7
Figure 2.4: Controlled NCA polymerization using a primary amine hydrochloride salt [11] .....	8
Figure 2.5: NCA polymerization initiated by transition metals .....	9
Figure 2.6: ATRP reaction scheme [15] .....	11
Figure 2.7: Different compositions and architectures of polymers [15] .....	14
Figure 2.8: Huisgen 1,3-dipolar cycloaddition [18].....	15
Figure 2.9: $\alpha$ -Helix structure [23] .....	16
Figure 2.10: $\beta$ -Sheet structure [23] .....	17
Figure 2.11: Block copolymers of PEG-b-poly( $\gamma$ -methyl-L-glutamate).....	18
Figure 2.12: Block copolymers of PAA-b-PLVAL [30] .....	19
Figure 2.13: Schematic diagram of the morphology of PDMAEMA-b-PGA [35].....	21
Figure 2.14: "Schizophrenic" micelles of L-glutamic acid and L-lysine [39] .....	22
Figure 2.15: Block copolypeptides of leucine and lysine [20].....	24
Figure 2.16: Differential interference contrast images of poly-L-lysine-b-poly-L-leucine: (a) K <sub>20</sub> L <sub>20</sub> (sheets), (b) K <sub>40</sub> L <sub>20</sub> (fibrils), (c) K <sub>60</sub> L <sub>20</sub> (vesicles) and (d) K <sub>80</sub> L <sub>20</sub> (irregular) [40] .....	24
Figure 2.17: Self-assembled vesicles of poly-L-lysine-b-poly-L-leucine [40] .....	25
Figure 2.18: Barriers to successful gene delivery using non-viral vectors [47].....	27
Figure 3.1: Reaction scheme for the phosgenation of $\gamma$ -benzyl-glutamate .....	33
Figure 3.2: Reaction scheme for azide-functional amine initiator for NCA polymerization.....	33
Figure 3.3: NCA ring opening polymerization of $\gamma$ -benzyl-glutamate-NCA .....	34
Figure 3.4: Reaction scheme for alkyne-functional bromide initiator for ATRP .....	34
Figure 3.5: ATRP reaction scheme .....	35
Figure 3.6: Copolymerization using the Huisgen 1,3-dipolar cycloaddition .....	36
Figure 3.7: FTIR of $\gamma$ -benzyl-glutamate-NCA.....	37
Figure 3.8: <sup>1</sup> H NMR spectrum for $\gamma$ -benzyl-glutamate-NCA.....	38
Figure 3.9: <sup>1</sup> H NMR spectrum of 1-azido-3-aminopropane .....	38
Figure 3.10: <sup>1</sup> H NMR spectrum of PBLG.....	39

Figure 3.11: FTIR spectrum of PBLG.....	39
Figure 3.12: <sup>1</sup> H NMR of Propargyl-2-bromoisobutyrate .....	40
Figure 3.13: <sup>1</sup> H NMR spectrum of PDEAEMA .....	40
Figure 3.14: <sup>1</sup> H NMR spectrum for the block copolymer .....	41
Figure 3.15: NMR study of deprotected block copolymers in a) acidic solution, b) neutral solution and c) basic solution.....	42
Figure 4.1: Potentiometric titration curve for the G0 arborescent polymers .....	46
Figure 4.2: Comparison of pH curves for the generations of PLG.....	47
Figure 4.3: Comparison of pK <sub>a</sub> curves for the generations of PLG dendritic polymers.....	48
Figure 4.4: Comparison of Gibbs free energy required to abstract a proton .....	49
Figure 4.5: Structure of the G0 arborescent polymer with linear PLG grafts – the hexyl groups highlighted (x and y groups are randomly distributed along the chain) .....	50
Figure 4.6: Scattering intensity graph for G0 PLG at pH 10.....	52
Figure 4.7: Distribution functions for G0 PLG at pH 10.....	53
Figure 4.8: The q <sup>2</sup> dependence of the diffusion coefficient for G0 PLG at pH 10.....	54
Figure 4.9: Comparison of size and morphology by dendritic polymer generation .....	56
Figure 4.10: Distribution functions at 90° by generation .....	57
Figure 4.11: SLS data for LPLG at 2.0 g/L.....	58
Figure 4.12: Schematics illustrating the self-assembly mechanism for each generation of PLG, with the unimer in the left column and the proposed aggregated structure in the right column .....	59
Figure 5.1: Examples of self-assembled structures [3].....	61
Figure 5.2: Potentiometric titration curve of PLG-b-PDEAEMA.....	66
Figure 5.3: Protonation of the tertiary amine group of PDEAEMA.....	67
Figure 5.4: Neutralization of the carboxylic acid group of PLG.....	67
Figure 5.5: Critical micelle concentration at pH 3 .....	69
Figure 5.6: Critical micelle concentration at pH 10 .....	70
Figure 5.7: Critical micelle concentration at pH 7 .....	70
Figure 5.8: Distribution functions of PLG-b-PDEAEMA at pH 10.....	71
Figure 5.9: Diffusion coefficient angle dependency at pH 10.....	72
Figure 5.10: Electric double layer for a charged surface in solution [13] .....	73
Figure 5.11: Effect of pH on the hydrodynamic radius (R <sub>h</sub> ) and surface charge, where the dashed line corresponds to a zero zeta potential.....	74

Figure 5.12: Charge behavior of the polymer at different solution pHs .....	75
Figure 5.13: Zimm plot of PLG-b-PDEAEMA at pH 10.....	76
Figure 5.14: Effect of pH on the hydrodynamic ( $R_h$ ) and gyration radii ( $R_g$ ).....	77
Figure 5.15: Mechanism for self-assembly at pH 3, 7 and 10 .....	80
Figure 5.16: Agarose gel electrophoresis at different pH and N/P ratios, with the anode at the top of the figure and the cathode at the bottom of the figure .....	81
Figure 5.17: DNA condensation at different N/P ratios.....	82
Figure 5.18: Fluorescence micrographs (10x) of gene expression .....	83

## List of Tables

Table 3.1: Comparison of different peptide synthesis techniques.....	30
Table 4.1: Characteristics of arborescent poly( $\gamma$ -benzyl-L-glutamate) [6] .....	44
Table 4.2: Summary of Gibbs free energy for each arborescent polymer generation .....	50
Table 4.3: Summary of CAC results by generation.....	52
Table 4.4: Summary of size and morphology results by generation at 2 g/L.....	55
Table 5.1: pK <sub>a</sub> Values for the PLG-b-PDEAEMA system.....	67
Table 5.2: R <sub>g</sub> / R <sub>h</sub> ratio at different pH conditions .....	78
Table 5.3: Static light scattering results at solution pH 3, 7 and 10 .....	78



# Chapter 1

## Introduction

Intracellular delivery has become an important topic in the development of innovative methods in medicine. Much work has been done in order to develop systems for the delivery of genes, drugs and therapeutic proteins, with focus on controlled release and targeted delivery. Systems that have been developed include hydrogels, liposomes, cell penetrating peptides, polymeric structures and magnetic nanoparticles for the encapsulation and delivery of therapeutic agents. However, many problems exist and are important considerations for the development of new systems.

Many issues exist, from the complexation with the therapeutic agent, the translocation inside the cells, the release of the therapeutic agent and the stability in the case of the drug and protein, and gene expression in the case of the gene delivery. Complexation is an important aspect, as the therapeutic agents need to be protected from degradation.

Furthermore, the complexes must be stable in physiological media and enter the cells. The most commonly exploited pathway for delivery is endocytosis, however, protein and drugs can be degraded at this stage. The therapeutic protein needs to be protected at this point and needs a path to escape the endosome. The endosomal pH is more acidic than the cell environment, which needs to be taken into consideration for the system design. pH responsive polymers have an advantage, as the polymer can act as a proton sponge to buffer the drop in pH, which would cause the endosome to swell and rupture, releasing the contents into the cell.

This research focuses on the development of hybrid peptide block copolymers of glutamic acid and 2-(diethylamino)ethyl methacrylate for gene delivery. Glutamic acid was chosen for its pH responsive character and biodegradability, whereas DEAEMA was chosen for its intracellular delivery applications, as well as its pH responsive behaviour. At physiological pH, this system has a negative

surface charge, in comparison to the commonly used positive surface charged particles. Although positively charged surfaces are more effective for endocytosis, the designed polymer is pH responsive and changes structure once pH is lowered, thus disrupting the endosome and releasing therapeutic agents into the cell.

Another focus is to understand the physical properties of dendritic peptide systems, in particular dendritic polymers of L-glutamate. Peptides display a range of unique solution properties, but dendritic polymers composed of peptides, however, are not well understood. This research will provide a better understanding of these peptides, so that the dendrimers can be optimized for various applications.

## **1.1 Project Motivation**

The first motivation for this project is to develop a novel polymeric system that is pH-responsive, with a pKa around the endosomal and lysosomal pHs, to facilitate endolysosomal escape within the cell. The chosen DEAEMA-glutamate block copolymers form "schizophrenic vesicles", due to the zwitterionic character of the polymer, depending on the pH of the system. At high pH, the polymers self-assemble into negatively charged structures with glutamic acid on the corona. At low pH, the polymers self-assemble into positively charged structures with DEAEMA on the corona. This switch between the oppositely charged particles occurs around a pH of 5, which is within the endolysosomal pH range. The intracellular delivery of the polymer will then be investigated. The polymer will be complexed with plasmid DNA and in vitro delivery to a cell culture will be tested. Based on the results, an improved polymeric system can be developed.

The second motivation of this project is to characterize the poly(L-glutamate) arborescent polymers. The dendrimers, provided in collaboration by another research group, are pH sensitive due

to the carboxylic acid group of glutamic acid and soluble in basic solution. A more thorough understanding of the physical properties can be obtained.

## **1.2 Project Objectives**

The main objectives of this project are to synthesize the block copolymers, characterize the physical properties and self-assembly at different solution pHs, and to test the application of the polymers for intracellular delivery.

The first objective is to synthesize PLG-b-PDEAEMA with controlled molecular weight and low polydispersity. Due to the incompatibility of the synthetic chemistry of the two blocks, each block was synthesized separately and then linked together. An advantage of this method is that individual blocks can be tested for molecular weight and polydispersity prior to the block formation, giving greater control over the final block copolymer. Synthesizing well-defined block copolymers is important.

The second objective is to understand the physical properties of the block copolymer. Solution pH plays an important role as intracellular entry, particularly through the endocytosis pathway, is generally more successful for particles that are pH responsive. Due to the carboxylic and amine functional groups, the pH-responsiveness of the polymer plays a major role in the self-assembled structures of the block copolymer. The solution pH alters the solubility of each block, affecting the self-assembly. Above and below the isoelectric point, oppositely charged particles are formed. Additionally, the size and morphology of the self-assembled structures change close to the isoelectric point due to the increase in electrostatic charges. For intracellular delivery, an understanding of the polyplex formation between the polymer and DNA is necessary, followed by delivery of the polyplexes to a cell culture. This will assess the potential of the polymer as a nonviral gene delivery agent.

The third objective of this project is to understand the physical properties of the poly(L-glutamate) arborescent polymers. An important aspect that will be investigated is the pH responsive behaviour and solubility of the different generations of dendritic polymers. Furthermore, a thorough study of the aggregation behaviour of the dendritic polymers at high solution pH will be carried out.

### **1.3 Organization of Thesis**

This thesis is divided up into 5 main chapters. The second chapter will give an overview of the current work in peptide-based polymeric materials. Topics that will be covered include synthetic strategies used for peptides and synthetic polymers, the self-assembly and physical behaviour of these systems as well as some of the applications being explored.

The third chapter outlines the synthetic scheme of the PLG-b-PDEAEMA system. The block copolymer was successfully synthesized with low polydispersity and controlled molecular weight.

The fourth chapter describes the physical characterization of the poly(L-glutamate) dendritic polymers. Linear poly(L-glutamate) up to the third generation was investigated and the results are discussed in this chapter.

The fifth chapter of this thesis describes the physical characterization and applications of the PLG-b-PDEAEMA block copolymer system. In particular, the self-assembly and pH-responsive characteristics of the polymer in aqueous solution are discussed. The gene delivery applications are then discussed – the interactions between the polymer and plasmid DNA are explored and the delivery of the polymer/DNA complexes to a cell culture is investigated.

## **Chapter 2**

### **Literature Review: Peptide-Based Block Copolymers**

The use of peptides for biomedical applications rather than synthetic polymers is motivated mainly by their biological compatibility and degradability. Natural proteins and peptides are biological polymers, made of amino acids. Despite their simplicity, proteins and peptides can form complex, ordered structures.

In comparison to polymers, synthetic peptides are made of simple components, the amino acids. Traditionally, peptides were synthesized through a chemical polymerization reaction, the ring opening polymerization of N-carboxyanhydrides. The problem with this approach is side reactions, and as a result, it is difficult to synthesize peptides with specific properties [1].

Furthermore, much of the initial work on synthetic peptides focused on polyelectrolyte homopolypeptides. However, strongly charged peptides are difficult to use in biomedical applications due to charge interactions and solubility problems in biological media. As a result, synthetic polypeptides were conjugated to synthetic polymers for use in drug delivery applications [2]. Recent advances in peptide and polymer synthesis provide us with more control over the syntheses, leading to greater control over the sequence, composition and architecture of both peptide and polymer segments [1, 3].

#### **2.1 Synthesis**

##### **2.1.1 Peptide Synthesis**

Several methods exist for the synthesis of polypeptides. For polypeptides with control over the amino acid sequence, recombinant DNA methods, solid-phase synthesis and ligation methods are commonly used. Generally, for single amino acid polypeptides or random polypeptides, the polymerization of N-carboxyanhydrides (NCA) is used [4, 5].

### 2.1.1.1 DNA Recombinant Technology

Recombinant DNA methods can yield high molecular weight polypeptides. This method gives the best control over the amino acid sequence. The disadvantages of this method include the difficulty in modifying organisms, creating artificial genes, and separating the protein [4, 5].

### 2.1.1.2 Solid-State Peptide Synthesis

Solid-phase supported peptide synthesis can synthesize short polypeptides using a stepwise process. Larger polypeptides cannot be synthesized due to the limitations of this method – generally polypeptides with less than 20 units can be synthesized. The advantage of this approach, however, is that control over the amino acid sequence can be obtained. Ligation methods can be used in combination with solid-phase peptide synthesis, to attach shorter peptides together, creating larger polypeptides [4, 5].

### 2.1.1.3 Ring-Opening Polymerization of N-carboxyanhydrides

NCA polymerization is a chemical synthesis method (Figure 2.1). There is limited control over the amino acid sequence, unlike in the other two methods. However, longer chain polypeptides can be synthesized and the process can generate large quantities of polypeptide [1, 4, 6]. The amino acids need to be converted to  $\alpha$ -amino acid-N-carboxyanhydrides. This active species can then be polymerized - originally, amine-functional initiators were used, but the disadvantage of this strategy is that side reactions are common. Newer strategies for controlled NCA polymerization utilize transition metal initiators, primary amine hydrochloride initiators or different reaction conditions [6].

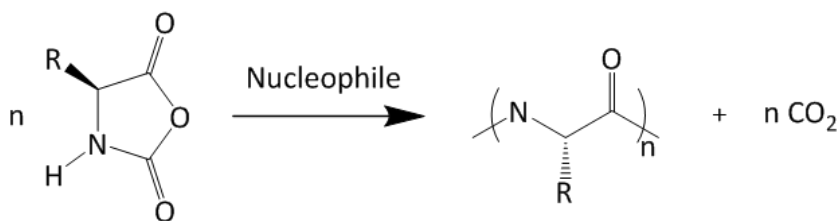


Figure 2.1: NCA ring opening polymerization

### 2.1.1.3.1 Preparation of $\alpha$ -amino acid-N-carboxyanhydrides

Two general methods are used for the preparation of  $\alpha$ -amino acid-N-carboxyanhydrides: the Fuchs-Farthing Method, by carbonylation of a free amino acid with a phosgenation reaction (Figure 2.2) [7], and Leuch's Method, by cyclization of N-alkoxycarbonyl-amino acids with a halogenation reaction (Figure 2.3) [8].

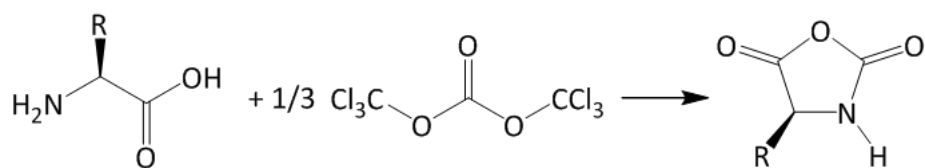


Figure 2.2: Phosgenation of an amino acid using triphosgene

### 2.1.1.3.2 Living Polymerizations

Conventional NCA polymerizations are initiated with nucleophiles and bases. The optimal initiator for each amino acid-NCA polymerization system varies, depending on the properties of the NCA and the polymer, as well as the side reactions in the process. Due to the lack of control with conventional initiators for NCA polymerization, in recent years, new methods have been developed to control polymerization and limit side reactions [6].

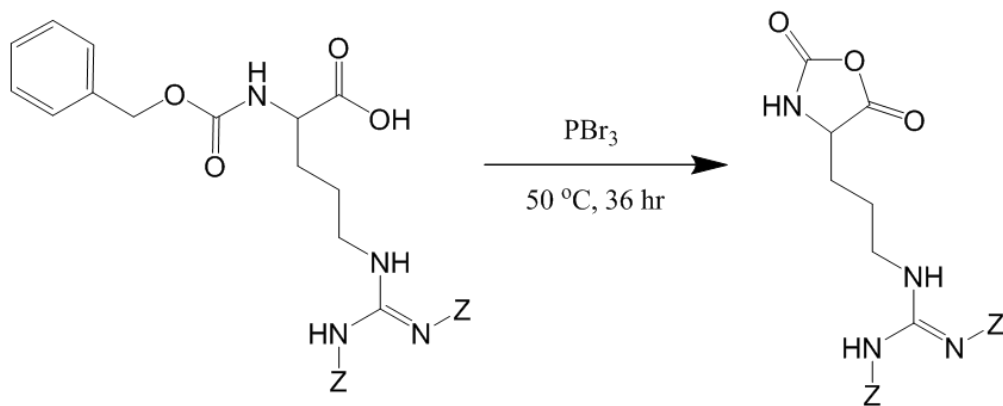


Figure 2.3: NCA formation using Leuch's method, shown here for  $Z_3$ -arginine, where Z is a urethane protecting group

Improvements can be made to the conventional amine initiated systems by changing the reaction conditions. This includes performing the polymerization under high vacuum [9] or at low temperatures, where the propagation reaction is more favourable than side reactions, due to the activation barrier for the reactions [10].

Another method is to use a different initiator, such as primary amine hydrochloride salts as an initiator instead of a primary amine (Figure 2.4). The salt is less reactive and good control over the polymerization is obtained [11]. Another option is to use transition metal initiators, specifically zero-valent nickel and cobalt, for living polymerization of NCAs (Figure 2.5). A wide range of molecular weights was thus obtained with low polydispersity ( $M_w/M_n < 1.20$ ). Control over the composition was also obtained. The drawback is that the metal has to be removed by precipitation or dialysis after polymerization [12, 13].

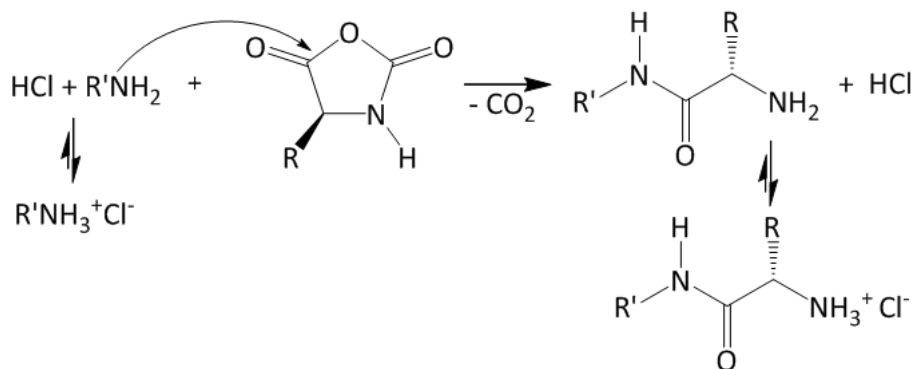


Figure 2.4: Controlled NCA polymerization using a primary amine hydrochloride salt [11]

#### 2.1.1.3.3 Copolymerization

Copolymers can also be formed by NCA polymerization. For random copolypeptides, a mixture of  $\alpha$ -amino acid-N-carboxyanhydrides are polymerized together. However, there is no control over the amino acid sequence. Block copolymers can also be formed. First, a homopolypeptide is synthesized followed by the functionalization of the end group to initiate the polymerization of the second block. Another approach to form block copolymers, using coupling strategies, is by synthesizing the

individual segments, functionalizing the chain ends and using methods, such as click chemistry, to connect the segments [14].

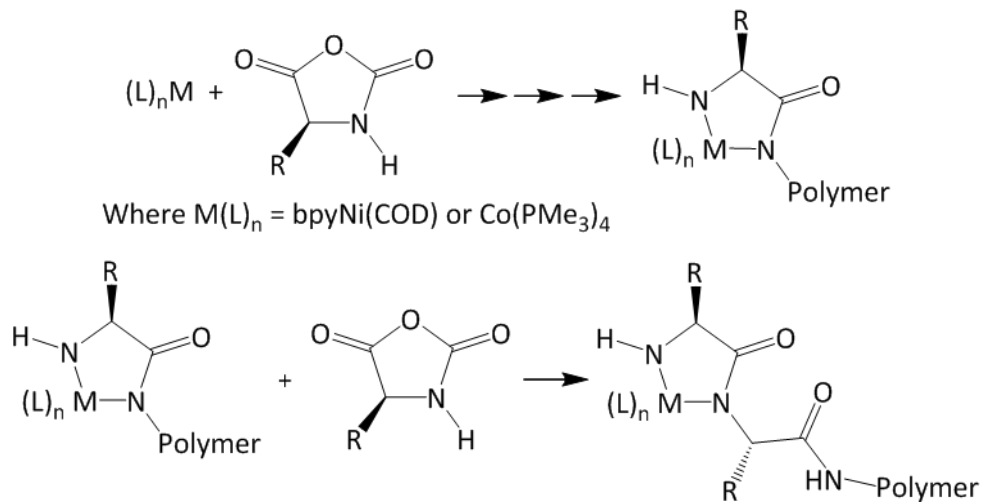


Figure 2.5: NCA polymerization initiated by transition metals

### 2.1.2 Conventional Polymerization

Synthetic polymers from olefins can be made by a wide range of processes, such as chain growth polymerization by free radical, anionic, cationic and coordination polymerization. Chain growth polymerization consists of initiation of the active species, propagation of the polymer chain and termination of the chain. The main difference between the chain growth methods depends on the active species, whether it is a free radical, anion, cation or transition metal center.

The advantage of free radical polymerization over the other processes is that a greater range of monomers can be used in comparison to the other methods. However, there are problems associated with free radical polymerization, which includes the lack of control over the molecular weight and polydispersity of the polymers produced. Furthermore, the polymer structure, as well as the chain end groups are difficult to control [15, 16].

### 2.1.2.1 Atom Transfer Radical Polymerization

In order to produce polymers with specific properties, better control is required. Controlled radical polymerization, or living radical polymerization, uses an organometallic catalyst to control the reaction. The catalyst creates a dynamic equilibrium with the propagating radical, called the persistent radical effect (PRE). The radicals deactivate into a dormant species, which can reactivate back to the active species, generally spontaneously, or by external means such as heat [15].

Propagation in controlled radical polymerization, in comparison to free radical polymerization, is longer due to the deactivation/activation process. The initiation process in controlled radical polymerization is fast, so all the chains grow at the same rate, resulting in a narrow molecular weight distribution, unlike free radical polymerization. Also, the kinetics are determined by the deactivation/activation of the propagating radical, rather than initiation/termination as in free radical polymerization [15].

The advantages over free radical polymerization include low polydispersity and controllable molecular weight, based on the monomer consumption and initiator concentration. Also, the polymer end groups can be functionalized, whether with a specific group or with another polymer. The main disadvantage is that stereoselectivity in the reaction remains a problem due to the reactivity of free radicals [16].

#### 2.1.2.1.1 Mechanism

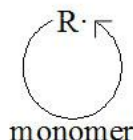
The mechanism that the polymerization follows is similar to radical polymerization, with a few notable differences shown in Figure 2.6. The polymerization initiates through cleavage of an alkyl halide,  $RX$ , by the catalyst,  $M^0/L_m$ . A radical is generated and the species  $M^{n+1}X/L_m$ , is formed. The radical can either propagate with the monomer, or deactivate due to the catalyst,  $R-X$  and  $M^0/L_m$ , which can activate again due to the equilibrium between the dormant and active species. The radical

terminates either through combination or disproportionation, or remains with the halogenated end group depending on the reaction conditions [15].

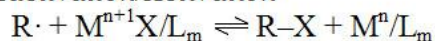
*Initiation*



*Propagation*



*Deactivation/Activation*



*Termination*

**Combination**



**Disproportionation**



Figure 2.6: ATRP reaction scheme [15]

The kinetics in ATRP are determined by the deactivation/activation of the radical species. The ATRP equilibrium constant is given in Equation (2.1). In general, for ATRP to be controlled successfully, the activation rate constant must be smaller than the deactivation rate constant - the equilibrium is shifted in favour of the dormant species [15].

$$K_{ATRP} = \frac{k_{act}}{k_{deact}} \quad (2.1)$$

Furthermore, in order to obtain better control over the polymerization, the halide needs to transfer quickly between the catalyst and the growing chain; typically chlorine or bromine is used [15, 17].

There are many factors that determine the kinetics of the polymerization: the monomer, initiator, catalyst, ligands on the catalyst, solvent, temperature, reaction time and additives.

The most successful monomers in ATRP are those with substituents to stabilize the radicals formed in the process. These include styrenics, acrylates, acrylamides, dienes and acrylonitrile. Acidic monomers have been unsuccessful due to protonation of the ligand and the formation of salts. Halogenated olefins are generally not reactive in radical polymerization. Furthermore, each monomer reacts differently based on the catalytic system, so optimizing the conditions can be difficult [17].

Initiation is an important process, as it determines the number of growing chains in the polymerization and subsequently the molecular weight of the resulting polymers. The process must be fast in order to obtain a low polydispersity. Furthermore, initiators with multiple halogen groups can initiate the polymerization in several directions. The most commonly used initiators are alkyl halides, but benzylic halides, haloesters, haloketones, halonitriles and sulfonyl halides have also been used to initiate ATRP [17].

The catalyst determines the equilibrium constant so an appropriately selected catalyst is vital for polymerization. For a catalyst to be effective, the transition metal must have 2 stable oxidation states differing by one electron, be attracted to the halogen group and the ligand should be strongly bonded to the metal [17]. Catalysts generally used for ATRP are Cu(I) and Ru(II), though research on Ni(II), Fe(II), Rh(II) and Te has demonstrated that they can catalyze ATRP as well [16].

Ligands, as mentioned before, must bond strongly to the catalyst. Furthermore, ligands are necessary for the solubility of the catalyst and are also important due to their effect on catalytic activity. Typical ligands used for Cu(I) are bipyridine, or multidentate amines and phosphine for other catalysts [17].

The solvent can have an important impact on the polymerization, but it is not necessarily needed as polymerization can occur in bulk. In the cases where a solvent is used, solvent selection is based on

the solubility of the reagents and the polymer formed. Additionally, side reactions need to be minimized [17].

Like all reactions, the temperature and reaction time play important roles. An increase in temperature increases the rate of polymerization, however, at higher temperatures the catalyst may decompose and side reactions are more likely to occur, so the temperature needs to be optimized to find ideal reaction conditions [17]. The incorporation of additives has been found to increase the rate of polymerization depending on the additive and the reaction system [17].

#### 2.1.2.1.2 Applications

ATRP can make a range of polymeric materials, by varying composition such as in copolymers, by changing the structure, like linear or branched polymers, as well as customizing functional groups on the polymers [16].

Functionality in a polymer results from the monomer, the initiator and the end groups. Monomers are chosen based on the properties of functional groups that are sought after in the polymer. Functionality from the initiator, the group forming the start of the propagating chain, must be stable with respect to the catalyst and radicals in the process. Functionality in the end group is selected by replacing the halogen group with the desired group [17].

A variety of polymers with different composition can be formed, such as statistical, gradient and block copolymers, shown in Figure 2.7. The longer reaction time in ATRP gives greater opportunity to form different segments of polymers. Gradient polymers, which are a mixture between statistical and block copolymers, can also be formed using ATRP and have unique properties, different from both statistical and block copolymers [17].

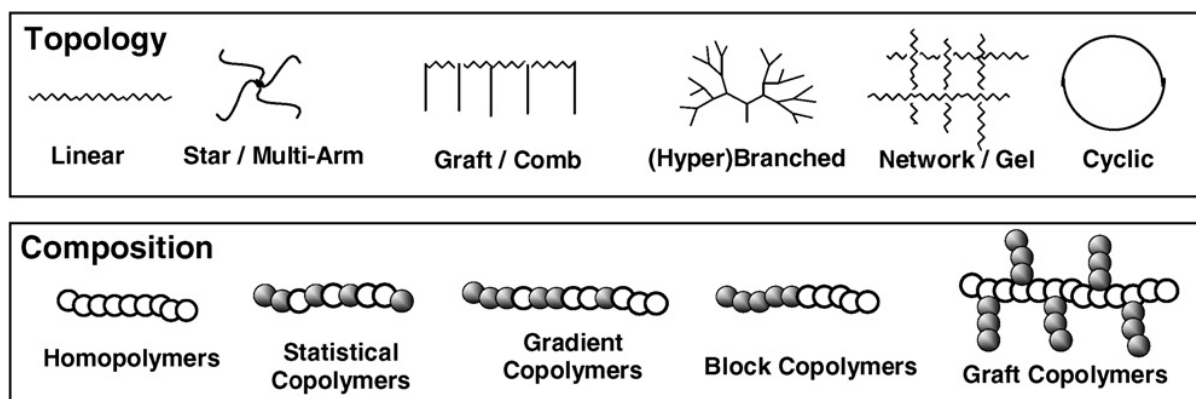


Figure 2.7: Different compositions and architectures of polymers [15]

ATRP gives a large range of possible architecture for polymers, ranging from linear, to branched structures, such as graft copolymers, polymers grafted to a linear organic chain, an inorganic chain, or a surface. Star polymers and highly branched polymers can be synthesized as well [17]. See Figure 2.7 for diagrams of potential architectures.

### 2.1.3 Click Chemistry

The click reaction consists of reactions that are simple, fast, have a high conversion of reagents, functional group tolerance and works in both aqueous and non-aqueous solvents as well as homogeneous and heterogeneous solutions. Furthermore, the reaction conditions are mild and because of the high conversion, the removal of unreacted reagents and side products is a minor concern. Click chemistry can be combined with living radical polymerization processes for further functionalization of the polymers [18, 19].

The different classes of click reactions include cycloaddition, nucleophilic ring-opening, non-aldol carbonyl chemistry and addition to carbon-carbon multiple bonds [19]. The most important click reaction, the azide-alkyne reaction, or the Huisgen 1,3-dipolar cycloaddition reaction, shown in Figure 2.8, is a catalyzed reaction between a terminal carbon triple bond and a carbon-nitrogen triple bond, forming 1,4- and 1,5-triazoles [18].

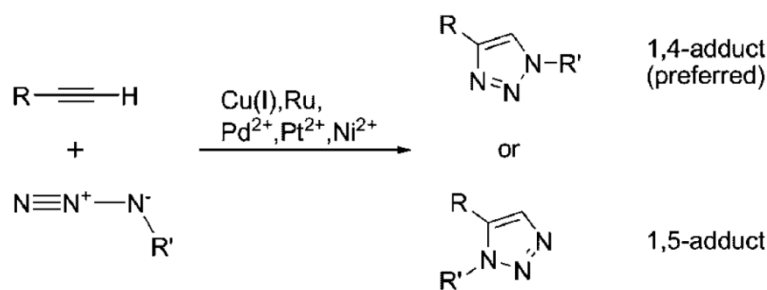


Figure 2.8: Huisgen 1,3-dipolar cycloaddition [18]

## 2.2 Self-Assembly

Surfactant-type peptides and polymers are amphiphilic, so in solution, the polymers will self-assemble into structures to minimize free energy [20]. Block copolymers and copolypeptides can form vesicles, which can be used for a range of applications including the delivery of therapeutic agents, sensors and separations. Micelles, vesicles, rod-shaped structures and hydrogels are a few examples of block copolymer self-assembled structures. Concentration plays a role in the self-assembly, with the peptides and polymers forming assemblies above of the critical micelle concentration. Furthermore, at higher concentrations, gelation can occur due to increased interactions between the polymer chains. The self-assembly will also change in the solid-state, which will not be discussed in this review.

### 2.2.1 Factors affecting self-assembly

The factors affecting self-assembly include intramolecular interactions, leading to secondary structure formation in peptides, intermolecular interactions between the chains and interactions with the solvent. The main solution properties that affect the aggregation are the pH and electrolytes [21]. The effect of these, however, depends on the composition. Polymers with pH-responsive functional groups will assemble differently depending on the pH of the solution. In some cases, polymer solubility may only be evident over certain pH ranges. Furthermore, charged peptide segments will assemble in a different fashion in the presence of electrolytes. Charged peptide segments will repel

each other when aggregated, however, electrolytes interact with the charged segments, decreasing the electrostatic repulsion [22].

Secondary structure formation in peptides is also an important consideration. The basic secondary structures of polypeptides are  $\alpha$ -helices,  $\beta$ -sheets, random coils and turns. The  $\alpha$ -helix is a secondary structure in peptides that is in the shape of a spiral, shown in Figure 2.9. The carbonyl oxygen and the amide hydrogen are bonded through a hydrogen bond, with an average of 3.6 residues per turn. Since the polar groups of the amino acids are involved in bonding, the polarity of the peptide is determined by the side chains of the amino acids. The  $\beta$ -sheet is another secondary structure common in peptides and has the structure shown in Figure 2.10.  $\beta$ -Strands are tightly packed through hydrogen bonding within or between adjacent peptides. The polarity is determined by the orientation of the peptide bonds, whether the peptides are parallel or antiparallel to each other. The random coil is another secondary structure, but unlike the other structures, it is not well-defined. The reverse turn is a short

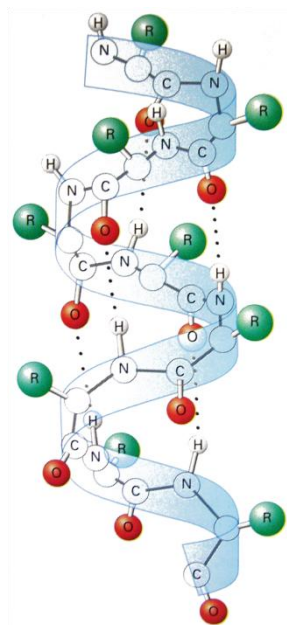


Figure 2.9:  $\alpha$ -Helix structure [23]

strand which form a U-shaped secondary structure due to hydrogen bonding at the end of the residues. They are common on the surface of proteins, with the backbone facing the inside, which helps proteins pack more tightly [23].

### 2.2.2 Hybrid peptide block copolymers

Hybrid peptide block copolymers consist of both a peptide chain and a synthetic polymer block. The advantage of these systems is the ability to exploit the characteristics of peptides - biocompatibility, complexity and secondary structure formation, as well as the variety of synthetic polymers available to customize the properties of the copolymer.

In general, there are three categories: hybrid block copolymers with the peptide forming the core, block copolymers with the peptide forming the corona of the self-assembled structures and systems where the peptide can form both the core and corona, depending on the solution conditions. In the case of the core-forming peptide copolymers, a hydrophobic amino acid is used, generally with a soluble synthetic polymer chain. The secondary structure of the peptide will have an important effect on the self-assembly. For corona-forming peptide systems, a hydrophilic amino acid is usually selected, with a hydrophobic synthetic polymer. Because of interactions with the solution, secondary structure formation is less important. In reversible systems, the peptide block can be either core-forming or corona-forming, depending on the solution conditions [20].

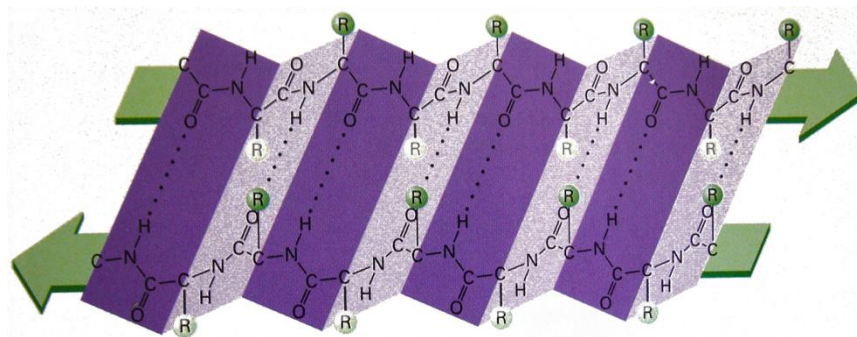


Figure 2.10:  $\beta$ -Sheet structure [23]

### 2.2.2.1 Core-forming peptides

Core-forming peptide block copolymers consist of an insoluble peptide block, forming the core of the self-assembled structures. The majority of the work uses poly(ethylene glycol) as the soluble block for its biocompatibility, but other polymer blocks have also been used based on their properties.

Yonese et al. studied block copolymers of PEG and poly( $\gamma$ -methyl-L-glutamate), which were found to form self-assembled structures, shown in Figure 2.11. The secondary structure of the  $\gamma$ -methyl-L-glutamate was found to be a contributor to the self-assembly [24]. Cho et al. studied a similar system, PEG-b- $\gamma$ -benzyl-L-glutamate which also formed large aggregates [25]. A similar system was studied, using poly(N-isopropylacrylamide) (PNIPAM), in order to study the effect of the LCST of PNIPAM on the aggregation. However, no major change was observed above and below the LCST [26].

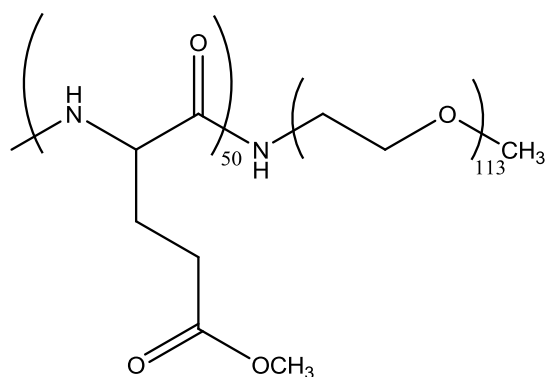


Figure 2.11: Block copolymers of PEG-b-poly( $\gamma$ -methyl-L-glutamate)

In addition to charged amino acids, hydrophobic amino acids have been used as well. Naka et al. studied poly(N-acetyliminoethylene)-b-poly(L-phenylalanine), which were found to form large micelles due to hydrogen bonding between the amino acids in the core of the micelles [27]. Dong et al. studied the self-assembly of poly(2-acryloyl ethyllactoside)-b-poly(L-alanine). The polymer was found to form large multi-lamellar vesicles [28]. Tam et al. studied poly(acrylic acid)-b-poly(L-valine), shown in Figure 2.12, which was found to form micelles [29] due to the  $\beta$ -sheet structure within their core [30].

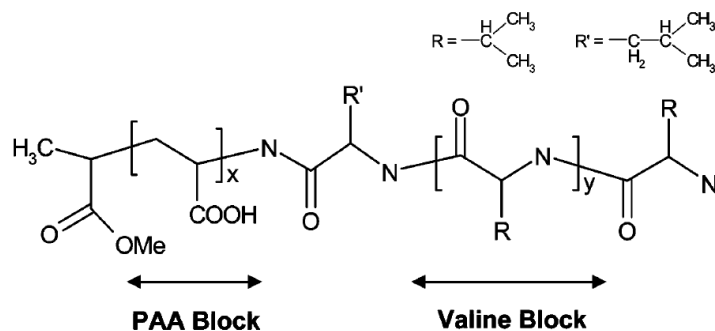


Figure 2.12: Block copolymers of PAA-b-PLVAL [30]

### 2.2.2.2 Corona-forming peptides

Corona-forming peptide block copolymers are composed of a soluble peptide block and an insoluble synthetic polymer block. The peptide block generally consists of a  $\alpha$ -helix forming amino acid.

Two groups, Schlaad et al. [31] and Lecommandoux et al. [32], studied the self-assembly of polybutadiene-b-poly(L-glutamate). The block copolymers were found to assemble into micelles or vesicles. Secondary structure was apparent at lower pHs and a random coil was observed at high solution pH, but did not affect the self-assembly. Another system, studied by Lecommandoux et al., was poly(isoprene)-b-poly(L-lysine). These formed micelles and similarly to the PB-b-PLG system, a transition could be observed between a random coil at low pH and  $\alpha$ -helix structure at high pH. Unlike the glutamate system, the self-assembled structures at high pH, with a  $\alpha$ -helix formation were smaller by nearly 50 % [33].

Most of the self-assembled structures observed were spherical micelles or vesicles. One group, however, observed cylindrical micelles with polystyrene-b-poly(L-lysine) regardless of the number of L-lysine units [34]. The difference in self-assembly, however, could not be explained and the mechanism is still poorly understood.

### 2.2.2.3 Reversible core-corona peptides

Reversible peptide block copolymers are both core- and corona-forming, depending on the solution conditions. The novelty of these systems is the potential to fine-tune the system for specific applications.

One system, studied by the Lecommandoux group, is poly[2-(dimethylamino)ethyl methacrylate]-b-poly(glutamic acid). The polymers were both pH responsive, due to the amine group of PDMAEMA and the glutamic acid group of PGA, and temperature responsive due to PDMAEMA. At high pH below the LCST of PDMAEMA, the polymer was soluble in water and present as free chains in solution. Above the LCST, PDMAEMA became insoluble and the polymer self-assembled into micelles or vesicles, depending on the degree of polymerization of PGA. At low pH, due to the high solubility of the PDMAEMA group, the polymers were soluble and self-assembly was not observed. Close to the isoelectric point, electrostatic vesicles were formed as both blocks are charged [35]. A schematic of the self-assembly behaviour is shown in Figure 2.13.

### 2.2.3 Block copolypeptides

Block copolypeptides consist only of peptide chains. Unlike hybrid peptide block copolymers, much less work has been done in this field.

#### 2.2.3.1 Non-ionic block copolypeptides

The Deming group formed vesicles from uncharged block polypeptides of L-leucine and ethylene glycol modified L-lysine. Block copolypeptides with lengths of 60 to 200 amino acids were formed, with leucine, the hydrophobic segment, ranging from 10 to 75 residues [36]. Since both leucine and lysine tend to form  $\alpha$ -helix structures, strong  $\alpha$ -helical behaviour was observed in this case with

circular dichroism [37]. The length of the hydrophobic and hydrophilic segments had a large impact on the assembly [1, 36]. The stability was tested by entrapping a fluorophore in the vesicles – there was no release of the fluorophore with time (a few weeks), with temperature (up to 90 °C), pH (between 3 – 10) and solutes (below 1.0 M) [36].

The advantage of non-ionic block copolymers is that the uncharged residues do not interact with charged biomaterials. PEG, which is one of the most commonly used polymers due to its biocompatibility and solubility. PEG will not illicit an immune response [38]. Because of the lack of polyelectrolyte segments, these polymers tend to be stable towards ions, pH and biological molecules. However, their disadvantage is that very rigid membranes are formed – in the case of peptides a result of the secondary structure formation. Another disadvantage of these systems is the lack of flexibility and functionality limiting their drug delivery applications [1, 36].

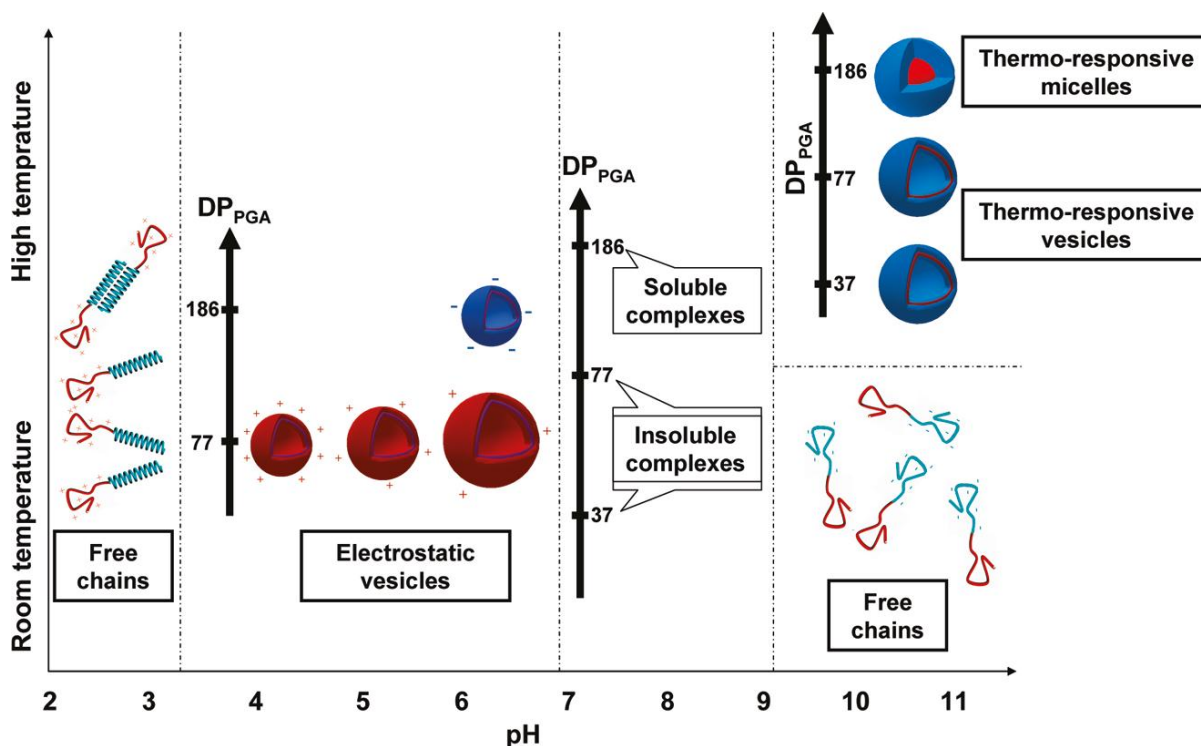


Figure 2.13: Schematic diagram of the morphology of PDMAEMA-b-PGA [35]

### 2.2.3.2 Zwitterionic block copolypeptides

In contrast to the neutral block copolymers, zwitterionic block copolymers are highly pH sensitive due to functional groups on each block of the polymer. A novel block copolypeptide of L-glutamic acid and L-lysine was investigated for drug delivery by the Lecommandoux group. The block lengths were small, with 15 residues of amino acid in each segment. The assembly of the polypeptides was largely dependent on the polyelectrolytic properties of each peptide segment and the pH of the system. The system was found to form "schizophrenic" micelles depending on the pH of the solution, as can be seen in Figure 2.14 [39].

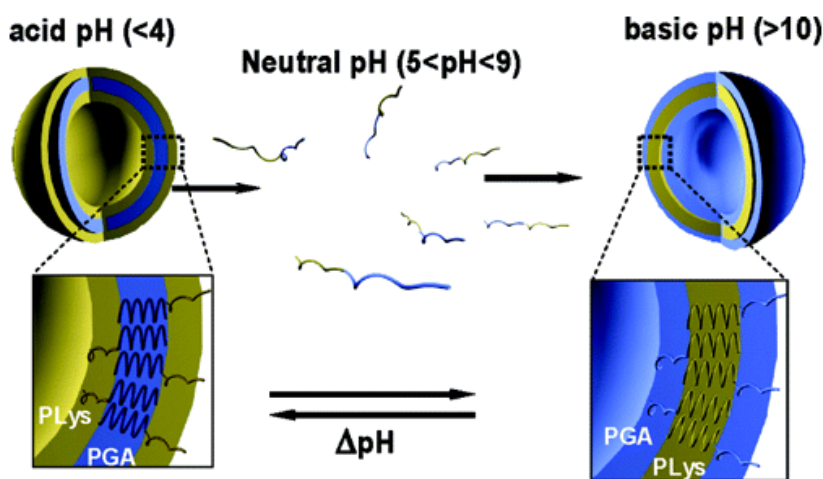


Figure 2.14: "Schizophrenic" micelles of L-glutamic acid and L-lysine [39]

It was found that around neutral pH,  $5 < \text{pH} < 9$ , both segments of the block copolypeptide were soluble in water. Under acidic conditions,  $\text{pH} < 4$ , the L-glutamic acid segment was neutralized and therefore less soluble in water, leading to the self-assembly of vesicles with a positively charged surface. Under basic conditions,  $\text{pH} > 10$ , the L-lysine segment was neutralized and the hydrophobicity of the block led to the formation of vesicles with a negatively charged surface. For both segments, when neutralized, the secondary structure changed from a charged, random coil to a compact  $\alpha$ -helical structure. Nuclear magnetic resonance spectroscopy and fluorescence spectroscopy were used to examine the pH dependence of micellization. Using dynamic light scattering, the

diameter of the vesicles under acidic and basic conditions was 220 and 350 nm, respectively [39]. The polymer was found to encapsulate pyrene at both high and low pH, showing potential drug delivery applications.

### 2.2.3.3 Block copolypeptides with a polyelectrolyte segment

The majority of the work on block copolymers for drug delivery revolves around a combination of ionic and non-ionic segments. The hydrophobic segment directs self-assembly and the hydrophilic segment can be selected for the desired properties and further functionalized.

The Deming group investigated block copolypeptides of L-lysine and L-leucine (Figure 2.15) as well as L-glutamic acid and L-leucine. The size of the blocks ranged from 20 to 80 residues for the charged segment, and 10 to 30 residues for the hydrophobic segment. A range of structures was observed, including membrane sheets, fibrils, micelles, vesicles and irregularly shaped aggregates depending on the length of each block, see Figure 2.16. The optimal lysine-leucine system had residue length ratio of lysine to leucine of 60 to 20, which formed unilamellar vesicles, as can be seen in Figure 2.17. Similarly, the glutamic acid-leucine system with a residue length ratio of 60 to 20 also formed vesicles. The assembly depended strongly on the lysine to leucine ratio - a low ratio did not have enough polyelectrolyte to stabilize and solubilize the hydrophobic segment and a high ratio has greater polyelectrolyte repulsion between the chains, destabilizing the membranes. Additionally, the structures were found to be rigid, due to the  $\alpha$ -helical structure of the polypeptides. As a result, the vesicles were quite large, ranging in diameter from 0.8 to 5  $\mu\text{m}$ , depending on the method used. However, extrusion of the vesicles through a polycarbonate membrane gave better control over the vesicle diameter. The vesicles were also found to be stable over time and at high temperatures (up to 80 °C) [40].

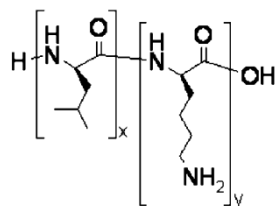


Figure 2.15: Block copolypeptides of leucine and lysine [20]

The ability of the vesicles to entrap drugs was tested with Texas Red labelled dextran. The vesicles entrapped a reasonable amount of the dextran and were stable over a period of a week. An investigation into the osmotic stress on the vesicles found that the vesicles were permeable to water. Also, high salt concentrations would rupture the vesicles, resulting in the formation of membranes. This was likely due to ionic interactions of the salt with the charged peptide segment. The vesicles were stable at high salt concentrations in a 100 mM phosphate-buffered saline solution. Overall, the lysine-leucine system was found to be a good potential drug delivery agent [40].

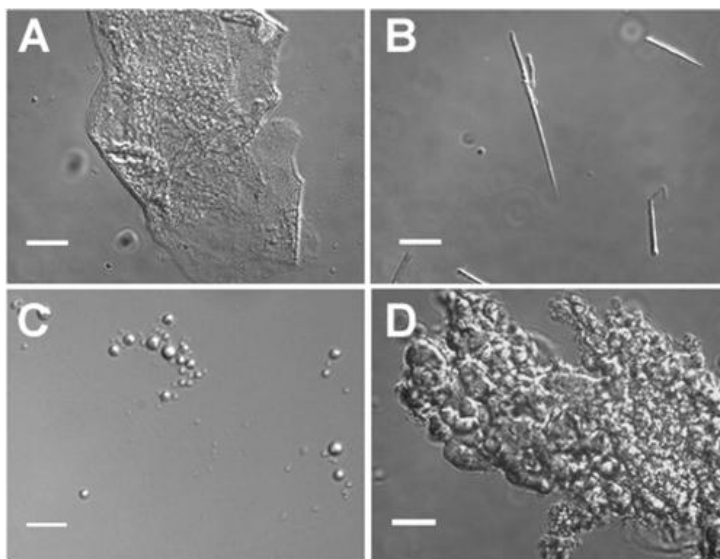


Figure 2.16: Differential interference contrast images of poly-L-lysine-b-poly-L-leucine: (a)  $K_{20}L_{20}$  (sheets), (b)  $K_{40}L_{20}$  (fibrils), (c)  $K_{60}L_{20}$  (vesicles) and (d)  $K_{80}L_{20}$  (irregular) [40]

Another system investigated by the Deming group was a block copolypeptide of L-arginine and L-leucine. Arginine was chosen because a peptide derived from the HIV-1 Tat-protein, which is rich in arginine residues, has been found to deliver drugs effectively at the cellular level. Studies have found that the guanidinium group of arginine is an important component of the Tat-peptide and that a simple homopolypeptide of arginine is sufficient [41]. The system was found to be similar to the lysine-leucine system. Additionally, the vesicles could transport between the hydrophilic and hydrophobic environments without disruption of the vesicles. As a result, the vesicles were investigated for intracellular delivery in vitro for epithelial and endothelial cells. The vesicles, around 100 nm, easily entered the cells despite their large size. The main problem with the arginine-leucine system is the toxicity of the polyarginine chain, which needs further investigation [42].

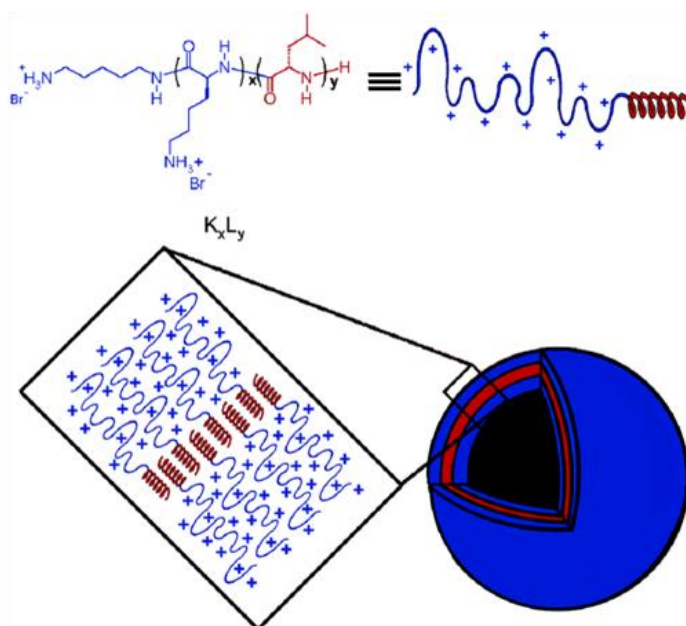


Figure 2.17: Self-assembled vesicles of poly-L-lysine-b-poly-L-leucine [40]

### 2.3 Applications

Synthetic polypeptides and polymers can be used for a range of biomedical applications. The majority of research in this field concerns their use as non-viral vectors of gene delivery and membranes for

drug delivery [43]. In addition to drug delivery, polypeptides and polymers can be used as hydrogel scaffolds to mimic extracellular matrices, for medical adhesives, as well as antimicrobial and immuno-modulating applications [1].

### **2.3.1 Gene Therapy**

An important field of biomedical research is gene therapy, which is the delivery of genes in order to treat genetic diseases [44].

Initially, viral vectors were explored for gene therapy, as viruses are natural gene delivery agents and have efficient mechanisms for delivering genetic material. Two of the most commonly used viruses are the adenovirus [45] and the retrovirus [46]. The genetic material of the virus is replaced by the therapeutic gene and the virus is modified to be safe. However, problems exist with viral vectors – such as an immune response and the possibility that the virus becomes pathogenic.

An alternative to viral vectors is the use of non-viral vectors such as lipids, synthetic polymers and peptides. In comparison to viral vectors, non-viral vectors have lower transfection rates and gene expression. However, polymers and peptides can be designed to be safer and more efficient in delivering genetic material [47].

Non-viral vectors typically bind to DNA or RNA and condense the genetic material into small nanoparticles in order to protect it and facilitate its entry into cells. As DNA and RNA are negatively charged, cationic lipids, polymers and peptides are typically used to bind through electrostatic interactions. A range of problems surrounding gene delivery with non-viral vectors include protection and condensation of the genetic material, polyplex stability in serum and extracellular material, targeting to specific cells, cellular entry typically through the endosome, escape from the endosome or lysosome, transport through the cytoplasm and entry into the nucleus, as shown in Figure 2.18. Furthermore, the vector needs to be non-toxic, non-immunogenic and non-pathogenic for safety

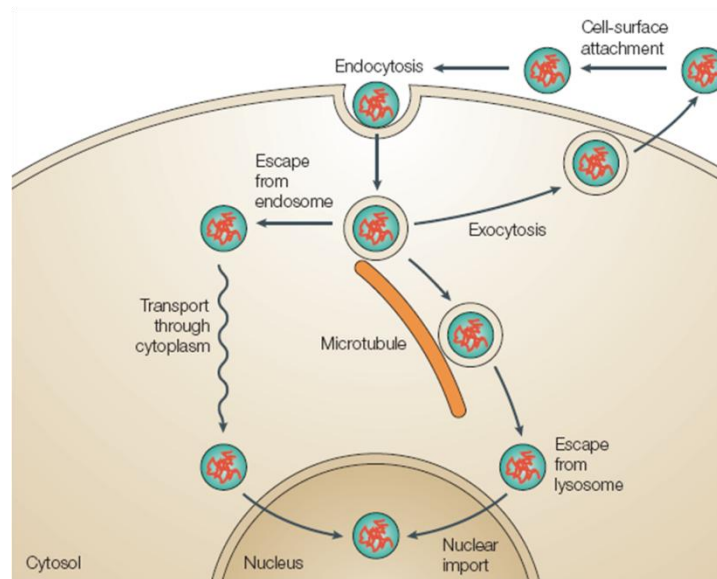


Figure 2.18: Barriers to successful gene delivery using non-viral vectors [47]

concerns [47]. Although gene therapy using non-viral vectors can become quite complicated, by understanding existing delivery systems, improved non-viral vectors can be designed and developed.

The majority of the work on non-viral vectors used commercially available cationic polymers, such as polylysine, polyethylenimine (PEI) and polyamidoamine (PAMAM).

As polylysine is a peptide, the advantage for intracellular delivery is its biodegradability. Although the polyplexes are taken up by cells, low transfection efficiency is observed and is likely due to limited endosomal escape [48]. The transfection efficiency has been improved by the addition of agents, such as chloroquine, a weak base, which changes the pH within the endosomes, leading to endosomal swelling and the release of the genes into the cell [49]. This effect is the proton-sponge hypothesis [50]. Despite attempts to increase the transfection efficiency of polylysine, it is generally not used as a gene delivery agent as many polymers have higher transfection efficiencies [48].

PEI has been shown to be an effective polymer for gene delivery [51]. Unlike polylysine, no additional agents are necessary since PEI has a  $pK_a$  between the physiological and the lysosomal pHs,

and so it is believed that the polyplex is able to escape the endosome due to the proton-sponge hypothesis [50]. Modifications to PEI with targeting ligands have been performed and were successful for in vivo gene delivery. However, the main disadvantage of PEI is its high toxicity [48].

The latest commercially available polymer is the PAMAM dendrimer. Like PEI, PAMAM is believed to be an effective proton sponge and has high transfection efficiency [50, 52]. The higher generations were found to have improved transfection efficiency [53] as well as partially fractured PAMAM dendrimers, which have more flexibility [54].

In order to develop better polymers and peptides for non-viral gene therapy, several pathways are explored, focusing on different barriers in the intracellular delivery process. The main approach, which exploits the proton-sponge hypothesis, uses functional groups which have a  $pK_a$  between physiological and endosomal pH, such as imidazoles that have a  $pK_a$  around 6, to assist in endolysosomal escape. For imidazoles, two approaches are generally taken either to incorporate the group directly into the chain, such as polyhistidines [55], or to link an imidazole group to an existing polymer chain [56]. Another interesting approach is the use of charge-conversional functional groups, such as citraconic amide and cis-aconitic amide, which degrade around pH 5.5 [57].

Other approaches have been developed to make existing polymers, such as PEI, biodegradable and less cytotoxic. Low molecular weight PEI is non-toxic, but not as effective as higher molecular weight PEI for gene delivery. However, linking together low molecular weight PEI has been found to be a non-toxic option [58]. Cross-linking using disulfide bonds is a unique approach, as the bonds are degradable within the cell [59, 60].

Another approach is the use of block copolymers, with the second block chosen to enhance the polyplex stability and lower its toxicity [61]. One of the most commonly used polymers is PEG, which increases the steric stability of polymeric complexes and minimizes interactions with proteins

and biological components, thereby improving the complexes for intracellular delivery [62]. In vivo tests of polylysine polyplexes, in comparison to PEG-polylysine polyplexes, have shown less toxicity with the PEG-polylysine system but lower transfection efficiency was observed [63].

## **2.4 Outlook**

Improvements in the synthesis of both synthetic peptides and polymers allow for more diverse materials to be created. For block copolypeptides and hybrid synthetic-peptide block copolymers, the different blocks can be selected for interactions with therapeutic agents or the environment, solubility, pH-responsiveness, non-toxicity, biodegradability, secondary structure formation and so on.

The ability to customize these polymeric materials allow for a range of different applications. By building on published research, improved polymeric systems can be designed for various biomedical applications.

## Chapter 3

### Synthesis of Peptide-based Block Copolymers

#### 3.1 Introduction

A variety of synthetic schemes exist for the synthesis of peptide-based block copolymers. Due to the different synthetic chemistry of each block, a separate synthesis is required. The two general schemes used are: the preparation of the first polymeric chain, which is functionalized to act as a macroinitiator for the polymerization of the second polymeric chain [1] and the preparation of the two blocks individually, which are then coupled together [2].

The three main methods used for the synthesis of peptides are: solid-state peptide synthesis, recombinant DNA technology and NCA ring opening polymerization. The advantages and disadvantages of each method are outlined in Table 3.1. For the synthetic polymer block, many of the typical controlled polymerization techniques are used to synthesize controlled molecular weight and monodispersed samples.

Table 3.1: Comparison of different peptide synthesis techniques

<b>Synthesis Method</b>	<b>Sequence</b>	<b>Chain length</b>	<b>Scale</b>
Solid-state synthesis	Controlled	Short	Small scale
Gene expression	Controlled	Controlled	Potential for larger scale using bio-reactors
NCA polymerization	Random	Controlled	Allows large scale synthesis

The synthetic scheme for this project was based on that developed by Lecommandoux and coworkers for the synthesis of PBLG-b-PDMAEMA [2]. Although the polymer is similar, modification of the approach will be made when necessary. For the polymerization of DEAEMA, differences in solubility due to the ethyl groups, in comparison to the methyl groups of PDMAEMA, made it difficult to precipitate the polymer. PDEAEMA was used in its liquid form for the subsequent

polymerizations. Another modification prior to the polymerization of PBLG was to limit the side reactions in NCA polymerization. The synthesis was performed at low temperatures in order to obtain a peptide with low polydispersity [3].

## **3.2 Experimental**

### **3.2.1 Materials**

The solvents used in the synthesis were purified and dried as follows. Tetrahydrofuran (THF), methylene chloride and hexane were passed through an alumina column under nitrogen. N,N-dimethylformamide (DMF) was dried over molecular sieves and distilled under vacuum. 2-(diethylamino)ethyl methacrylate was passed through a basic alumina column twice immediately before the polymerization. All chemicals used in the synthesis were purchased from Sigma-Aldrich and used as received. Deuterated solvents were purchased from Cambridge Isotope Laboratories.

### **3.2.2 Instrumentation**

$^1\text{H}$  NMR spectra were recorded using a Bruker AV300 instrument. All runs were performed at room temperature. The polymerization initiators were run in deuterated chloroform ( $\text{CDCl}_3$ ), the protected polymer products and monomers were run in deuterated DMSO ( $d_6$ -DMSO) and the final polymer was run in deuterated water, ( $\text{D}_2\text{O}$ ), with deuterium chloride (DCl) and sodium deuterioxide (NaOD) used to adjust the pH of the aqueous solution.

FTIR was run using a Bruker Tensor 27 instrument at room temperature using a KBr pellet under nitrogen flow. The spectra were recorded from 4000 to 400  $\text{cm}^{-1}$ .

The molecular weight and polydispersity of the samples were recorded using gel permeation chromatography. The system consisted of a 500 mm x 10 mm Jordi Gel DVB Mixed Bed column with a linear polystyrene molecular weight range of  $10^2$ - $10^7$ , a Waters 510 HPLC pump, a 50 mL injection loop and Waters 2410 differential refractometer (DRI) detector. HPLC grade N,N-

dimethylacetamide with 1 g/L LiCl, to prevent aggregation of polymers, was used at a flow rate of 1.0 mL/min at room temperature was used.

### 3.2.3 Synthetic Protocols

#### 3.2.3.1 Synthesis of PBLG

The monomer for the polymerization was prepared by protecting L-glutamic acid with a benzyl group, synthesizing the N-carboxyanhydride of the protected glutamate using phosgenation, followed by polymerization using an azide-functional amine initiator.

**Preparation of  $\gamma$ -benzyl-glutamate:** The carboxylic acid group of the side chain of glutamic acid was protected with a benzyl group using a published procedure [4]. L-glutamic acid was dissolved in benzyl alcohol and hydrochloric acid with rigorous stirring under high heat. Once the amino acid was dissolved, the solution was cooled in an ice bath and added to a solution of 15 % pyridine in ethanol. The mixture was left in the fridge overnight for the product to precipitate. The precipitate was recovered and then dissolved in a 5 % ethanol solution. This solution was neutralized to pH 7 using sodium bicarbonate and left overnight in the fridge for the product to crystallize. The precipitate was recovered, washed with water, ethanol and diethyl ether, and dried under vacuum. The  $\gamma$ -benzyl-glutamate was stored at -20 °C.

**Preparation of  $\gamma$ -benzyl-glutamate-NCA:**  $\gamma$ -Benzyl-glutamate-NCA was synthesized using a published procedure [5], which utilized the Fuchs-Farthing Method – a phosgenation reaction [6]. The synthetic scheme is shown in Figure 3.1.  $\gamma$ -Benzyl-glutamate was added to anhydrous THF and the mixture was warmed to 50 °C. 1/3 Molar equivalent of triphosgene was then added. The mixture was degassed with nitrogen gas and vented to ammonium hydroxide to neutralize any hydrogen chloride produced in the reaction. The mixture was stirred until the solution became homogeneous, typically 1 h. The solution was added slowly to approximately 3 times its volume in hexanes. This solution was

left overnight in a freezer at  $-20\text{ }^{\circ}\text{C}$  to allow the NCA to fully crystallize out of solution. The NCA was recrystallized using THF/hexane (1:3).

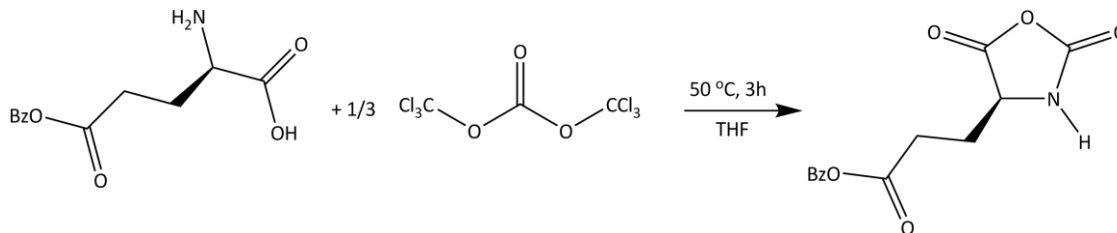


Figure 3.1: Reaction scheme for the phosgenation of  $\gamma$ -benzyl-glutamate

**Preparation of Azide-Functional Amine:** 1-Azido-3-aminopropane was synthesized using the published procedure [7]. The reaction scheme is summarized in Figure 3.2. 3-Chloropropylamine hydrochloride and sodium azide were dissolved in water and the solution was heated at  $80\text{ }^{\circ}\text{C}$  for 15 h. The solution was then cooled in an ice bath with potassium hydroxide added to the solution. The aqueous solution was extracted 3 times with diethyl ether. The organic solution was dried over anhydrous sodium sulfate and the solvent was removed using a rotary evaporator. The amine was then purified by distillation.

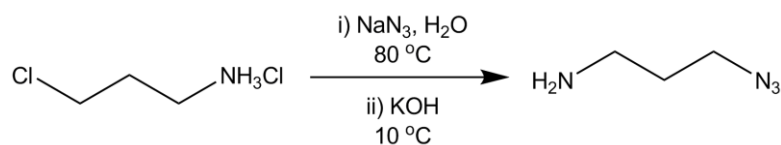


Figure 3.2: Reaction scheme for azide-functional amine initiator for NCA polymerization

**NCA Polymerization:** The NCA ring opening polymerization was performed at low temperature ( $0\text{ }^{\circ}\text{C}$ ) [3]. The reaction scheme is shown in Figure 3.3.  $\gamma$ -Benzyl-glutamate-NCA was dissolved in anhydrous DMF and the solution was cooled to  $0\text{ }^{\circ}\text{C}$  under nitrogen gas in a jacketed reaction flask. An appropriate amount of the azide-functional amine was added using a nitrogen purged syringe. The solution was stirred at  $0\text{ }^{\circ}\text{C}$  for two to seven days, depending on the desired chain length. The chain

length was observed using gel permeation chromatography. The polymerization was stopped by the addition of the solution to diethyl ether to precipitate the peptide and dried in a vacuum oven.

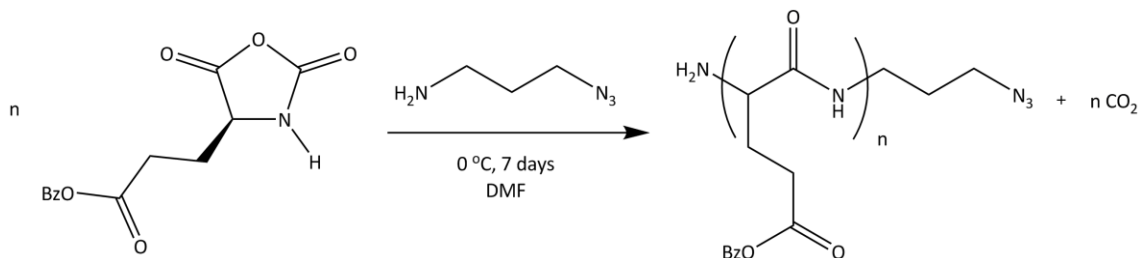


Figure 3.3: NCA ring opening polymerization of  $\gamma$ -benzyl-glutamate-NCA

### 3.2.3.2 Synthesis of PDEAEMA

**Preparation of Alkyne-Functional Bromide Initiator:** The initiator for ATRP, propargyl-2-bromoisobutyrate, was prepared using a published procedure [8]. The reaction scheme is shown in Figure 3.4. Equimolar amounts of propargyl alcohol and 2-bromoisobutyric acid were dissolved in methylene chloride in an ice bath. A solution of dicyclohexylcarbodiimide in methylene chloride was added slowly to the solution, followed by the slow addition of a solution of 4-(dimethylamino)pyridine, also in methylene chloride. This solution was stirred in an ice bath for 1 h, followed by stirring overnight at room temperature. The precipitate was removed and propargyl-2-bromoisobutyrate was recovered by removing methylene chloride using a rotary evaporator and distilling the product under vacuum.

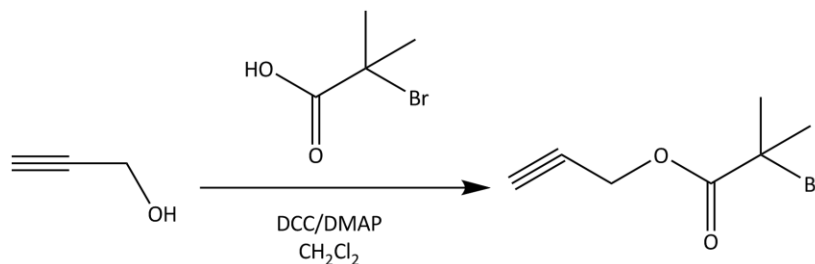


Figure 3.4: Reaction scheme for alkyne-functional bromide initiator for ATRP

**Atom Transfer Radical Polymerization (ATRP):** Using the alkyne-functional bromide initiator, 2-(diethylamino)ethyl methacrylate was polymerized using ATRP. The reaction scheme is shown in Figure 3.5. DEAEMA was dissolved in anhydrous THF with the initiator and the catalyst, CuBr, in a flame dried Schlenk flask. This solution was then degassed using three freeze-thaw cycles. The solution was heated to 60 °C and the degassed ligand, hexamethyltriethylenetetramine, was added to initiate the polymerization reaction. After 1 h, the polymerization was stopped by the addition of THF. The solution was passed through a basic alumina column to remove the copper catalyst and the solvent was removed using a rotary evaporator.

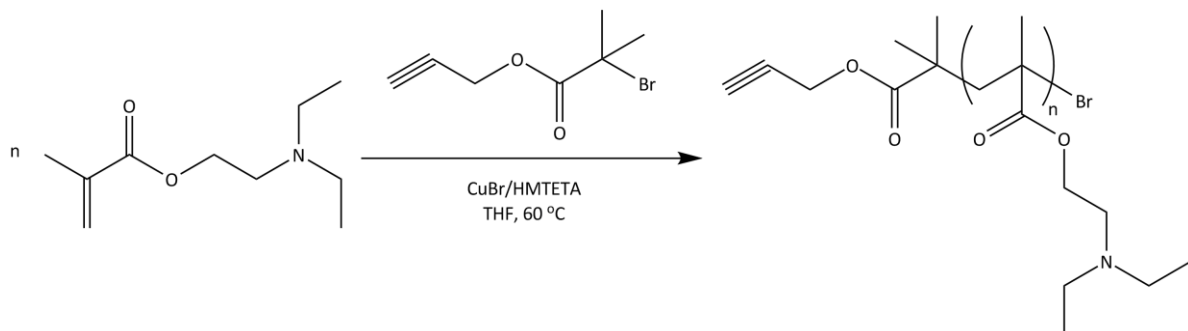


Figure 3.5: ATRP reaction scheme

### 3.2.3.3 Block Copolymer Synthesis

**Huisgen 1,3-dipolar cycloaddition:** The reaction scheme can be seen in Figure 3.6. The two blocks were dissolved in anhydrous DMF with the ligand, pentamethyldiethylenetriamine, in a flame dried Schlenk flask. The solution was degassed using three freeze-thaw cycles and transferred via canula to a degassed Schlenk flask containing catalyst, CuBr. The flask was stirred overnight at room temperature. The reaction was passed through a neutral alumina column to remove the catalyst. The majority of the solvent was removed using a rotary evaporator and the resulting solution was precipitated in diethyl ether. The block copolymer was dried in a vacuum oven.

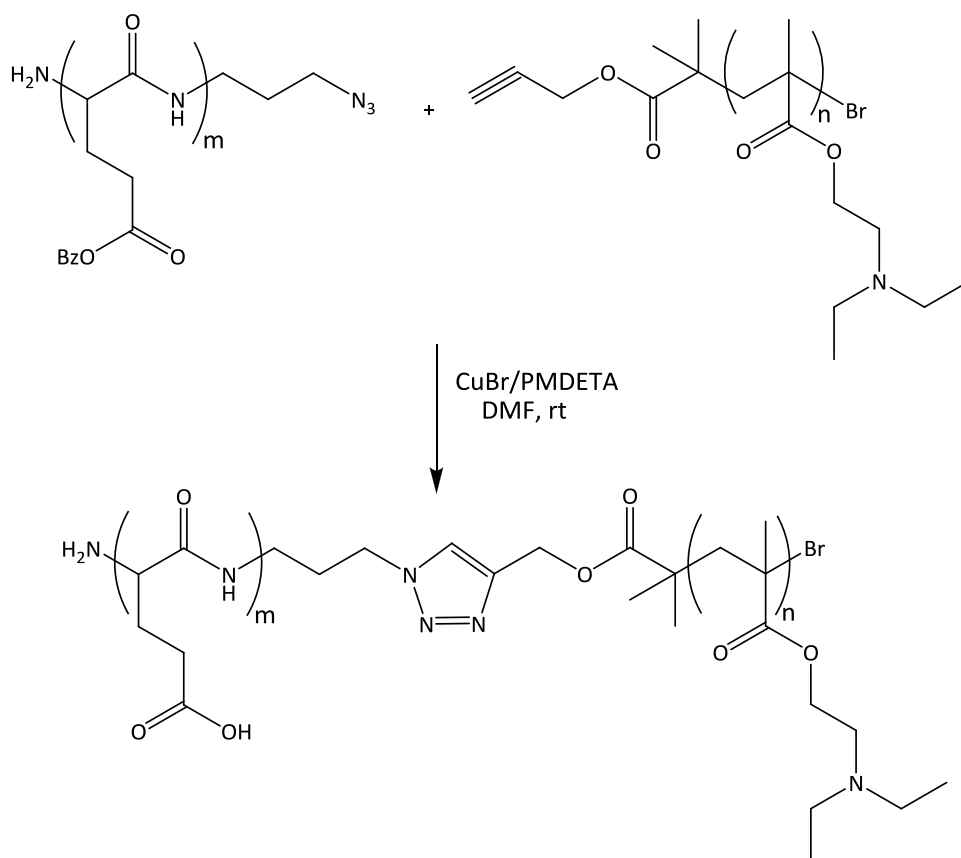


Figure 3.6: Copolymerization using the Huisgen 1,3-dipolar cycloaddition

**Deprotection:** The benzyl protecting group was removed using a strong base. The block copolymer was dissolved in THF and concentrated KOH was added to the solution. The mixture was sonicated until the solution became cloudy. The polymer was centrifuged out of solution at 5000 rpm and dried under vacuum.

### 3.3 Results and Discussion

To synthesize the block copolymer comprising polyglutamate and PDEAEMA segments with controlled molecular weight and low polydispersity, each block was prepared individually before linking the blocks together.

### 3.3.1 PBLG

In order to synthesize polyglutamate, the carboxylic acid group of the side chain of glutamic acid was protected using a benzyl group, which is the most common protecting group used for glutamic acid in NCA polymerization. Once glutamic acid was successfully protected, the N-carboxyanhydride was synthesized through phosgenation. The NCA was purified and the FTIR spectrum of the final product is shown in Figure 3.7. The resonances at 1790 and 1850  $\text{cm}^{-1}$  are indicative of the anhydride bond. The NMR spectrum is depicted in Figure 3.8.

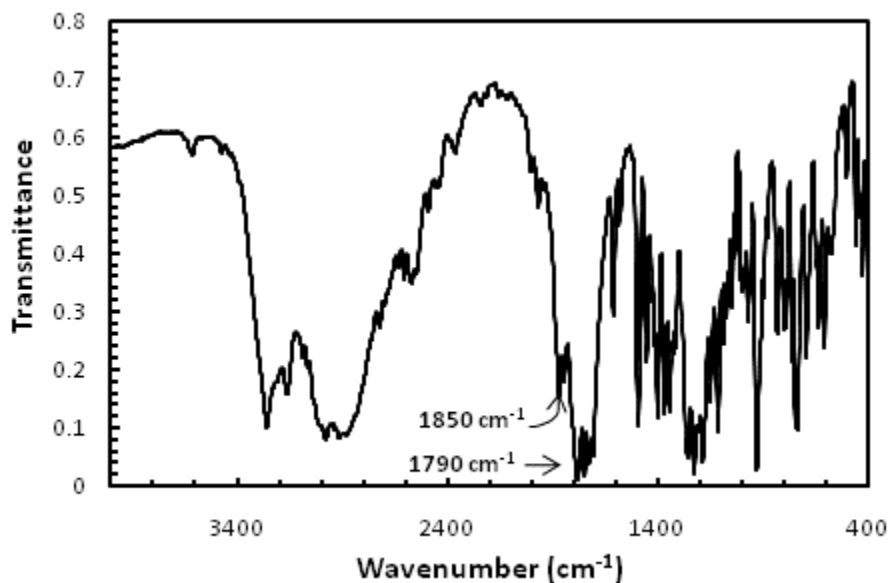


Figure 3.7: FTIR of  $\gamma$ -benzyl-glutamate-NCA

Before the NCA could be polymerized, an amine initiator was synthesized. 1-Azido-3-aminopropane contains an amine group for initiating NCA polymerization and an azide group for the block synthesis in subsequent steps. The initiator was successfully synthesized, which was confirmed by the NMR spectrum (Figure 3.9).

PBLG was synthesized using the azide-functional amine initiator at low temperature in order to minimize side reactions and under nitrogen gas to decrease moisture in the system. The molecular

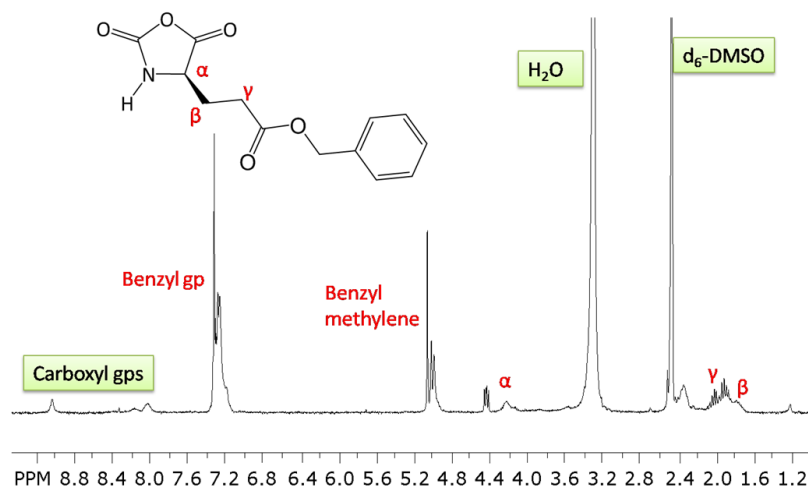


Figure 3.8:  $^1\text{H}$  NMR spectrum for  $\gamma$ -benzyl-glutamate-NCA

weight of the peptide was controlled by examining the MW of the samples throughout the polymerization using the gel permeation chromatography (GPC). The reaction was stopped once the desired absolute molecular weight was obtained. Based on GPC, the polydispersity of the sample was determined to be 1.10 and the molecular weight was approximately 5000 Da, indicating that there were around 20 repeat units. NMR spectroscopy was run and based on the NMR, there were approximately 16 repeat units. The NMR spectrum is shown in Figure 3.10. The FTIR is depicted in Figure 3.11 and the resonances at  $1660$  and  $1555\text{ cm}^{-1}$  are indicative of peptide bonds. The anhydride bond resonances seen in the FTIR of the NCA (Figure 3.7) are no longer present.

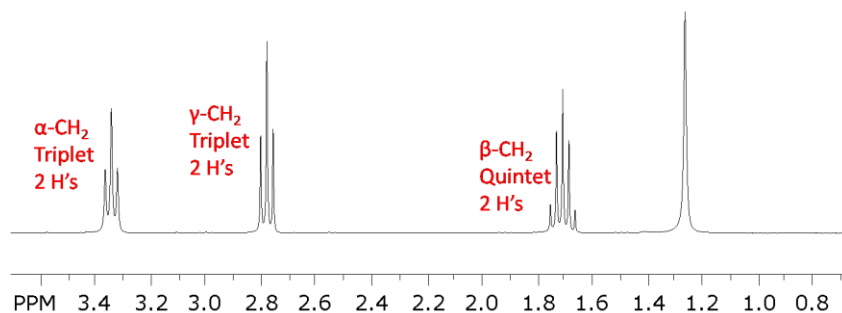


Figure 3.9:  $^1\text{H}$  NMR spectrum of 1-azido-3-aminopropane

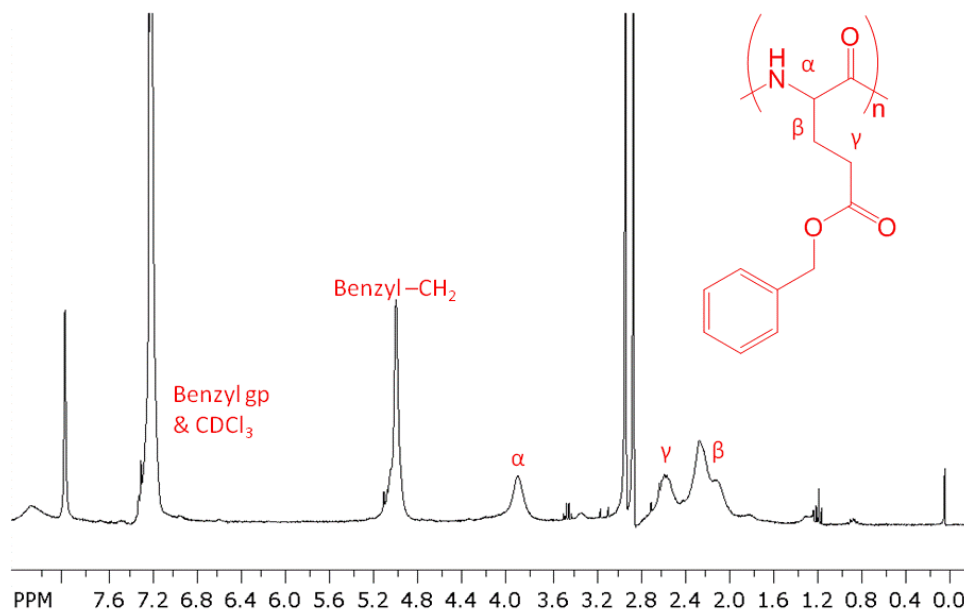


Figure 3.10: <sup>1</sup>H NMR spectrum of PBLG

### 3.3.2 PDEAEMA

Prior to the ATRP of DEAEMA, an alkyne-functional bromine initiator, propargyl-2-bromoisobutyrate was synthesized. The NMR spectrum obtained is shown in Figure 3.12.

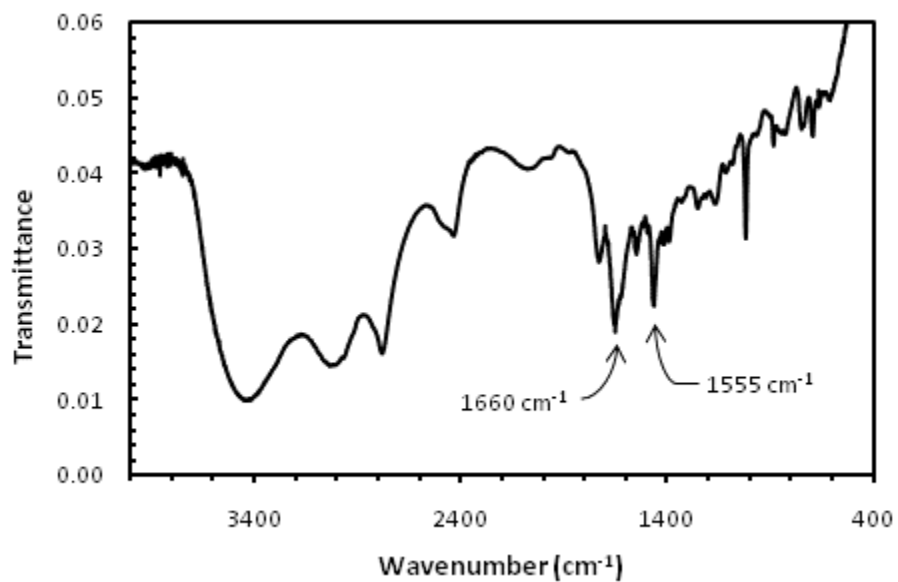


Figure 3.11: FTIR spectrum of PBLG

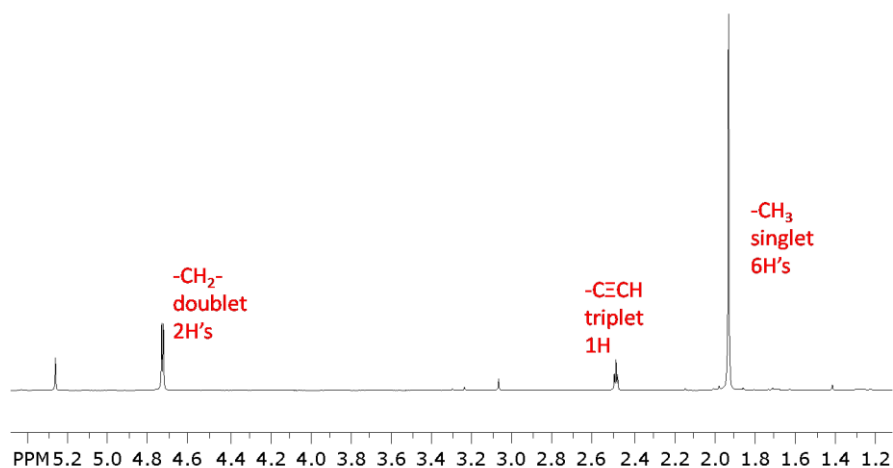


Figure 3.12:  $^1\text{H}$  NMR of Propargyl-2-bromoisobutyrate

The alkyne-functional bromide initiator was used for the polymerization of DEAEMA. The molecular weight and polydispersity measured using GPC were approximately 7400 Da and 1.06. Based on GPC, there are approximately 40 repeat units. Based on the NMR spectra (Figure 3.13), there are approximately 35 repeat units.

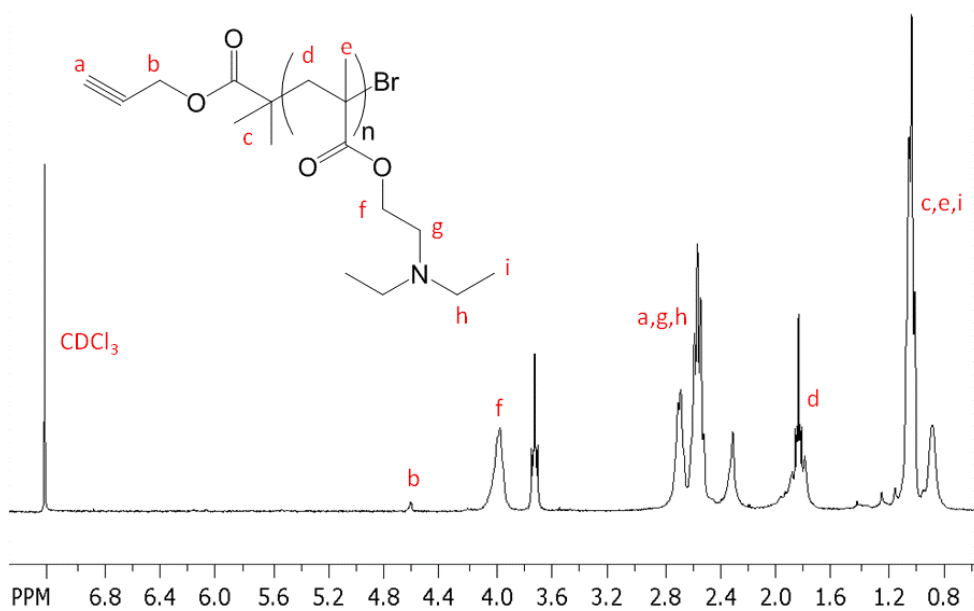


Figure 3.13:  $^1\text{H}$  NMR spectrum of PDEAEMA

### 3.3.3 Block Copolymer Synthesis

The block copolymer was synthesized using the azide-functionalized PBLG and the alkyne-functionalized PDEAEMA using the Huisgen 1,3-dipolar cycloaddition. Equimolar amounts of PBLG and PDEAEMA were used. The addition of the two blocks was confirmed by GPC – one peak was present with molecular weight and polydispersity index of 10 000 Da and 1.15. NMR spectroscopy provided additional confirmation, where the spectra contain chemical shifts from both PBLG and PDEAEMA (Figure 3.14).

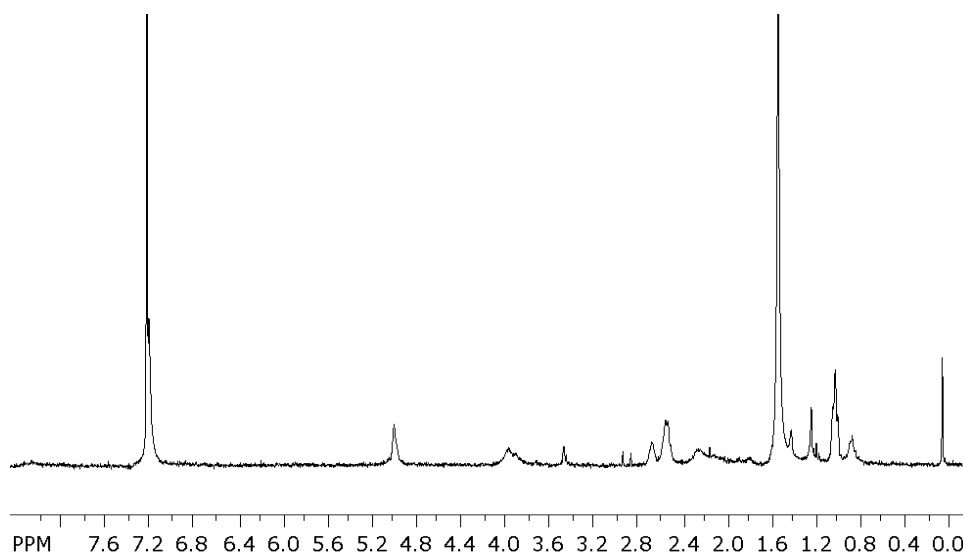


Figure 3.14:  $^1\text{H}$  NMR spectrum for the block copolymer

The benzyl groups were removed and this was confirmed using  $^1\text{H}$  NMR spectroscopy. The NMR study was performed in deuterated water in acidic, neutral and basic solutions. In self-assembled structures,  $^1\text{H}$  NMR spectroscopy only provides signals for the groups on the outer shell. Figure 3.15 depicts the NMR spectrum of the self-assembled structures. At low pH, the chemical shifts correspond to the groups of DEAEMA and at neutral and high pH, the chemical shifts correspond to the groups of glutamic acid. These results confirm that the block copolymers of PLG and PDEAEMA

were successfully synthesized. Furthermore, these results confirm the reversible micellization of the block copolymer at both high and low pH.

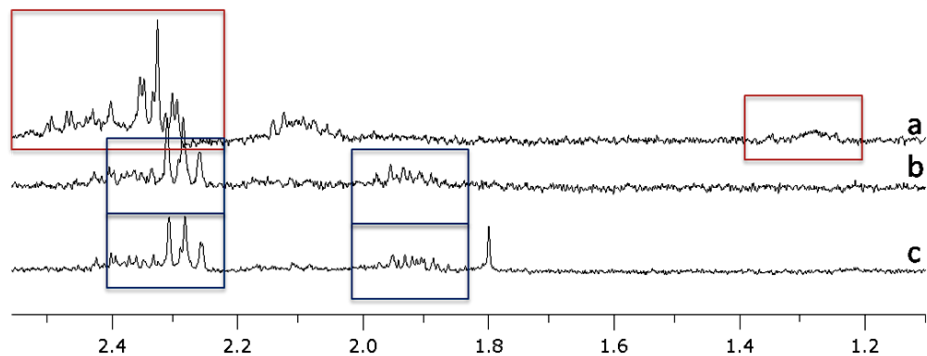


Figure 3.15: NMR study of deprotected block copolymers in a) acidic solution, b) neutral solution and c) basic solution

### 3.4 Conclusions

A block copolymer of polyglutamate and PDEAEMA was successfully synthesized with a molecular weight of approximately 10 000 Da and polydispersity of 1.15. The polymer contains around 18 repeat units of glutamate and 38 repeat units of DEAEMA. The NMR results confirmed that reversible micellization occurs at high and low pH.

## Chapter 4

### Characterization of Poly(L-glutamate) Arborescent Polymers

#### 4.1 Introduction

With improvements in peptide synthesis, which include solid-state peptide synthesis, recombinant DNA technology and  $\alpha$ -amino acid-N-carboxyanhydride (NCA) ring opening polymerization, a wide range of synthetic peptides can be produced [1]. Solid-state peptide synthesis allows for the synthesis of short, sequence specific peptides. Recombinant DNA technology utilizes gene expression with an artificial gene in a modified organism, and collecting the expressed peptide. NCA polymerization is a chemical synthesis method, generally used for the synthesis of homopolypeptides or peptides with a random sequence [1, 2]. The focus of this chapter is peptides synthesized using NCA polymerization due to its simplicity in the synthesis of homopolypeptides, in comparison to the other methods.

The majority of work on peptides synthesized through NCA polymerization is for surfactant-type peptides – mainly block copolymers or branched structures with both hydrophobic and hydrophilic moieties [1, 3]. Well-defined dendritic structures, which are common for synthetic polymers, such as polyamidoamine, are not as common in peptide systems and offer a range of unique structural properties. In comparison to branched polymer architectures, dendrimers are perfectly branched due to several successive synthesis steps. Due to the numerous end groups, dendrimers are highly functional and thus are attractive systems for many applications [4].

Highly branched poly(L-lysine) has been synthesized by Klok et al. [5]. The polymer, however, was not monodisperse or uniform in structure. As a result, any physical characterization of the polymer would be highly dependent on the sample tested [5]. Poly( $\gamma$ -benzyl-L-glutamate) arborescent polymers were synthesized by Gauthier and co-workers with a low polydispersity index (1.03 – 1.06) and a controlled molecular weight, ranging from 48 kDa to 1 060 kDa from generations 0 to 3,

respectively [6]. This research will discuss the physical properties and their self-assembly of poly(L-glutamate) arborescent polymers in aqueous solution.

## 4.2 Experimental

### 4.2.1 Polymer Synthesis

The arborescent polymers were prepared by Gregory Whitton and Timothy Hall, under the supervision of Professor Mario Gauthier in the Department of Chemistry at the University of Waterloo.  $\gamma$ -Benzyl-L-glutamate was polymerized using NCA ring opening polymerization with n-hexylamine as the initiator at 0 °C. For the various generations of arborescent polymer, linear PLG chains were grafted onto the pre-existing chains. The characteristics of the benzyl protected polymers are shown in Table 4.1. Prior to the characterization experiments, the benzyl group was removed using a 33 % HBr/acetic acid solution. [6].

Table 4.1: Characteristics of arborescent poly( $\gamma$ -benzyl-L-glutamate) [6]

Sample Number	M <sub>n</sub> Side Chains <sup>a</sup>	DRI	MALLS		Grafting Yield (%) <sup>b</sup>	Branching Functionality <sup>c</sup>
		M <sub>n</sub> <sup>app</sup>	M <sub>n</sub>	M <sub>w</sub> /M <sub>n</sub>		
G0	4300	17 400	48 000	1.04	38	9
G1	4000	39 300	133 000	1.06	63	21
G2	3900	83 100	486 000	1.03	46	90
G3	3900	134 000	1 060 000	1.03	32	147

<sup>a</sup> <sup>1</sup>H NMR (absolute values), <sup>b</sup> DRI detector, <sup>c</sup> MALLS detector (absolute values)

### 4.2.2 Instrumentation

#### 4.2.2.1 Potentiometric Titration

A Metrohm titration system with a pH meter and a conductivity meter was used for potentiometric titrations. Samples were prepared in a basic solution, with the addition of concentrated NaOH and titrated with a 50 mM HCl solution. The experiments were carried out in a 100 mL titration vessel at

25 °C under constant stirring. For dosing, a lag time of 15 sec was set to allow sufficient time for the solution to reach equilibrium.

#### 4.2.2.2 Laser Light Scattering

A Brookhaven BI-200SM goniometer and laser light scattering system was used for both the static and dynamic light scattering experiments. A BI-9000AT digital autocorrelator with a HeNe laser was used, with the detector set to 636 nm. To analyze the correlation functions for the dynamic light scattering experiments, the GENDIST software was used to find the inverse Laplace transform of REPES. The density was set to 12 and the probability to reject was 0.5. The samples were prepared in borosilicate glass test tubes in 25 mM buffer. Milli-Q grade water was used. In addition, all buffers and water used were passed through 0.1  $\mu\text{m}$  filters to remove dust. The experiments were carried out at 25 °C.

### 4.3 Results and Discussion

In order to obtain a thorough understanding of the PLG dendritic polymers, the pH-responsive characteristics were studied using potentiometric titration along with the self-assembly of the polymers studied using dynamic and static light scattering.

#### 4.3.1 Potentiometric Titration

The carboxylic acid groups of L-glutamic acid plays an important role in the physical properties of the arborescent polymers, particularly the solution properties. At solution pHs above the  $\text{pK}_a$  the carboxylic acid groups are deprotonated, increasing the solubility of the polymers, and at solution pHs below the  $\text{pK}_a$ , the polymers become hydrophobic and are insoluble in water. The degree of neutralization/deprotonation,  $\alpha$ , for the carboxylic acid group is defined by Equation (4.1). In order to obtain a better understanding of the solubility and the differences between the different generations, a

potentiometric titration was conducted on a 0.01 wt% polymer solution in a basic solution by titrating with a 50 mM HCl solution.

$$\alpha = \frac{[COO^-]}{[COOH]_{total}} \quad (4.1)$$

The titration curve, shown in Figure 4.1, can be divided into three regions. The first region shows a decrease in the conductivity and pH, corresponding to the neutralization of excess NaOH with HCl. The second region is marked by a change in conductivity and the inflection of the pH curve. This is the buffering region of the polymer, where the solution pH stays relatively constant, and is typical behaviour for weak polyacids due to the dissociation equilibrium. The deprotonation/neutralization equilibrium and the constant are shown in Equations (4.2) and (4.3). In the third region, the polymer has been completely deprotonated and the addition of excess HCl contributes to the decrease in pH and the increase in solution conductivity.

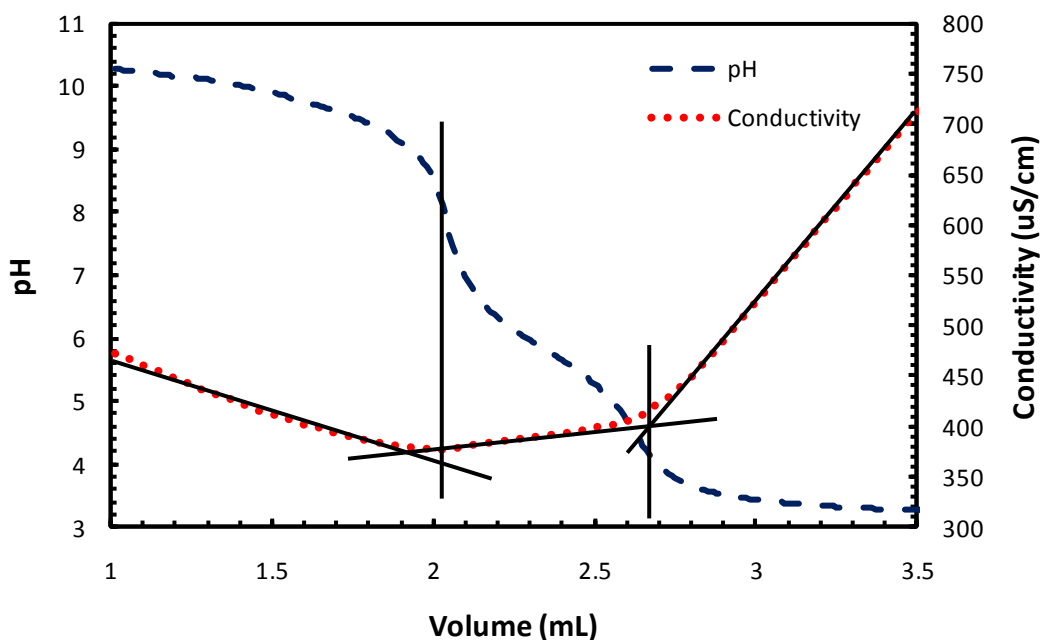


Figure 4.1: Potentiometric titration curve for the G0 arborescent polymers



$$K_a = \frac{[COO^-][H^+]}{[COOH]} \quad (4.3)$$

In order to compare the different generations of poly(L-glutamate) arborescent polymers, the charge density and pH data were extracted from the potentiometric titration data as shown in Figure 4.2. In general, the pH of the buffering region increases with the generation number. Linear PLG shows the lowest pH profile. The G0 and G1 dendritic polymers show similar profiles with a slightly higher pH compared to the linear chain. The G2 and G3 dendritic polymers also show a similar profile at a higher pH, however, the G2 dendritic polymer shows a higher pH buffering region in comparison to the G3.

In order to obtain a better understanding of the pH behaviour, the charge density was compared to the apparent  $pK_a$ , using the Henderson-Hasselbalch equation, derived from Equations (4.1) and (4.3), and shown in Equation (4.4). The apparent  $pK_a$  is related to both the solution pH and charge density,

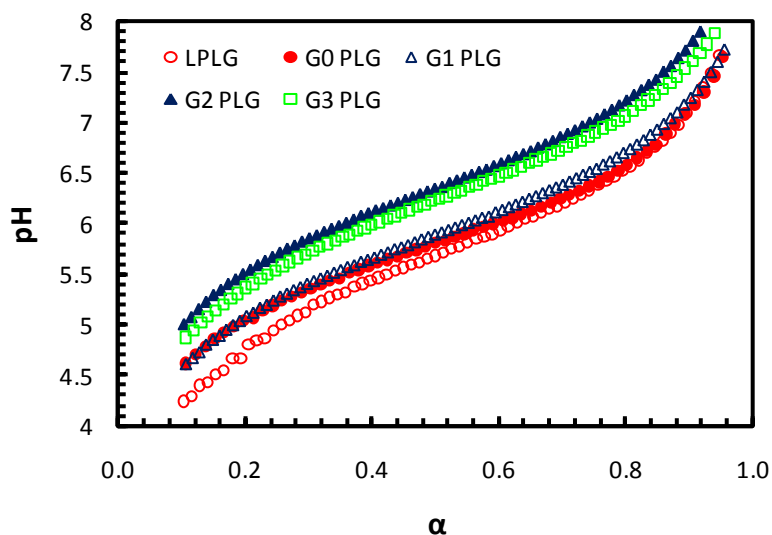


Figure 4.2: Comparison of pH curves for the generations of PLG

thus giving better insight on the differences between the various generations of dendritic polymers as shown in Figure 4.3.

$$pK_a = pH + \log \frac{1 - \alpha}{\alpha} \quad (4.4)$$

In general, for all the generations of arborescent polymer, there is an increase in  $pK_a$  with increasing  $\alpha$ . This increase is due to the higher electrostatic forces and the difficulty in abstracting a proton from the polymer chain. In comparing the  $pK_a$  of the various generations of dendritic polymer, the  $pK_a$  increases with generation, except for the G2 polymer, which has a higher  $pK_a$  than the G3 dendritic polymer. This increase with generation is likely due to the greater number of carboxylic acid groups and the size and complexity of the arborescent polymers at higher generations, as shown in Table 4.1.

Another method to analyze the potentiometric titration data is to examine the Gibbs free energy required to abstract a proton from the polymer. The  $pK_a$  can be expressed as a sum of the intrinsic dissociation constant,  $pK_o$ , and the free energy for abstracting a proton,  $\Delta G_{el}$ , which accounts for the

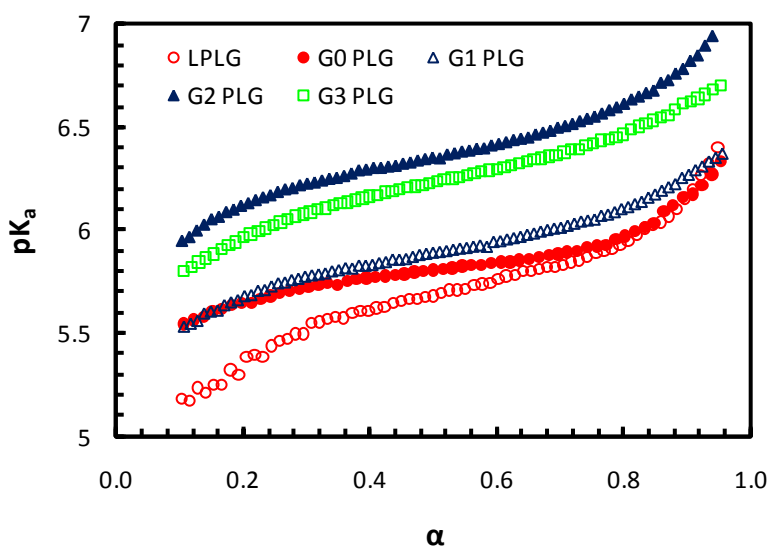


Figure 4.3: Comparison of  $pK_a$  curves for the generations of PLG dendritic polymers

electrostatic interactions, shown in Equation (4.5).  $pK_o$  was found by extrapolating the  $pK_a$  curve to  $\alpha = 0$ , R is the gas constant and T is the absolute temperature.  $\Delta G_{el}$  can be found by integrating Equation (4.5) to obtain Equation (4.6) [7].

$$pK_a = pK_o + 0.4343 \frac{dG_{el}}{RTd\alpha} \quad (4.5)$$

$$\Delta G_{el} = 2.30RT \int_0^1 [pK_{(\alpha)} - pK_o] d\alpha \quad (4.6)$$

Figure 4.4 and Table 4.2 show the Gibbs free energy required for each of the arborescent polymer generations. From G0 to G3, the amount of energy required increases from 2.16 to 3.22 kJ/mol. The difference of 1 kJ/mol appears to be the result of enhanced electrostatic interactions at higher generations. The linear PLG, however, has a higher Gibbs free energy than the dendritic polymers. This is most likely due to aggregation, resulting in greater electrostatic repulsion and more energy necessary to abstract a proton. This will be discussed in the critical aggregation in Section 4.3.2.

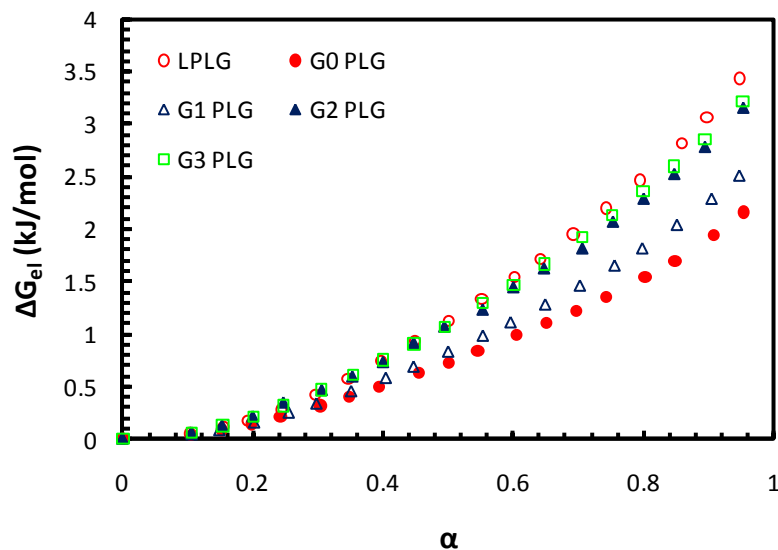


Figure 4.4: Comparison of Gibbs free energy required to abstract a proton

Table 4.2: Summary of Gibbs free energy for each arborescent polymer generation

Generation	$\Delta G_{el}$ (kJ/mol)
Linear	3.44
G0	2.16
G1	2.51
G2	3.16
G3	3.22

### 4.3.2 Critical aggregation concentration of the PLG arborescent polymers

Linear PLG was prepared using NCA polymerization with n-hexylamine used as the initiator. As a result, the end of each linear chain contained a hydrophobic hexyl group ( $C_6$ ). The dendritic structure was synthesized by grafting linear chains onto the earlier generations and as a result, the end of every PLG graft contains a hydrophobic hexyl group. Figure 4.5 shows the structure of the G0 PLG polymer. These hydrophobic groups play a role in the self-assembly of the arborescent polymers.

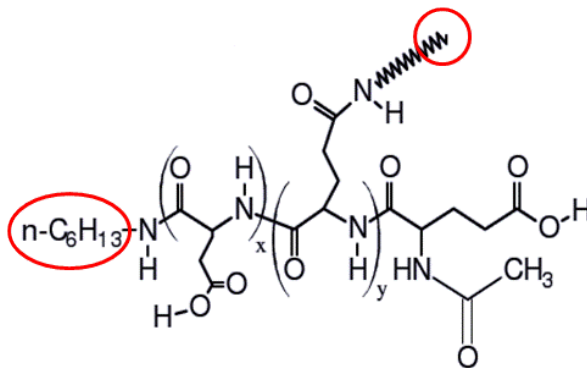


Figure 4.5: Structure of the G0 arborescent polymer with linear PLG grafts – the hexyl groups highlighted (x and y groups are randomly distributed along the chain)

At pH 10, the carboxylic acid groups of PLG are fully deprotonated and thus are hydrophilic. As a result of the hydrophilic PLG chains and the hydrophobic hexyl groups, the chains will self-assemble

in order to minimize free energy. Additional parameters that will affect the self-assembly include the amount of PLG to hexyl groups, the arborescent polymer flexibility at higher generations, etc.

The critical aggregation concentration (cac) was found using laser light scattering at a scattering angle of  $90^\circ$ . In a light scattering experiment, the scattering vector,  $\vec{q}$ , is the difference between the incident and scattered vectors, shown in Equation (4.7). Assuming that the light intensity does not change due to absorption by the sample, then Equation (4.8) applies [8].

$$\vec{q} = \vec{k}_i - \vec{k}_s \quad (4.7)$$

$$q = \frac{4\pi n}{\lambda} \sin \frac{\theta}{2} \quad (4.8)$$

At concentrations below the cac, there is no observable change in the scattering intensity, due to localization of the polymer at the air-water interface. However, at concentrations above the cac, the polymer self-assembles in order to minimize its free energy. These larger structures result in an increase in the light scattering intensity.

The plot for the G0 PLG is shown in Figure 4.6 and the cac results are summarized in Table 4.3. From the linear to the G1 dendritic polymer, the cac decreases from 0.60 g/L to 0.42 g/L. This decrease in cac is due to the increase in the hydrophobic and hydrophilic moieties. However, from the G1 to the G3 arborescent polymers, the cac increases. With increasing generation, the dendritic structure is increasing in size, resulting in the hydrophobic and hydrophilic groups dispersed all over the polymer and thus more difficulty in manoeuvring the hydrophobic moieties together. This results in the increase in cac with increasing generation.

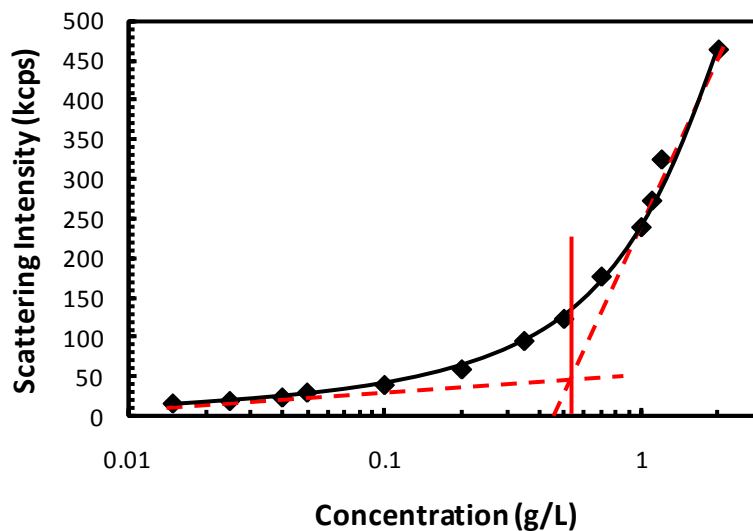


Figure 4.6: Scattering intensity graph for G0 PLG at pH 10

Relating back to the potentiometric titration results in Section 4.3.1, the cac for the linear PLG was found to be 0.60 g/L, whereas the concentration used in the titration was 0.10 g/L, which is significantly lower. From examining the light scattering intensity graphs compared to concentration (Figure 4.6), the micellization occurs over a range of concentrations and the potentiometric titration data shows that even on the lower end of the range, micellization is still apparent.

Table 4.3: Summary of CAC results by generation

Generation	CAC (g/L)
Linear	0.60
G0	0.52
G1	0.42
G2	0.48
G3	0.57

### 4.3.3 Self-Assembled Structures

In order to obtain a better understanding of the self-assembled structures, multi-angle dynamic and static light scattering experiments were conducted. The size and morphology of the assemblies were examined at pH 10 so that the carboxylic acid groups were fully deprotonated.

DLS is a time resolved experiment, where the time dependent changes in intensity are measured. For particle size, the Brownian motion of the particles can be measured – the change in the spectrum of scattered light is given by the frequency shift,  $\Delta\omega$ . The Fourier transform of the spectrum, the autocorrelation function, is the intensity at time  $t$ ,  $I(t)$  multiplied by the intensity at a time delay,  $\tau$ ,  $I(t + \tau)$ . The inverse of the time decay rate,  $\Gamma = 1/\tau$ , is related to diffusion coefficient, given in Equation (4.9). The distribution functions are multiple angles for G0 are shown in Figure 4.7.

$$\Gamma = Dq^2 \quad (4.9)$$

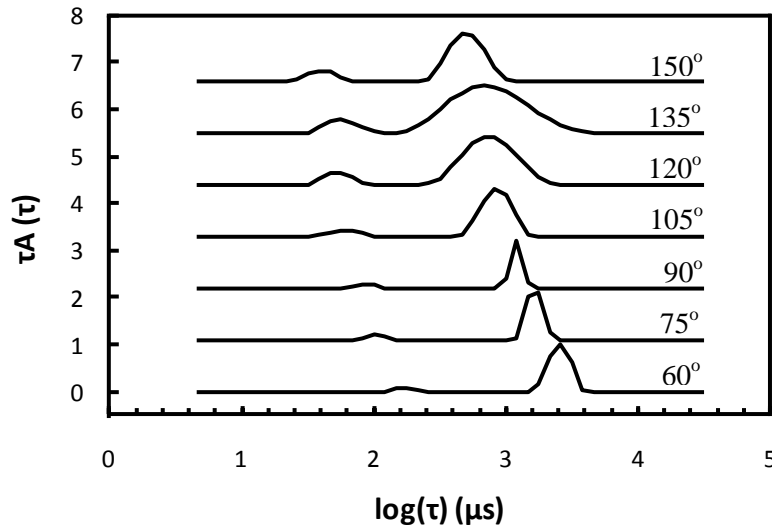


Figure 4.7: Distribution functions for G0 PLG at pH 10

With the diffusion coefficient, the particle size was determined using the Stokes-Einstein expression, shown in Equation (4.10), where  $R_h$  is the hydrodynamic radius,  $k$  is Boltzmann's constant,  $T$  is the temperature,  $\eta$  is the viscosity and  $D_0$  is the diffusion coefficient. For the multi-

angle experiments, the diffusion coefficient was averaged over various angles. Figure 4.8 shows the  $q^2$  dependence of the diffusion coefficient. Similarly to the DLS results at one angle, the particle size was found using the Stokes-Einstein expression, shown in Equation (4.10).

$$R_h = \frac{kT}{6\pi\eta D_o} \quad (4.10)$$

From examining the distribution functions (G0 PLG shown in Figure 4.7), two peaks can be observed, indicating the presence of two distinct aggregates. The diffusion coefficient and hydrodynamic radius were determined for both diffusive species as shown in Figure 4.8. The smaller size corresponds to the unimer and the larger size comprises of the aggregate formed by the polymers. The results of the DLS experiments are summarized in Table 4.4.

In general, the radii of the arborescent polymers increase with increasing generation. A graphical comparison of the aggregates is shown in Figure 4.9. For the polymer aggregates, the hydrodynamic radius increases slightly, likely due to the larger structures, but the difference is subtle.

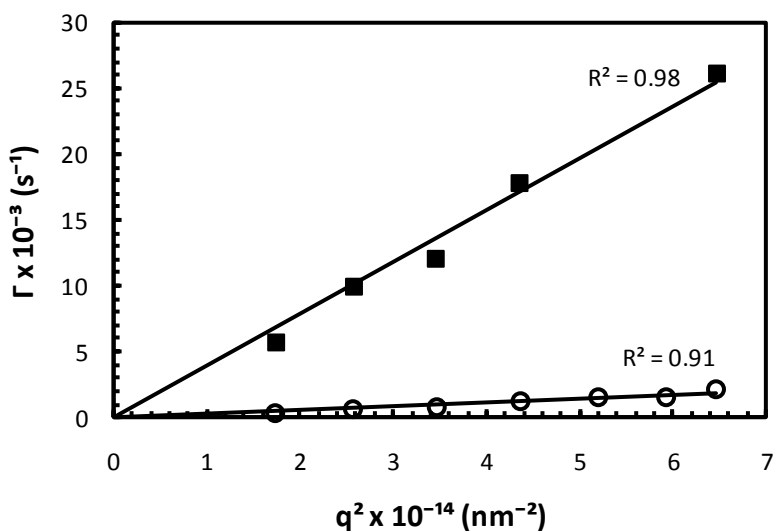


Figure 4.8: The  $q^2$  dependence of the diffusion coefficient for G0 PLG at pH 10

Table 4.4: Summary of size and morphology results by generation at 2 g/L

Generation	$R_{h,1}$ (nm)	$R_{h,2}$ (nm)	$R_g$ (nm)	$R_g/R_h$	$N_{agg}$
Linear	-	111.1	89.5	0.81	41.7
G0	6.22	87.1	77.0	0.88	19.5
G1	8.46	109.2	73.1	0.67	4.8
G2	12.5	113.3	31.2	0.28	1.7
G3	15.1	115.7	46.5	0.40	2.1

Using static light scattering, the aggregation number, radius of gyration and 2<sup>nd</sup> virial coefficient were determined. The scattered light intensity is averaged over a predetermined observation time at a range of scattering angles, as given by Equation (4.11). The SLS data were analyzed using the Debye Equation (Equation (4.12)), where  $M_w$  is the apparent molecular weight,  $C$  is the concentration,  $A_2$  is the 2<sup>nd</sup> virial coefficient,  $q$  is the intensity (given in Equation (4.8)) and  $\Delta R_\theta$  is the Rayleigh ratio, using toluene as a standard. The instrument optical parameter,  $K$ , is shown in Equation (4.13), where  $\lambda$  is the wavelength of the laser,  $N_A$  is Avogadro's number,  $n_o$  is the refractive index of the solvent, and  $dn/dc$  is the differential refractive index increment.

$$I(\theta) = \lim_{T \rightarrow \infty} \frac{1}{T} \int_0^T I(\theta, t) dt \quad (4.11)$$

$$\frac{KC}{\Delta R_\theta} = \frac{1}{M_w} \left( 1 + \frac{1}{3} R_g^2 q^2 \right) + 2A_2 C \quad (4.12)$$

$$K = \frac{2\pi^2}{\lambda^4 N_A} \left( n_o \frac{dn}{dc} \right)^2 \quad (4.13)$$

The radii of gyration and the  $R_g / R_h$  ratios for the different arborescent polymers at pH 10 are summarized in Table 4.4 and Figure 4.9. In general, the  $R_g$  are smaller at higher generations, though this reduction is most drastic for the G2 system. Furthermore, the  $R_g$  of the G3 polymer is slightly higher than that of G2. As a result, the  $R_g/R_h$  ratio decreases significantly, with a slight increase at G3.

The rationale for this behaviour is that the mechanism for self-assembly for G0 and G1 is different than for G2 and G3, most likely due to the larger size of G2 and G3.

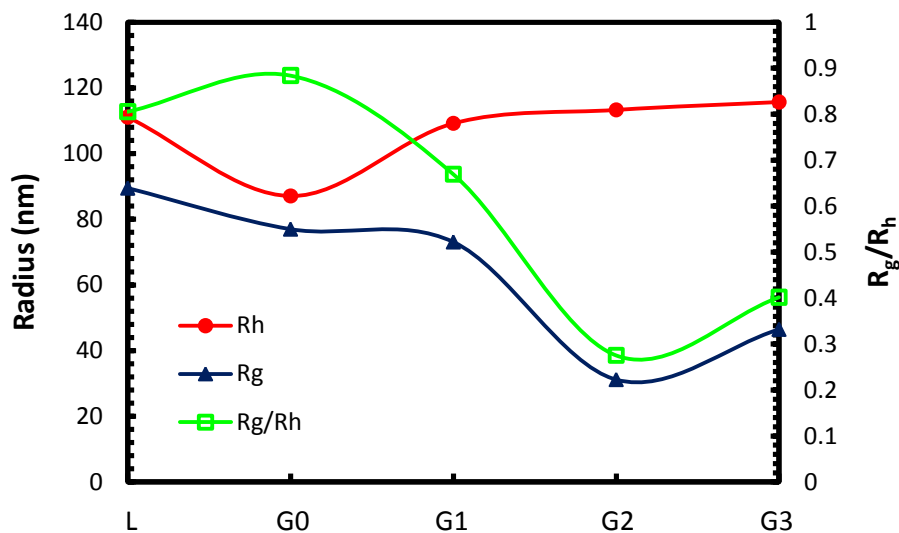


Figure 4.9: Comparison of size and morphology by dendritic polymer generation

In order to obtain a more comprehensive comparison of the effect of the generation of arborescent polymers, the distribution functions at 90° were obtained and they are summarised in Figure 4.10. The linear PLG forms only aggregated species. In the distribution functions for G0 and G1, both the aggregated structure and the unimer are observed. In comparing these two, a greater number of the G1 PLG is present in unimeric form compared to the G0 PLG. The G2 and G3 PLG arborescent polymers show a different trend. A greater number of the polymers are present in the unimeric form, with a small amount of the aggregated polymer. Furthermore, in comparing the two, it appears as though there are more aggregated G3 polymers than G2, indicating that the G2 unimer is likely more stable than the G3 dendritic polymer and thus G3 PLG prefers to aggregate in solution.

The SLS data were analyzed and plotted in the form of Zimm plots, where  $KC/\Delta R_\theta$  was plotted against  $\sin^2(\theta/2) + kC$ , where  $k$  is an adjustable constant, as shown in Figure 4.11 for LPLG. The data

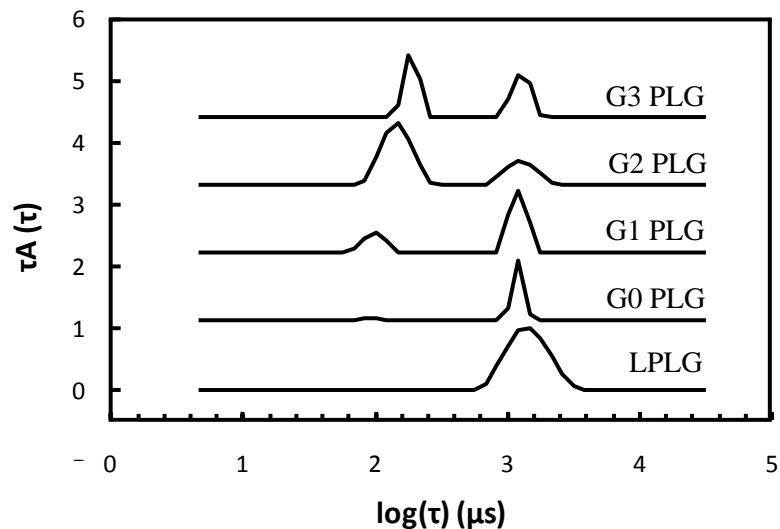


Figure 4.10: Distribution functions at 90° by generation

was extrapolated to zero angle, which was used to find the apparent molecular weight and aggregation number, where the results are summarized in Table 4.4. The aggregation number decreases as the generation of arborescent polymer increases, which is likely to be due to a change in the morphology of the micelle. The micelles formed for the G0 and G1 aggregates require a greater number of polymer chains whereas the G2 and G3 aggregates require fewer.

The aggregate size over a range of concentrations was tested for each generation of arborescent polymer, ranging from 1 g/L to 3 g/L. However, no discernable change in the aggregate size was observed over this range. Based on this result, it was concluded that the aggregates assemble via a closed-association mechanism.

Based on the light scattering data, the self-assembly mechanism for each of the generations of dendritic polymer is summarized in Figure 4.12. The morphology of the aggregates changes depending on the generation, though all of the aggregated systems are spherical structures, as the  $R_g / R_h$  ratios were less than one. Linear, G0 and G1 have a higher ratio, ranging from 0.67 to 0.88, indicating micelles with more uniform densities. G2 and G3 have geometric ratios ranging from 0.28

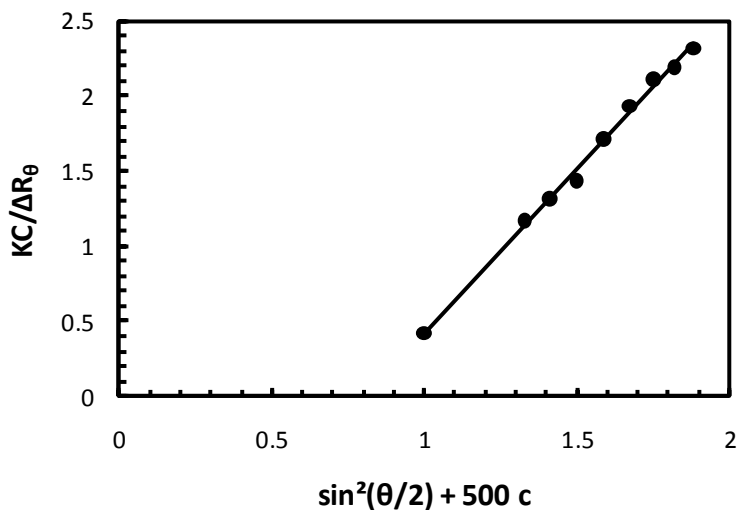


Figure 4.11: SLS data for LPLG at 2.0 g/L

to 0.40, indicating core-shell structures with a highly dense core. Examining the stability of the aggregated structures against the unimer, at lower generations, aggregation is more likely to occur for the linear, G0 and G1 PLG as the unimers are more flexible. In the case of higher generations, the branched structure makes self-assembly into aggregates less favourable. Moreover, compact structures are less favourable due to electrostatic repulsion within, and between, the anionic poly(L-glutamate) chains.

#### 4.4 Conclusion

The physical properties of poly(L-glutamate) arborescent polymers were investigated. The acid-base characteristics were explored using potentiometric titration. The  $pK_a$  of the polymers ranged from 5.7 to 6.4, with a general increase in  $pK_a$  with arborescent polymer generation. The Gibbs free energy required to abstract a proton increased from 2.16 kJ/mol to 3.21 kJ/mol for the G0 to G3 PLG due to greater electrostatic forces. The linear PLG had a higher Gibbs free energy change of 3.43 kJ/mol as a result of micellization.

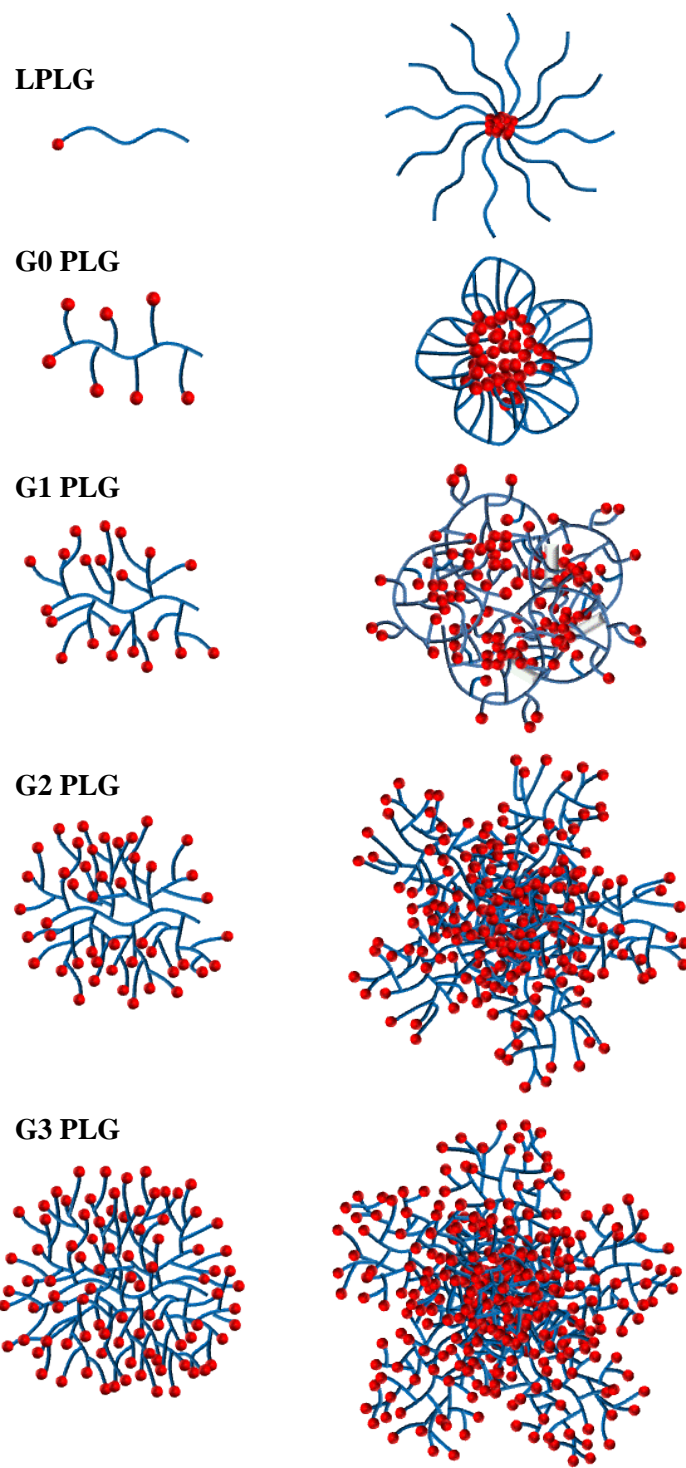


Figure 4.12: Schematics illustrating the self-assembly mechanism for each generation of PLG, with the unimer in the left column and the proposed aggregated structure in the right column

Due to the dendritic structure containing a hydrophobic hexyl group at the end of every hydrophilic negatively charged poly(L-glutamate) chain, the arborescent polymers self-assemble in aqueous solution. The critical aggregation concentration was found to range from 0.60 g/L for the linear chains, decreasing to 0.42 g/L for the G1 and increasing again to 0.57 g/L for the G3 polymer. This is influenced by the increase in hydrophobic moieties at higher generations, decreasing the  $c_{ac}$ , counteracted by the size of the arborescent polymers, increasing the  $c_{ac}$ .

With the exception of linear PLG, the dendritic aggregates exhibited a bimodal size distribution with both the unimers and the aggregated structures at equilibrium. For increasing arborescent polymer generations, the unimer was more favourable than the aggregate as polymer flexibility is lost at higher generations. The hydrodynamic radius of the aggregated structures was similar for all generations, ranging from 90 – 110 nm. The radius of gyration dropped from 89.5 nm to 31.2 nm for increasing dendritic polymer generations and the  $R_g / R_h$  ratio dropped from approximately 0.88 to 0.28, indicating that the aggregates were forming more core dense structures at higher generations.

## Chapter 5

# Self-Assembly Behaviour and Applications of Poly(L-glutamate)-b-poly(2-(diethylamino)ethyl methacrylate)

### 5.1 Introduction

Many studies have been done on the self-assembly of amphiphilic block copolymers in aqueous solution. Depending on the hydrophobicity and hydrophilicity of the blocks, the polymer can self-assemble into various types of nanostructures. The components of the two blocks can vary greatly, depending on the monomer that can have specific functional groups as well as the chain length. Furthermore, depending on the polymeric blocks, the structure can be affected by the solution properties, such as the pH and ionic strength, which are very important for various applications [1].

Similarly to surfactants, amphiphilic block copolymers are surface active due to their hydrophobic and hydrophilic moieties and above a certain concentration, they will self-assemble into ordered structures, with the hydrophobic part in the core of the structure, and the hydrophilic, soluble block at the corona [2]. The different structures that can form are micelles, cylindrical micelles, vesicles, rods as well as irregular aggregates. Examples of these self-assembled structures are shown in Figure 5.1 [3].

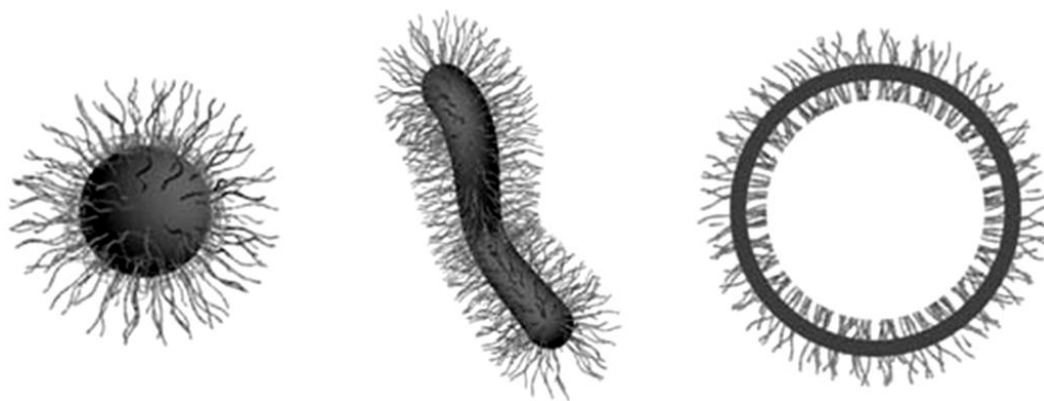


Figure 5.1: Examples of self-assembled structures [3]

In structures that contain pH-sensitive groups, such as carboxylic acids and amines, the solution pH plays a major role in the self-assembly. In the case of block copolymers, the solubility of the pH-responsive block depends strongly on the solution pH. This affects the size and morphology of the self-assembled structure [4].

After the physical properties of a polymeric system are understood, appropriate tests for applications are necessary. Gene therapy consists of the delivery of plasmid DNA to the organs or tissues affected by a genetic disease. Viruses, which are natural gene delivery vehicles, were initially pursued [5 – 6], however, problems associated with viral vectors, such as immunogenicity and pathogenicity, lead to increased use of non-viral vectors such as lipids, polymers and peptides for gene therapy [7].

Non-viral vectors typically bind to DNA through electrostatic interactions, as DNA is negatively charged. Cationic lipids, polymers and peptides are generally used for binding and condensing DNA and the resulting polyplex is delivered to the cells. However, many problems exist at this stage, such as polyplex stability and entry into the cells. Cellular entry is one of the major barriers – after a polyplex enters a cell through endocytosis, the polyplex must escape from the endosome and travel to the nucleus. Furthermore, safety concerns are an important consideration and the polyplex needs to be non-toxic and not illicit an immune response [7 – 9]. As it is difficult to address all of these issues, this research will attempt to develop a biodegradable and non-toxic hybrid peptide-polymeric system and study its potential applications and in vitro transfection.

## **5.2 Experimental**

### **5.2.1 Materials**

The synthesis of PLG-b-PDEAEMA was discussed in Chapter 3. ATRP was used for the preparation of PDEAEMA and  $\alpha$ -amino acid-N-carboxyanhydride ring opening polymerization was used for the

preparation of PLG. The two blocks were linked using the Click reaction, Huisgen-1,3-dipolar cycloaddition.

The samples were dissolved in an aqueous solution and stored in the refrigerator. Solutions for potentiometric titration were prepared at high pH, with the addition of concentrated NaOH. Samples prepared for laser light scattering measurements were prepared in a 25 mM buffered solution.

Buffers at low pH were prepared using sodium citrate and citric acid. Buffers at physiological pH were prepared using a HEPES buffer, and buffers at high pH were prepared using sodium carbonate and sodium bicarbonate. The buffers were filtered through a 0.1  $\mu\text{m}$  filter to remove dust and microorganisms and stored in the fridge.

Ethidium bromide solution (EtBr) was supplied by Biorad. HEPES and tris acetate EDTA (TAE) were purchased from Sigma and agarose was purchased from Promega (Madison, WI).

The plasmid DNA (pIRES-EGFP-EV71) used in this experiment expresses enhanced green fluorescent protein (eGFP). The plasmid DNA was prepared by Sarah Ho, working under Professor H. P. Too at the University of Singapore.

## **5.2.2 Instrumentation**

### **5.2.2.1 Potentiometric Titration**

See experimental section of Chapter 4.

### **5.2.2.2 Laser Light Scattering**

See experimental section of Chapter 4.

### **5.2.2.3 Zeta Potential Measurements**

A Brookhaven 90 Plus particle size analyzer, with an attached ZetaPALS phase analyzing light scattering system, was used to measure zeta potential. A 35 mW diode laser was used at a  $90^\circ$

scattering angle. Palladium electrodes with acrylic supports were used for the measurements. The samples were prepared in polystyrene cuvettes and the measurements were carried out at 25 °C.

#### 5.2.2.4 Agarose Gel Electrophoresis

An agarose gel was used to examine the electrophoretic mobility of the polymer/DNA polyplexes. The gel was prepared using 1.0 % agarose and 5 µg EtBr in TAE buffered solution. The polyplexes were prepared in a 25 mM HEPES buffer at pH 7.5 and incubated for 15 min. The gel was run at 120 V for 30 min and photographed on an ultraviolet transilluminator at 254 nm.

#### 5.2.3 Cell Culture

Neuroblastoma cells (N2a) obtained from the American Type Culture Collection (CCL-131, ATCC, USA) were used. The cells were incubated in Dulbecco's modification of Eagle's medium (DMEM) with 10 % fetal bovine serum (FBS, Hyclone, Logan, UT) and 1 % penicillin and streptomycin under a humidified atmosphere with 5 % carbon dioxide (CO<sub>2</sub>) at 37 °C.

For cell transfection experiments, N2a cells were seeded in a 12-well plate at a density of 40 000 cells per well and incubated for 24 hr at 37 °C under a humidified atmosphere with 5 % CO<sub>2</sub>. All materials used, except for the polymer, were passed through a 0.2 µm filter to remove dust and microorganisms. The polyplexes were prepared in a 25 mM HEPES buffered solution at different N/P ratios – the ratio between the number of amine groups of the polymer to the number of phosphate groups on the plasmid DNA. The polyplexes were vortexed and incubated at room temperature for 15 min, followed by 10x dilution with serum-free media and incubated for an additional 15 min. One ml of the diluted polyplex solution was added to the wells and incubated at 37 °C for 1 hr. The wells were then centrifuged at 500 g for 5 min. The media was removed, rinsed with phosphate buffered saline (PBS), replaced with DMEM with 10 % FBS and incubated for 24 hr at 37 °C. To view the transfection efficiency, the media was removed, rinsed with PBS three times and viewed with PBS

under a fluorescence microscope. The efficiency was compared to a negative control, a solution containing only plasmid DNA and a positive control, a solution of the PEI/DNA polyplex at N/P 20.

## 5.3 Results and Discussion

### 5.3.1 Potentiometric Titration of PLG-b-PDEAEMA

Due to the carboxylic acid and amine groups on the glutamate and DEAEMA respectively, the block copolymer is responsive to changes in solution pH. The charge density of each individual segment is an important aspect for the self-assembly, which depends on the degree of neutralization and protonation/deprotonation.

The two groups that will affect the charge of the polymer are the carboxylic acid group of the side chain of PLG and the tertiary amine group of the PDEAEMA. The degree of neutralization/deprotonation of the carboxylic acid group is given in Equation (5.1) and the degree of neutralization/protonation of the amine is given in Equation (5.2).

$$\alpha_1 = \frac{[COO^-]}{[COOH]_{total}} \quad (5.1)$$

$$\alpha_2 = \frac{[N(R)_3^+]}{[N(R)_3]_{total}} \quad (5.2)$$

The degree of neutralization and protonation/deprotonation of the polymer chain was found using potentiometric titration of a 0.01 wt% polymer solution with a 50 mM solution of HCl. The graph can be seen in Figure 5.2. The curve can be separated into 4 regions, separated by three points, which are indicated by changes in the conductivity of the solution. At high pH, before the first end point, A, is the neutralization of excess base by HCl, which accounts for the drop in conductivity.

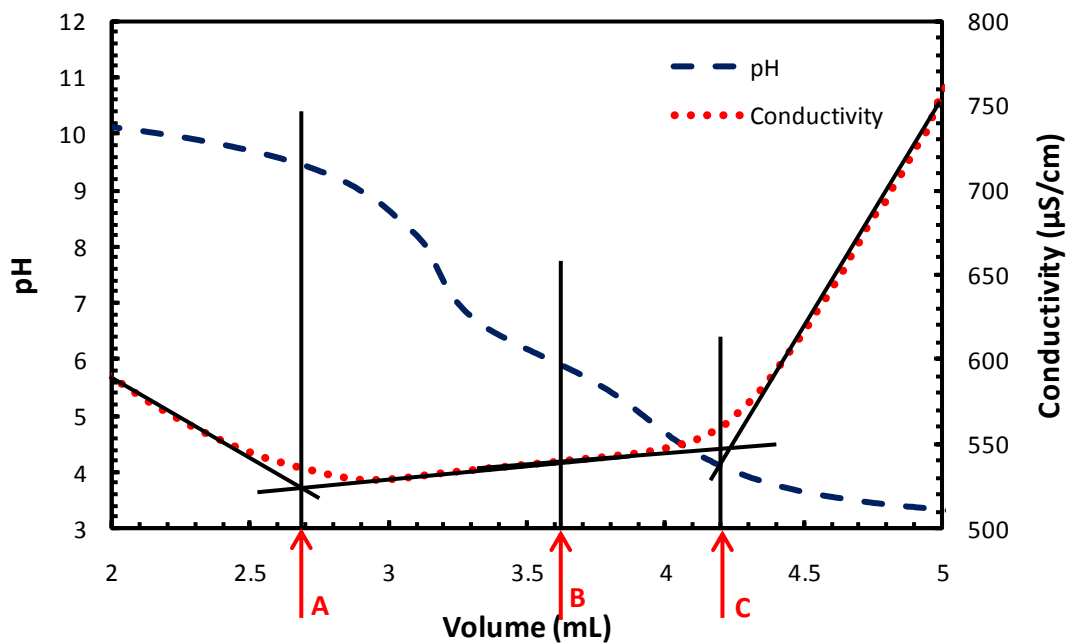


Figure 5.2: Potentiometric titration curve of PLG-b-PDEAEMA

From points A to B, the tertiary amine group of PDEAEMA was titrated with 50 mM HCl, and the protonation of the amine function groups are shown in Figure 5.3 and Equation (5.3). From points B to C, the carboxylic acid groups of PLG were protonated to form carboxylic acid and the dissociation reaction and equilibrium equation are shown in Figure 5.4 and Equation (5.4) respectively. From point C onwards, excess acid was titrated to solution, causing an increase in conductivity.

$$K_{a2} = \frac{[NR(Et)_2][H^+]}{[NR(Et)_2H^+]} \quad (5.3)$$

$$K_{a1} = \frac{[COO^-][H^+]}{[COOH]} \quad (5.4)$$

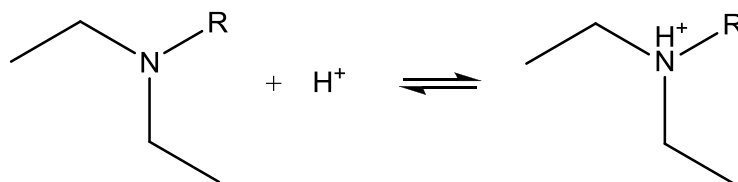


Figure 5.3: Protonation of the tertiary amine group of PDEAEMA

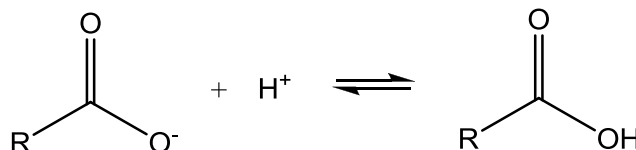


Figure 5.4: Neutralization of the carboxylic acid group of PLG

In comparing regions A to B and B to C in Figure 5.2, region A to B is much larger, as there are approximately twice the repeat units of DEAEEMA in comparison to glutamate. By comparing the amount of acid needed in the titration for each region and taking into consideration the amount of polymer titrated, there are 18 repeat units of glutamate and 35 repeat units of DEAEEMA. This is similar to the repeat units found using NMR and GPC. On average between the three methods, there are 18 repeat units of glutamate and 37 repeat units of DEAEEMA.

The  $pK_a$  for each of the pH-sensitive groups corresponds to the point of half-neutralization. For the polymer, these values are summarized in Table 5.1. The  $pK_a$  values are comparable to published values for each of the functional groups. For the glutamate functional group, the carboxylic acid group is much higher than published values of 4.0 [10]. For the amine group of DEAEEMA, the  $pK_a$  ranges from 5 – 8 depending on the salt concentration [11]. However, there is still significant overlap between the titration of the two functional groups, which may be the reason for inaccuracies in the  $pK_a$  values.

Table 5.1:  $pK_a$  Values for the PLG-b-PDEAEMA system

$pK_{a1}$	4.88
$pK_{a2}$	7.87

### 5.3.2 Critical Micellization Concentration

The critical micelle concentration is an important property of block copolymers – it is the concentration at which the polymers will form self-assembled structures. Generally, the cmc is observed by a change in solution properties, such as light intensity, surface tension, viscosity or conductivity.

The critical micelle concentration (cmc) was found using laser light scattering at an angle of 90°. In a light scattering experiment, the scattering vector,  $\vec{q}$ , is the difference between the incident and scattered vectors, as shown in Equation (5.5). Assuming that the light intensity does not change,  $k_i = k_s$ , then Equation (5.6) applies [12].

$$\vec{q} = \vec{k}_i - \vec{k}_s \quad (5.5)$$

$$q = \frac{4\pi n}{\lambda} \sin \frac{\theta}{2} \quad (5.6)$$

The cmc of PLG-b-PDEAEMA was investigated using dynamic light scattering at 90°. At concentrations below the cmc, there is no observable change in scattering intensity, due to localization of the polymer in solution and at the air-water interface. However, at concentrations above the cmc, the polymer forms micellar structures as the solution becomes saturated, resulting in an increase in the light scattering intensity, shown in Figure 5.5, which shows the change in intensity at pH 3.

In order to obtain an understanding of the PLG-b-PDEAEMA system, the cmc was investigated at pH 3, 7 and 10. At low pH, the PDEAEMA block is charged, and possesses hydrophilic characteristics, whereas the PLG block is protonated and is hydrophobic, which is the driving force in the micellization of the polymer. The change in intensity occurs around 320 µg/ml as shown in Figure 5.5.

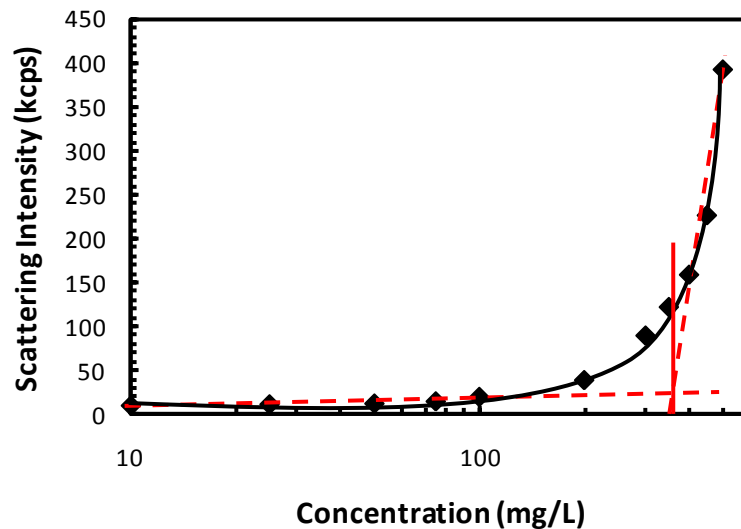


Figure 5.5: Critical micelle concentration at pH 3

At high pH, the reverse case is true, with the PDEAEMA block now hydrophobic and the PLG block hydrophilic. This results in a reverse micellization of the block copolymer. The cmc was approximated to be 61  $\mu\text{g/ml}$ , shown in Figure 5.6. At pH 7, the micellization is similar to high pH as the pH is above the isoelectric point of the polymer. However, the PDEAEMA is partially protonated and more soluble. Furthermore, electrostatic interactions may also play a role in the cmc. The cmc was found to be 72  $\mu\text{g/ml}$ , shown in Figure 5.7. The higher cmc is most likely due to the higher solubility of the PDEAEMA block, and thus a stronger driving force is necessary for micellization, in comparison to high pH.

The lower critical micelle concentration at high pH, in comparison to low pH, is likely due to the longer PDEAEMA segment and the shorter PLG block. Based on GPC analysis, there are approximately 18 glutamate units and 38 DEAEMA units. At high pH, greater hydrophobicity of the DEAEMA block likely causes micellization at a lower concentration.

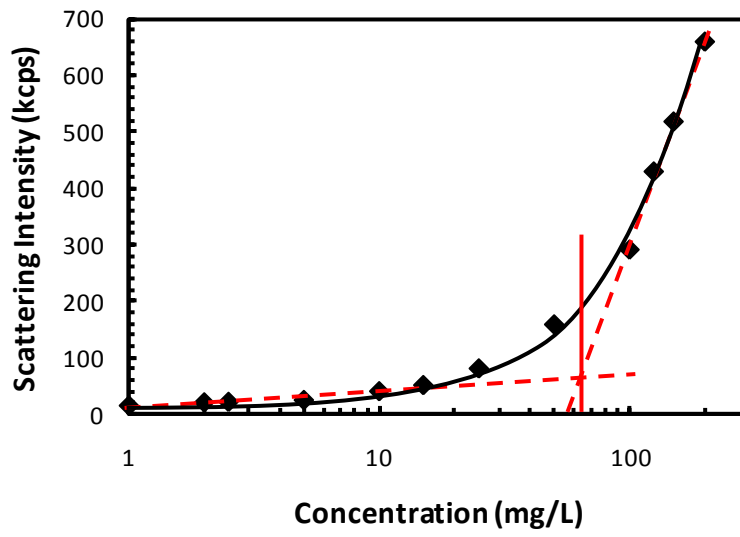


Figure 5.6: Critical micelle concentration at pH 10

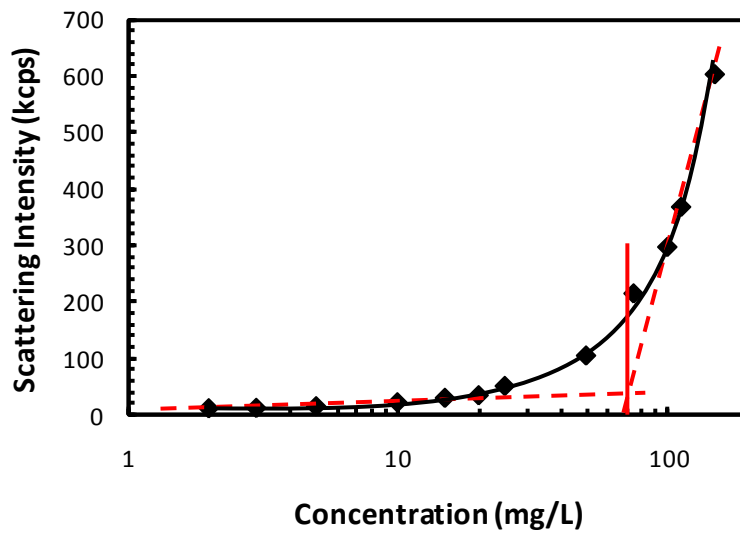


Figure 5.7: Critical micelle concentration at pH 7

### 5.3.3 pH-Dependent Self-Assembly of PLG-b-PDEAEMA

The size, surface charge and morphology of the self-assembled structures were studied at different pHs, ranging from pH 3 to 10. A thorough study of the PLG-b-PDEAEMA polymer was performed using dynamic and static light scattering and zeta potential measurements.

### 5.3.3.1 Effect of pH on Size and Surface Charge

The effect of pH conditions on the surface charge and size of the self-assembled structures were observed using DLS and zeta potential.

DLS is a time resolved experiment, where time dependent changes in intensity can be measured. This is utilized to measure electrophoretic motion to determine the  $\zeta$ -potential of samples. For particle size, the Brownian motion of the particles can be measured – the change in the spectrum of scattered light is given by the frequency shift,  $\Delta\omega$ . The Fourier transform of the spectrum, the autocorrelation function, is the intensity at time  $t$ ,  $I(t)$  multiplied by the the intensity at a time decay,  $\tau$ ,  $I(t + \tau)$ . The distribution function of the time decay for pH 10 is shown in Figure 5.8. Only one distinct peak is observed with relaxation times increasing at higher angles.

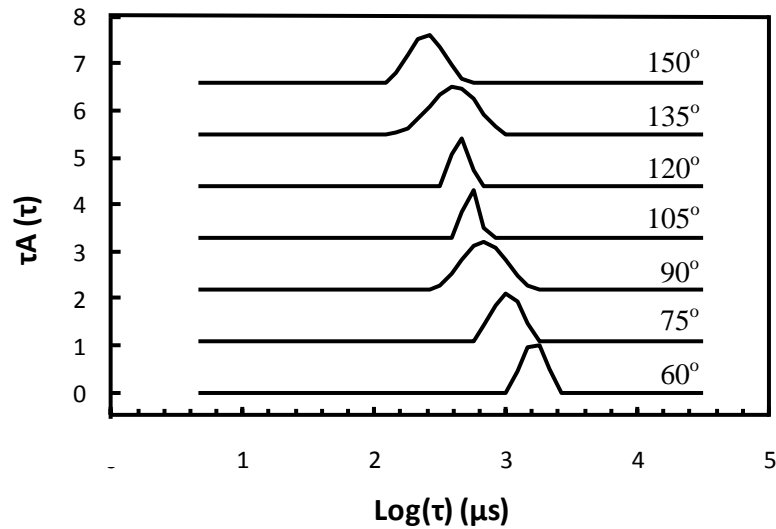


Figure 5.8: Distribution functions of PLG-b-PDEAEMA at pH 10

The inverse of the time decay,  $\Gamma = 1/\tau$ , is related to diffusion coefficient, given in Equation (5.7). The decay rate was plotted against the scattering vector, with a representative plot shown in Figure 5.9 at pH 10, to find the diffusion coefficient.

$$\Gamma = Dq^2 \quad (5.7)$$

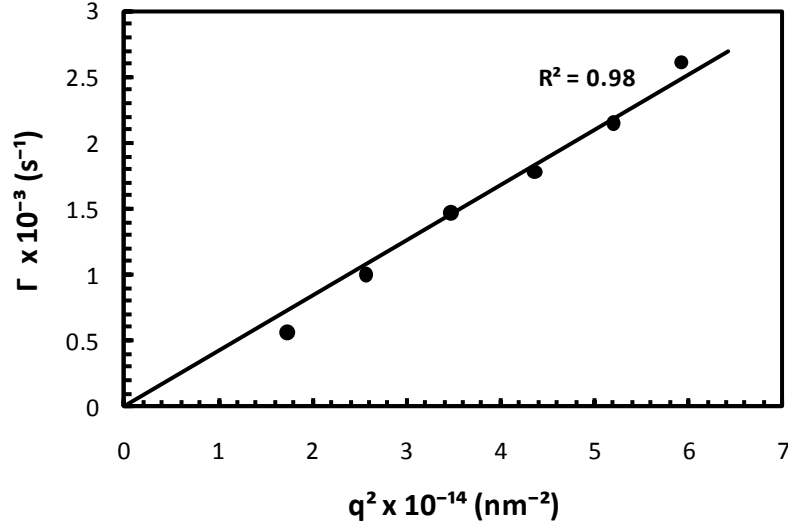


Figure 5.9: Diffusion coefficient angle dependency at pH 10

The diffusion coefficient was determined and the particle size was found using the Stokes-Einstein expression, shown in Equation (5.8), where  $R_h$  is the hydrodynamic radius,  $k$  is Boltzmann's constant,  $T$  is the temperature,  $\eta$  is the viscosity, and  $D_o$  is the diffusion coefficient. For the multi-angle experiments, the average diffusion coefficient was found and similar to the DLS results at one angle, the particle size was found using the Stokes-Einstein expression, as shown in Equation (5.8).

$$R_h = \frac{kT}{6\pi\eta D_o} \quad (5.8)$$

The surface charge density of the particles is related to the solution pH, which is related to the stability of the particles. Electrostatic effects play an important role at the interface in solution between charged particles and the liquid medium. An electrical double layer forms at the interface due to the surface charge density and the ions in solution, as shown in Figure 5.10. The first layer, the Stern layer, consists of tightly bound ions at the particle surface and the second layer, the diffuse layer, has a decrease in potential towards the bulk solution. The boundary between the two layers is the shear surface, and the potential at this point is the zeta potential,  $\zeta$ . This is given by Equation

(5.9), relating the zeta potential to the charge,  $q$ , particle radius,  $R_s$  and the position dependence,  $\epsilon$  [13].

$$\zeta = \frac{q}{4\pi\epsilon R_s} \quad (5.9)$$

The zeta potential measurements determine the electrophoretic mobility,  $u$ , which is the particle movement based on an applied electric field. The Hückel equation, which correlates the electrophoretic mobility to the zeta potential, is shown in Equation (5.10) [13].

$$u = \frac{2\epsilon\zeta}{2\eta} \quad (5.10)$$

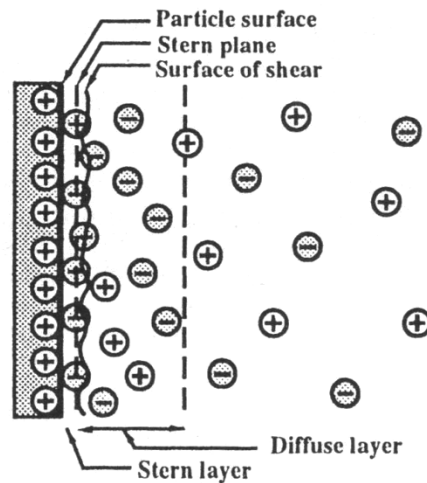


Figure 5.10: Electric double layer for a charged surface in solution [13]

The results are summarized in Figure 5.11. At  $\text{pH} < 4$ , the hydrodynamic radius is approximately 90 nm and the nanostructures possess a positive surface charge. At  $\text{pH} > 7$  the hydrodynamic radius is around 50 nm with a negative surface charge. This change in size and surface charge demonstrates that the mechanism for self assembly is strongly affected by pH.

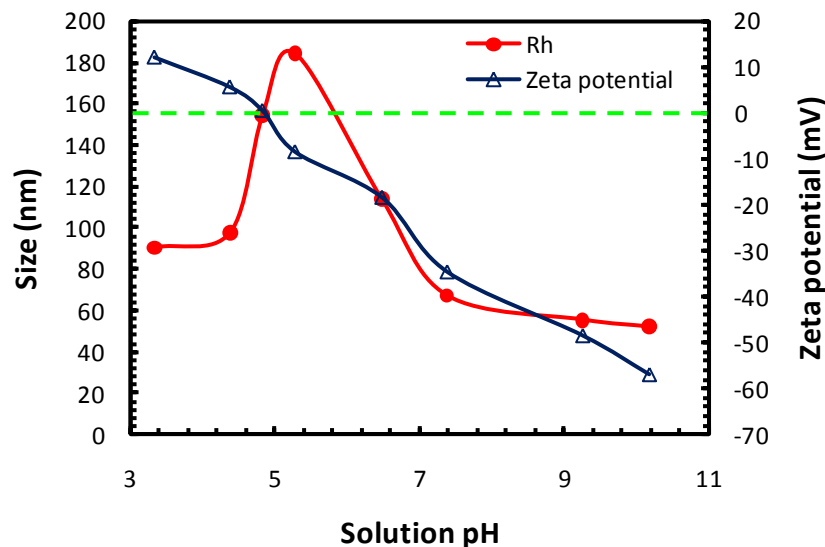


Figure 5.11: Effect of pH on the hydrodynamic radius ( $R_h$ ) and surface charge, where the dashed line corresponds to a zero zeta potential

In the low pH range, the carboxylic acid groups of glutamate are neutralized and the majority of the amine groups of DEAEMA are protonated as shown in Figure 5.12. Due to the differences in the solubility, the block copolymers self-assemble into nanostructures comprising of a DEAEMA shell to impart positive charge characteristics to the particle. At the higher pH range, the amine groups of DEAEMA are neutralized and the carboxylic acid groups of glutamates are deprotonated yielding negatively charge particles (Figure 5.12). In contrast to low pH, the glutamate block is now soluble and the DEAEMA block is insoluble. This leads to an inverse assembly of the block copolymer, with glutamate on the surface on the structure leading to negatively charged nanostructures. In the mid-range pH values ( $4 < \text{pH} < 7$ ), both the glutamate moieties and the DEAEMA units are partially charged and electrostatic interactions play an important role in their aggregation behavior (Figure 5.12). The particle size increases to a maximum hydrodynamic radius around 180 nm and the surface charge is close to zero. By extrapolating to a surface charge of zero, the isoelectric point of the polymer is at pH 4.9.

The surface charge is an indicator of the stability of the self-assembled structures. In general, a high zeta potential,  $|\zeta| > 30$  mV, indicates a stable particle [12]. For the PLG-b-PDEAEMA system, at pH < 7, the zeta potential values are less than 30, implying that the particles are not very stable. At pHs close to the isoelectric point, the instability is due to aggregation between the polymer chains due to electrostatic interactions. At lower pHs, where the glutamate block is insoluble, the lower stability may be due to electrostatic repulsion between the longer PDEAEMA chains.

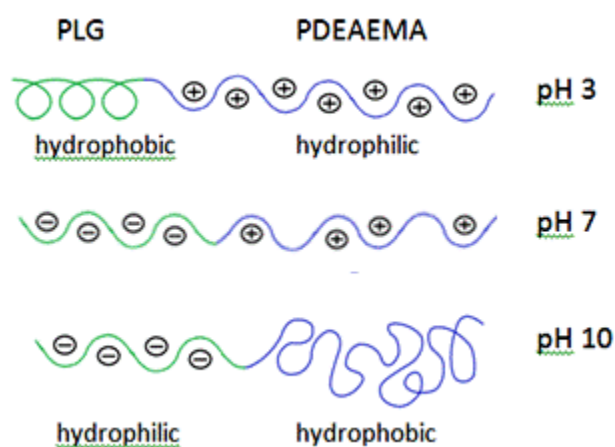


Figure 5.12: Charge behavior of the polymer at different solution pHs

### 5.3.3.2 Morphology of Self-Assembled Structures

Dynamic and static light scattering were used to elucidate the size and morphology of the self assembled structures as a function of the solution pH. For the DLS experiments, samples at different pH were measured at multiple scattering angles in order to obtain additional data for the determination of the morphology and structures.

Using static light scattering the aggregation number, radius of gyration and 2nd virial coefficient can be determined. For the measurements, the scattered light intensity was averaged over a defined observation time at different angles as described by Equation (5.11). The SLS data were analyzed using the Zimm Equation, shown in Equation (5.12), where  $M_w$  is the apparent molecular weight,  $C$  is

the concentration,  $A_2$  is the 2<sup>nd</sup> virial coefficient,  $q$  is the scattering vector as described earlier in Equation (5.6) and  $R(q)$  is the Rayleigh ratio.  $K$  is an instrument optical parameter, shown in Equation (5.13), where  $\lambda$  is the wavelength of the laser,  $N_A$  is Avogadro's number,  $n_o$  is the refractive index of the solvent, and  $dn/dc$  is the differential refractive index increment.

$$I(\theta) = \lim_{T \rightarrow \infty} \frac{1}{T} \int_0^T I(\theta, t) dt \quad (5.11)$$

$$\frac{KC}{\Delta R_\theta} = \frac{1}{M_w} \left( 1 + \frac{1}{3} R_g^2 q^2 \right) + 2A_2 C \quad (5.12)$$

$$K = \frac{2\pi^2}{\lambda^4 N_A} \left( n_o \frac{dn}{dc} \right)^2 \quad (5.13)$$

The data was plotted as a Zimm plot, where  $KC/\Delta R_\theta$  was plotted against  $\sin^2(\theta/2) + kC$ , where  $k$  is an adjustable constant. A representative Zimm plot at pH 10 is shown in Figure 5.13. The data was extrapolated to zero concentration and zero angle, which was used to find the radius of gyration, aggregation number and 2<sup>nd</sup> virial coefficient.

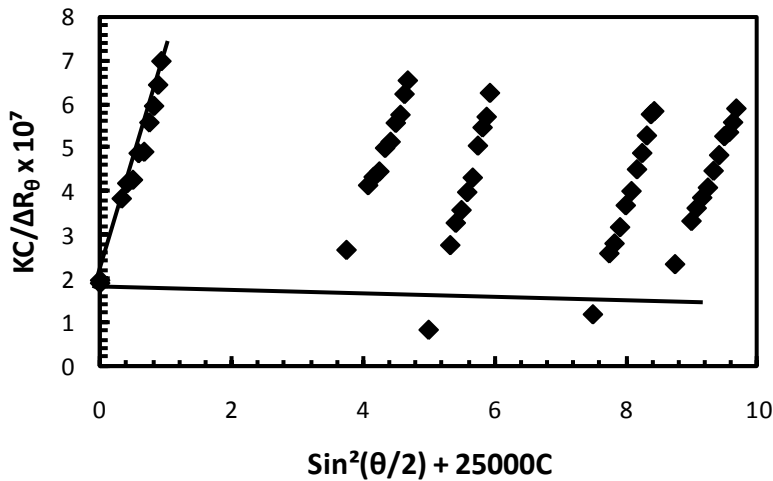


Figure 5.13: Zimm plot of PLG-b-PDEAEMA at pH 10

A summary of the DLS and SLS results is shown in Figure 5.14. The radii at low pH were much larger than at high pH, 90 nm in comparison to 50 nm. Furthermore, at low and high pH, both the hydrodynamic and gyration radii were similar to each other, whereas, at pH close to the isoelectric point, the radius of gyration was notably smaller than hydrodynamic radius. The  $R_g / R_h$  ratios are summarized in Table 5.2. At higher and lower pH values, the  $R_g / R_h$  ratios are approximately 1, indicating that the mass of the particles are centred on the outside. At pH close to the isoelectric point, the  $R_g / R_h$  ratios are around 0.74, which would indicate micelle formation, as the mass of the structures are more uniformly distributed within the particle. This is a result of the greater electrostatic charges in the polymer, causing large aggregates to form.

In order to further investigate the morphology, the aggregation number and 2nd virial coefficient were found from the Zimm plot. The aggregation number is found by comparing the apparent  $M_w$  to the molecular weight of the individual chains. For PLG-b-PDEAEMA, the  $M_w$  was found using GPC, which was discussed in Chapter 3. Using this information, an approximate number of chains forming the aggregates was found.

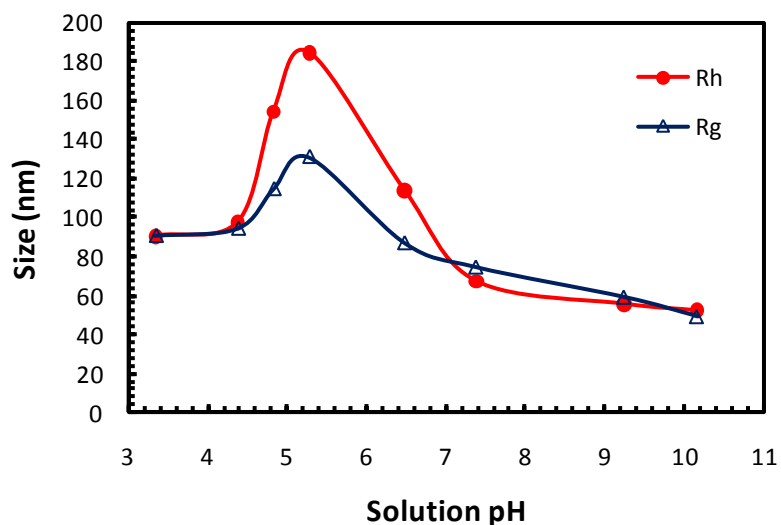


Figure 5.14: Effect of pH on the hydrodynamic ( $R_h$ ) and gyration radii ( $R_g$ )

Table 5.2:  $R_g / R_h$  ratio at different pH conditions

<b>pH</b>	<b><math>R_h</math> (nm)</b>	<b><math>R_g</math> (nm)</b>	<b><math>R_g / R_h</math></b>
3.34	90.4	90.8	1.00
4.38	97.4	94.5	0.97
4.83	154.2	114.7	0.74
5.28	184.4	131.1	0.71
6.48	113.7	87.1	0.77
7.38	67.1	74.7	1.11
9.25	55.4	59.3	1.07
10.2	52.1	49.4	0.95

A range of concentrations was used, depending on the solution pH and the critical micelle concentration at that pH. At pH 3, concentrations ranging from 350 – 500  $\mu\text{g/ml}$  were used. At pH 7 and 10, concentrations from 100 – 300  $\mu\text{g/ml}$  were measured. All samples were measured from 60 – 130°. The data was plotted as a Zimm plot, where  $KC/\Delta R_\theta$  was plotted against  $\sin^2(\theta/2) + kC$ , with  $k$  as an adjustable constant. The data was extrapolated to zero concentration and zero angle, which was used to find the radius of gyration, aggregation number and 2nd virial coefficient. The results obtained are summarized in Table 5.3.

Table 5.3: Static light scattering results at solution pH 3, 7 and 10

<b>pH</b>	<b><math>M_{w,\text{apparent}}</math> (g/mol)</b>	<b><math>A_2</math> (<math>\text{cm}^3 \text{mol/g}^2</math>)</b>	<b>Aggregation number</b>
3.34	$2.2 \times 10^7$	$-4.0 \times 10^{-6}$	2000
7.38	$4.5 \times 10^7$	$-4.3 \times 10^{-5}$	4500
10.2	$1.2 \times 10^7$	$-1.9 \times 10^{-4}$	1200

The aggregation numbers range from 1200 to 4500, indicating that thousands of polymer chains are necessary for each self-assembled structure. These values are typical of vesicle formation. Additionally, at low pH, the aggregation number is almost twice as large as that at high pH. This

corresponds with the particle size, as the particles at low pH are approximately 90 nm, in comparison to the size at high pH, 50 nm. The aggregation number at pH 7, however, is much larger, which is likely due to electrostatic forces between the polymer chains. As a result, there are more polymer chains per structure, despite a similar hydrodynamic radius in comparison to the self-assembled structures at high pH.

The 2<sup>nd</sup> virial coefficient at the three pHs measured was negative, indicating that water is a poor solvent for the block copolymer. Furthermore,  $A_2$  decreased with a decrease in pH, indicating that the PLG core is more stable than a PDEAEMA core. This may be due to  $\alpha$ -helix formation of the PLG block, however, a more indepth study of the secondary structure formation is necessary.

A schematic showing the mechanism for self-assembly is shown in Figure 5.15. At low pH, the glutamate groups form the core of the vesicles due to the hydrophobicity of the group, with the DEAEMA groups forming the corona due to its solubility. At high pH, in contrast, the DEAEMA groups form the core and the negatively charge glutamate groups form the corona of the vesicles.

At physiological pH, the polymer chain has partial positive and negative charges, yet based on the results in Table 5.2, vesicle structures are still being formed. Based on these results, it is expected that the polymer forms charged vesicles – rather than stabilization due to solubility, the vesicles are partially stabilized by electrostatic interactions between the polymer chains [14].

#### **5.3.4 Polyplex Formation**

Prior to the cell transfection experiments, a study of the polyplex formation between PLG-b-PDEAEMA was performed using agarose gel electrophoresis assay and laser light scattering.

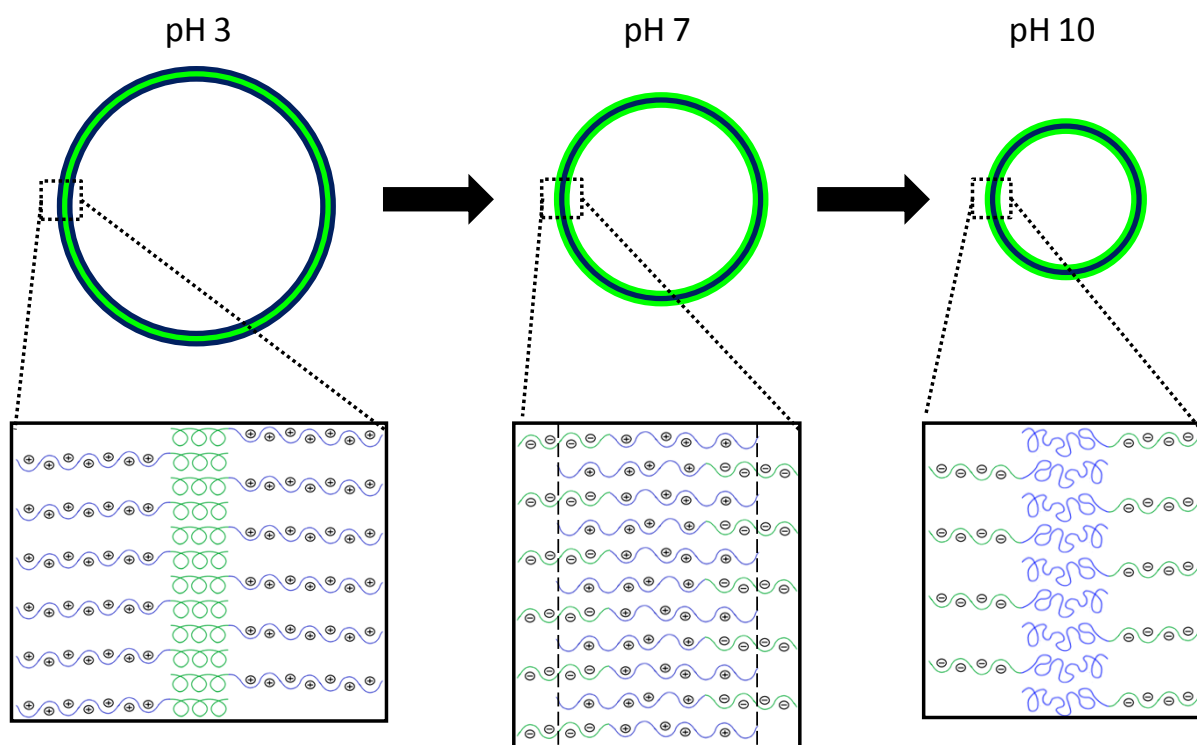


Figure 5.15: Mechanism for self-assembly at pH 3, 7 and 10

#### 5.3.4.1 Agarose Gel Electrophoresis Assay

The agarose gel electrophoresis assay was performed at N/P ratios of 0 – 20, where N/P 0 is a negative control with only plasmid DNA. Due to the applied electric field, negatively charged plasmid DNA will move through the agarose gel matrix towards the cathode. DNA that has been condensed by the polymer will remain stationary, as a certain degree of flexibility is necessary to pass through the agarose gel matrix. The fluorescent dye, EtBr, was added to the agarose gel as interactions with DNA increase its fluorescence.

The gel electrophoresis assay photographed under UV irradiation at pH 3, 7 and 10 is shown in Figure 5.16. At pH 3, which is expected to display increased polymer-DNA interactions due to a greater number of positively charged amine groups, a decrease in intensity is observed between N/P of 1 and N/P ratio of 0. At N/P = 5, the DNA is condensed by the polymer and thus no movement is

observed under the applied electric field. At pH 7, which is of interest for intracellular delivery, the intensity decreases with increasing N/P ratios, however, this decrease is more gradual than at pH 3. The plasmid DNA is condensed at N/P = 20. At pH 10, similarly to the results at pH 7, the intensity decreases with increasing N/P ratios and the DNA is condensed at N/P = 20.

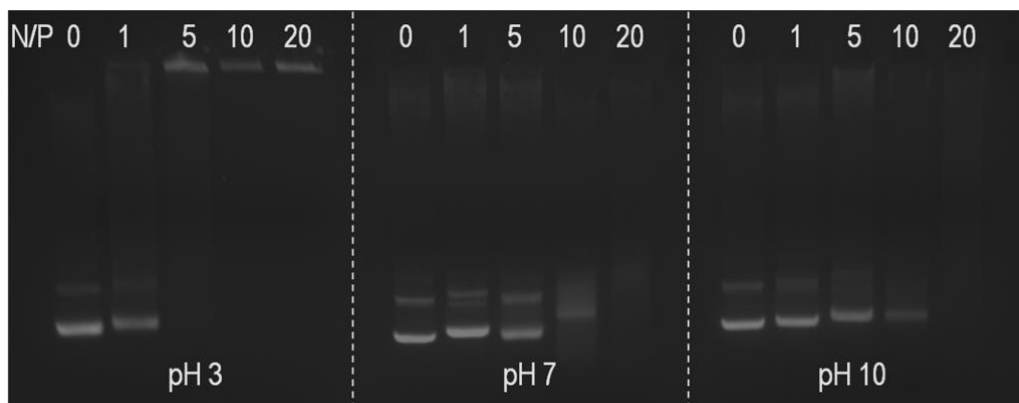


Figure 5.16: Agarose gel electrophoresis at different pH and N/P ratios, with the anode at the top of the figure and the cathode at the bottom of the figure

#### 5.3.4.2 Laser Light Scattering

The polyplex size was measured using multi-angle dynamic light scattering; see Sections 4.3.3 and 5.3.3 for more details on light scattering.

The hydrodynamic radius of the polyplexes is shown in Figure 5.17. With an increase of the N/P ratio the size decreases, indicating that the plasmid DNA is condensed. The polyplex at pH 7 exhibits the most significant reduction in size, from approximately 150 to 30 nm in size. The results are comparable to Figure 5.16, which shows that most of the plasmid DNA is condensed above N/P = 10. At pH 3 and pH 10 DNA was also condensed, but the change in radius was more moderate. At pH 3, the  $R_h$  drops from 120 to 80 nm and at pH 10, the size decreases from 70 to 50 nm. At pH 3, this may be due to the decrease in the negative DNA charge resulting in less DNA condensation, despite an increase in positive charge on the polymer. At pH 10, there is an increase in negative DNA charge,

coupled with a decrease in positively charge polymer, resulting in a less compact polyplex. The plasmid DNA is condensed most effectively at pH 7.

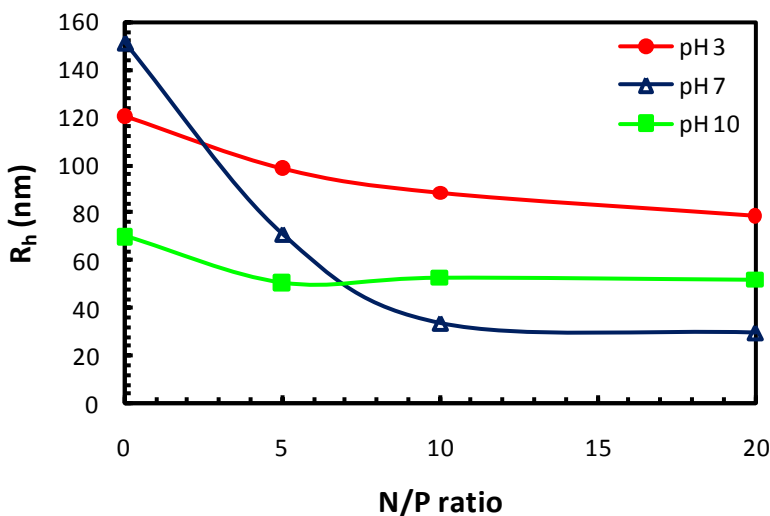


Figure 5.17: DNA condensation at different N/P ratios

### 5.3.5 Cell Transfection

The ability of PLG-b-PDEAEMA to deliver plasmid DNA to cells was tested on a N2a cell culture. The polyplexes were prepared and diluted with serum-free media. Serum-free media was used to minimize aggregation of the polyplexes. The diluted polyplexes were incubated over a short time period, as longer incubation times would result in differentiation of the cell culture. The cell culture was then incubated in media with 10 % FBS for an additional 24 h in order to allow the cell sufficient time to express the gene, if transfection was successful.

The plasmid DNA used expresses an eGFP protein, which will fluoresce under UV radiation. If transfection of the plasmid was successful, then the cells will fluoresce due to the eGFP. The results of the cell test are shown in Figure 5.18 after a 24 h incubation. In each of the sets of micrographs, the picture on the left is the cell culture and the picture on the right is the cell culture under UV radiation. All the micrographs are magnified ten-fold.

The first micrograph, at N/P of 0, is the negative standard used, with only the delivery of plasmid DNA on its own. As expected, no gene expression is observed. Free plasmid DNA is readily degraded by enzymes in the cellular environment. The positive standard, the LPEI/DNA polyplex at N/P of 20, shows successful transfection and expression of eGFP in the fluorescent micrograph. The polymer, PLG-b-PDEAEMA/DNA polyplexes were prepared at N/P ratios of 20 and 50. After a 24 h incubation time, no gene expression was observed, as observed in Figure 5.18. The cell culture was observed after an additional 24 h and there was still no gene expression observed.

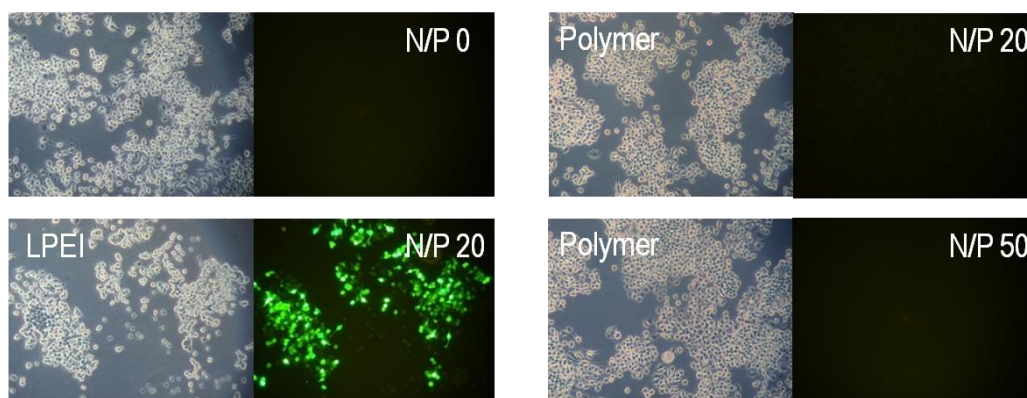


Figure 5.18: Fluorescence micrographs (10x) of gene expression

Based on these results, PLG-b-PDEAEMA was not able to deliver plasmid DNA. There are numerous barriers to overcome in gene delivery, such as endocytosis, endosome escape, reaching the nucleus and nuclear entry [7– 9]. Additional studies need to be performed to find the stage at which the delivery fails. Modifications can be made in order to optimize the polymer for successful gene therapy.

## 5.4 Conclusions

The self-assembly behaviour of PLG-b-PDEAEMA was discussed. The pH behaviour was investigated using potentiometric titration. The pH-sensitive groups observed are the carboxylic acid

of PLG and the tertiary amine of PDEAEMA. These groups inherently affect the self-assembly of the block copolymer.

Using zeta potential measurements and dynamic and static light scattering, the polymer was found to form “schizophrenic” vesicles at high and low pH. This was observed by a change in hydrodynamic radius and surface charge from a solution pH of 3 – 10, with a hydrodynamic radius of approximately 90 nm at low pH, 180 nm close to the isoelectric point, approximately pH 5, and 50 nm at high pH. Positively charged particles were found at solution pHs less than the isoelectric point and negatively charged particles were found at pH above the isoelectric point.

Furthermore, the reversible micellization was observed through the critical micelle concentration of the polymer and different solution pHs. At low pH, a polymer concentration of 320  $\mu\text{g/ml}$  was necessary to induce micellization and at high pH, a concentration of 61  $\mu\text{g/ml}$  was required. This shows a clear difference in the self-assembly mechanism based on pH.

The morphology of the aggregates was observed to be vesicles at high and low pH, due to the hydrophobic and hydrophilic properties of the functional groups at different pH. The aggregation number at high pH was 1200, lower than the aggregation number at low pH, due to the smaller size of the vesicles. At solution pH close to the isoelectric point, larger aggregates were observed due to the increased electrostatic forces within the polymer chains.

Lastly, the potential gene therapy applications of PLG-b-PDEAEMA were explored. Polymer/DNA polyplexes were prepared. The binding and size of the polyplexes were examined at different pH using agarose gel electrophoresis and dynamic light scattering. Based on the gel electrophoresis results, the DNA was condensed at lower N/P ratios at lower solution pH, but in general, the plasmid DNA would be condensed at N/P ratios of 20 and above. Based on the dynamic light scattering results, DNA was condensed most effectively at pH 7, from a hydrodynamic radius of 150 to 30 nm.

The polyplex size was highly dependent on the charge density of the polymer and DNA and dependent on the solution pH.

An in vitro cell test of the polyplexes was performed, however, no gene expression was observed and so the polymer was not capable of intracellular delivery. Further studies are necessary to determine which stage of cellular entry is failing, so that the polymer can be optimized for gene therapy applications.

## References

### Chapter 2 References

- [1] Deming, T. J. Synthetic polypeptides for biomedical applications. *Prog. Polym. Sci.* 32, 858 (2007).
- [2] Pratesi, G., Savi, G., Pezzoni, G., Bellini, O., Penco, S., Tinelli, S., and Zunino, F. Poly-L-aspartic acid as a carrier for doxorubicin – a comparative in vivo study of free and polymer-bound drug. *British J. Cancer* 52, 841 (1985).
- [3] Nicolas, J., Mantovani, G., and Haddleton, D. M. Living radical polymerization as a tool for the synthesis of polymer-protein/peptide bioconjugates. *Macromol. Rapid Commun.* 28, 1083 (2007).
- [4] Börner, H. G. and Schlaad, H. Bioinspired functional block copolymers. *Soft Matter* 3, 394 (2007).
- [5] Löwik, D. W. P. M., Ayres, L., Smeenk, J. M., and Van Hest, J. C. M. Synthesis of bio-inspired hybrid polymers using peptide synthesis and protein engineering. *Adv. Polym. Sci.* 202, 19 (2006).
- [6] Deming, T. J. Polypeptide and polypeptide hybrid copolymer synthesis via NCA polymerization. *Adv. Polym. Sci.* 202, 1 (2006).
- [7] Cotarca, L. and Eckert, H. Phosgenations. Wiley-VCH (2004).
- [8] Kricheldorf, H. R.  $\alpha$ -N-Carboxyanhydrides and Related Materials. Springer (1987).
- [9] Aliferis, T., Iatrou, H., and Hadjichristidis, N. Living polypeptides. *Biomacromolecules* 5, 1653 (2004).
- [10] Vayaboury, W., Giani, O., Cottet, H., Deratani, A., and Schué, F. Living polymerization of alpha-amino acid N-carboxyanhydrides (NCA) upon decreasing the reaction temperature. *Macromol. Rapid Comm.* 25, 1221 (2004).

- [11] Dimitrov, I. and Schlaad, H. Synthesis of nearly monodisperse polystyrene-polypeptide block copolymers via polymerisation of N-carboxyanhydrides. *Chem. Comm.* 23, 2944 (2003).
- [12] Deming, T. J. Amino acid derived nickelacycles: Intermediates in nickel-mediated polypeptide synthesis. *J. Am. Chem. Soc.* 120, 4240 (1998).
- [13] Deming, T. J. Cobalt and iron initiators for the controlled polymerization of alpha-amino acid-N-carboxyanhydrides. *Macromolecules* 32, 4500 (1999).
- [14] Agut, W., Agnaou, R., Lecommandoux, S., and Taton, D. Synthesis of block copolypeptides by click chemistry. *Macromol. Rapid Comm.* 29, 1147 (2008).
- [15] Braunecker, W. A. and Matyjaszewski, K. Controlled/living radical polymerization: Features, developments, and perspectives. *Prog. Polym. Sci.* 32, 93 (2007).
- [16] Shipp, D. A. Living radical polymerization: Controlling molecular size and chemical functionality in vinyl polymers. *J. Macromol. Sci. – Polymer Reviews* 45, 171 (2005).
- [17] Matyjaszewski, K. and Xia, J. H. Atom transfer radical polymerization. *Chem. Rev.* 101, 2921 (2001).
- [18] Binder, W. H. and Sachsenhofer, R. 'Click' chemistry in polymer and material science: An update. *Macromol. Rapid Commun.* 29, 952 (2008).
- [19] Hein, C. D., Liu, X.-M., and Wang, D. Click chemistry, a powerful tool for pharmaceutical sciences. *Pharm. Res.* 25, 2216 (2008).
- [20] Schlaad, H. Solution properties of polypeptide-based copolymers. *Adv. Polym. Sci.* 202, 53 (2006).
- [21] Hiemenz, P. C. and Rajagopalan, R. Principles of Colloids and Surface Chemistry. CRC Press, Taylor & Francis, 3<sup>rd</sup> edition (1994).

- [22] Deming, T. J. Polypeptide hydrogels via a unique assembly mechanism. *Soft Matter* 1, 28 (2005).
- [23] Lodish, H., Berk, A., Zipursky, S. L., Matsudaira, P., Baltimore, D., and Darnell, J. *Molecular Cell Biology*. Freeman and Company, 4<sup>th</sup> edition (2000).
- [24] Toyotama, A., Kugimiya, S.-I., Yamanaka, J., and Yonese, M. Preparation of a novel aggregate like sugar-ball micelle composed of poly(methylglutamate) and poly(ethyleneglycol) modified by lactose and its molecular recognition by lectin. *Chem. Pharm. Bull.* 49, 169 (2001).
- [25] Cheon, J.-B., Jeong, Y.-I., and Cho, C.-S. Self-assembly of rigid polypeptides. *Korea Polym. J.* 6, 34 (1998).
- [26] Cheon, J.-B., Jeong, Y.-I., and Cho, C.-S. Effects of temperature on diblock copolymer micelle composed of poly( $\gamma$ -benzyl L-glutamate) and poly(N-isopropylacrylamide) *Polymer* 40, 2041 (1999).
- [27] Naka, K., Yamashita, R., Nakamura, T., Ohki, A., and Maeda, S. Aggregates of peptide-containing block copolymers and their interactions with a lipase in aqueous solution. *Macromol. Chem. Phys.* 198, 89 (1997).
- [28] Dong, C.-M., Sun, X.-L., Faucher, K., Apkarian, R., and Chaikof, E. Synthesis and characterization of glycopolymer-polypeptide triblock copolymers. *Biomacromolecules* 5, 224 (2004).
- [29] Sinaga, A., Hatton, T. A., and Tam, K. C. Hydrogen bonded assembly of poly(acrylic acid)-block-poly(L-valine) in dilute solutions. *Macromolecules* 40, 9064 (2007).

- [30] Sinaga, A., Hatton, T. A., and Tam, K. C. Poly(acrylic acid)-block-poly(L-valine): Evaluation of beta-sheet formation and its stability using circular dichroism technique. *Biomacromolecules* 8, 2801 (2007).
- [31] Kukula, H., Schlaad, H., Antonietti, M., and Forster, S. The formation of polymer vesicles or "peptosomes" by polybutadiene-block-poly(L-glutamate)s in dilute aqueous solution. *J. Am. Chem. Soc.* 124, 1658 (2002).
- [32] Checot, F., Brulet, A., Oberdisse, J., Gnanou, Y., Mondain-Monval, O., and Lecommandoux, S. Structure of polypeptide-based diblock copolymers in solution: Stimuli-responsive vesicles and micelles. *Langmuir* 21, 4308 (2005).
- [33] Babin, J., Rodriguez-Hernandez, J., Lecommandoux, S., Klok, H.-A., and Achard, M.-F. Self-assembled nanostructures from peptide-synthetic hybrid block copolymers: Complex, stimuli-responsive rod-coil architectures. *Faraday Discuss* 128, 179 (2005).
- [34] Lubbert, A., Castelletto, V., Hamley, I., Nuhn, H., Scholl, M., Bourdillon, L., Wandrey, C., and Klok, H.-A. Nonspherical assemblies generated from polystyrene-b-poly(L-lysine) polyelectrolyte block copolymers. *Langmuir* 21, 6582 (2005).
- [35] Agut, W., Brûlet, A., Schatz, C., Taton, D. and Lecommandoux, S. pH and temperature responsive polymeric micelles and polymersomes by self-assembly of poly[2-(dimethylamino)ethyl methacrylate]-b-Poly(glutamic acid) double hydrophilic block copolymers. *Langmuir* 26, 13, 10546 (2010).
- [36] Bellomo, E. G., Wyrsta, M. D., Pakstis, L., J., P. D., and Deming, T. J. Stimuli-responsive polypeptide vesicles by conformation-specific assembly. *Nature Materials* 3, 244 (2004).

- [37] Yu, M., Nowak, A. P., Deming, T. J., and Pochan, D. J. Methylated mono- and diethyleneglycol functionalized polylysines: Nonionic, alpha-helical, water-soluble polypeptides. *J. Am. Chem. Soc.* 121, 12210 (1999).
- [38] Zalipsky, S. Chemistry of polyethylene-glycol conjugates with biologically-active molecules. *Adv. Drug Delivery Rev.* 16, 157 (1995).
- [39] Rodríguez-Hernández, J. and Lecommandoux, S. Reversible inside-out micellization of pH-responsive and water-soluble vesicles based on polypeptide diblock copolymers. *J. Am. Chem. Soc.* 127, 2026 (2005).
- [40] Holowka, E. P., Pochan, D. J., and Deming, T. J. Charged polypeptide vesicles with controllable diameter. *J. Am. Chem. Soc.* 127, 12423 (2005).
- [41] Brooks, H., Lebleu, B., and Vivés, E. Tat peptide-mediated cellular delivery: back to basics. *Adv. Drug Delivery Rev.* 57, 559 (2005).
- [42] Holowka, E. P., Sun, V. Z., Kamei, D. T., and Deming, T. J. Polyarginine segments in block copolypeptides drive both vesicular assembly and intracellular delivery. *Nature Mat.* 6, 52 (2007).
- [43] Haag, R. and Kratz, F. Polymer therapeutics: Concepts and applications. *Angew. Chem. Int. Ed.* 45, 1198 (2006).
- [44] Mulligan, R. C. The basic science of gene therapy. *Science* 260, 926 (1993).
- [45] During, M. J. The basic science of gene-therapy. *Adv. Drug Deliv. Rev.* 27, 83 (1997).
- [46] Vile, R. G., Tuszynski, A., and Castleden, S. Retroviral vectors - From laboratory tools to molecular medicines. *Mol. Biotechnol.* 5, 139 (1996).
- [47] Pack, D. W., Hoffman, A. S., Pun, S., and Stayton, P. S. Design and development of polymers for gene delivery. *Nature Reviews* 4, 581 (2005).

- [48] Zauner, W., Ogris, M., and Wagner, E. Polylysine-based transfection systems utilizing receptor-mediated delivery. *Adv. Drug Deliv. Rev.* 30, 97 (1998).
- [49] Seglen, P. O. Inhibitors of Lysosomal Function. *Methods Enzymol.* 96, 737 (1983).
- [50] Behr, J. P. The proton sponge: A trick to enter cells the viruses did not exploit. *Chimia* 51, 34 (1997).
- [51] Boussif, O., Lezoualch, F., Zanta, M. A., Mergny, M. D., Scherman, D., Demeneix, B. and Behr, J. P. A versatile vector for gene and oligonucleotide transfer into cells in culture and in-vivo – polyethylenimine. *Proc. Natl Acad. Sci.* 92, 7297 (1995).
- [52] Haensler, J. and Szoka, F. C. Polyamidoamine cascade polymers mediate efficient transfection of cells in culture. *Bioconjug. Chem.* 4, 372 (1993).
- [53] Tanaka, S., Iwai, M., Harada, Y., Morikawa, T., Muramatsu, A., Mori, T., Okanoue, T., Kashima, K., Maruyama-Tabata, H., Hirai, H., Satoh, E., Imanishi, J., Mazda, O. Targeted killing of carcinoembryonic antigen (CEA)-producing cholangiocarcinoma cells by polyamidoamine dendrimer-mediated transfer of an Epstein-Barr virus (EBV)-based plasmid vector carrying the CEA promoter. *Cancer Gene Ther.* 7, 1241 (2000).
- [54] Tang, M. X., Redemann, C. T., and Szoka, F. C. In vitro gene delivery by degraded polyamidoamine dendrimers. *Bioconjug. Chem.* 7, 703 (1996).
- [55] Midoux, P., LeCam, E., Coulaud, D., Delain, E., and Pichon, C. Histidine containing peptides and polypeptides as nucleic acid vectors. *Somat. Cell Mol. Genet.* 27, 27 (2002).
- [56] Midoux, P. and Monsigny, M. Efficient gene transfer by histidylated polylysine pDNA complexes. *Bioconjug. Chem.* 10, 406 (1999).

- [57] Lee, Y., Ishii, T., Cabral, H., Kim, H. J., Seo, J. H., Nishiyama, N., Oshima, H., Osada, K., and Kataoka, K. Charge-conversional polyionic complex micelles-efficient nanocarriers for protein delivery into cytoplasm. *Angew. Chem. Int. Ed.* 48, 5309 (2009).
- [58] Forrest, M. L., Koerber, J. T., and Pack, D. W. A degradable polyethylenimine derivative with low toxicity for highly efficient gene delivery. *Bioconjug. Chem.* 14, 934 (2003).
- [59] Deng, R., Yue, Y., Jin, F., Chen, Y., Kung, H. F., Lin, M. C. M., and Wu, C. Revisit the complexation of PEI and DNA - How to make low cytotoxic and highly efficient PEI gene transfection non-viral vectors with a controllable chain length and structure? *J. Control. Release* 140, 40 (2009).
- [60] Lee, Y., Mo, H., Koo, H., Park, J. Y., Cho, M. Y., Jin, G. W., and Park, J. S. Visualization of the degradation of a disulfide polymer, linear poly(ethylenimine sulfide), for gene delivery. *Bioconjug. Chem.* 18, 13 (2007).
- [61] Osada, K. and Kataoka, K. Drug and gene delivery based on supramolecular assembly of PEG-polypeptide hybrid block copolymers. *Adv. Polym. Sci.* 202, 113 (2006).
- [62] Trubetskoy, V. S. and Torchilin, V. P. Use of polyoxyethylene-lipid conjugates as long-circulating carriers for delivery of therapeutic and diagnostic agents. *Adv. Drug Deliv. Rev.* 16, 311 (1995).
- [63] Harada-Shiba, M., Yamauchi, K., Harada, A., Takamisawa, I., Shimokado, K., and Kataoka, K. Polyion complex micelles as vectors in gene therapy – pharmacokinetics and in vivo gene transfer. *Gene Ther.* 9, 407 (2002).

### Chapter 3 References

- [1] Deming, T. J. Polypeptide and polypeptide hybrid copolymer synthesis via NCA polymerization. *Adv. Polym. Sci.* 202, 1 (2006).
- [2] Agut, W., Taton, D., and Lecommandoux, S. A versatile synthetic approach to polypeptide based rod-coil block copolymers by click chemistry. *Macromolecules* 40, 5653 (2007).
- [3] Vayaboury, W., Giani, O., Cottet, H., Deratani, A., and Schué, F. Living polymerization of alpha-amino acid N-carboxyanhydrides (NCA) upon decreasing the reaction temperature. *Macromol. Rapid Comm.* 25, 1221 (2004).
- [4] Blout, E. R. and Karlson, R. H. Polypeptides 3. The synthesis of high molecular weight poly-gamma-benzyl-L-glutamates. *J. Am. Chem. Soc.* 78, 941 (1956).
- [5] Daly, W. H. and Poche, D. The preparation of N-carboxyanhydrides of alpha-amino-acids using bio(trichloromethyl)carbonate. *Tetrahedron Letters* 29, 5859 (1988).
- [6] Cotarca, L. and Eckert, H. Phosgenations. Wiley-VCH (2004).
- [7] Carboni, B., Benanlil, A., and Vaultier, M. Aliphatic amino azides as key building-blocks for efficient polyamine synthesis. *J. Org. Chem.* 58, 3736 (1993).
- [8] Tsarevsky, N. V., Sumerlin, B. S., and Matyjaszewski, K. Step-growth "click" coupling of telechelic polymers prepared by atom transfer radical polymerization. *Macromolecules* 38, 3558 (2005).

### Chapter 4 References

- [1] Deming, T. J. Polypeptide and polypeptide hybrid copolymer synthesis via NCA polymerization. *Adv. Polym. Sci.* 202, 1 (2006).
- [2] Kricheldorf, H. R.  $\alpha$ -N-carboxyanhydrides and related materials. Springer (1987).

- [3] Börner, H. G. and Schlaad, H. Bioinspired functional block copolymers. *Soft Matter* 3, 394 (2007).
- [4] Rodríguez-Hernández, J., Gatti, M., and Klok, H. M. Highly branched poly(l-lysine). *Biomacromolecules* 4, 249 (2003).
- [5] Stiriba, S.-E., Frey, H. and Haag, R. Dendritic polymers in biomedical applications: From potential to clinical use in diagnostics and therapy. *Angew. Chem. Int. Ed.* 41, 1329 (2002).
- [6] Gauthier, M. and Whitton, G. Paper presented at the IDS-6 Conference Stockholm, June 16, 2009.
- [7] Wang, C., Ravi, P., Tam, K. C. and Gan, L. H. Self-assembly behavior of poly(methacrylic acid-block-ethyl acrylate) polymer in aqueous medium: Potentiometric titration and laser light scattering studies. *J Phys. Chem. B* 108 (5), 1621 (2004).
- [8] Finsy, R. Particle sizing by quasi-elastic light scattering. *Adv. in Colloid and Interface Sci.* 52, 79 (1994).

## Chapter 5 References

- [1] Zhang, X. and Matyjaszewski, K. Synthesis of well-defined amphiphilic block copolymers with 2-(dimethylamino)ethyl methacrylate by controlled radical polymerization. *Macromolecules*, 32, 1763 (1999).
- [2] Eisenberg, A.; Rinaudo, M. Polyelectrolytes and ionomers. *Polym. Bull.* 24, 671 (1990).
- [3] Schlaad, H. Solution properties of polypeptide-based copolymers. *Adv. Polym. Sci.* 202, (2006).
- [4] Rodríguez-Hernández, J. and Lecommandoux, S. Reversible inside-out micellization of pH-responsive and water-soluble vesicles based on polypeptide diblock copolymers. *J. Am. Chem. Soc.* 127, 2026 (2005).

- [4] Lodish, H., Berk, A., Zipursky, S. L., Matsudaira, P., Baltimore, D., and Darnell, J. Molecular cell biology. Freeman and Company, 4<sup>th</sup> edition (2000).
- [5] During, M. J. Adeno-associated virus as a gene delivery system. *Adv. Drug Deliv. Rev.* 27, 83 (1997).
- [6] Vile, R. G., Tuszynski, A., and Castleden, S. Retroviral vectors - From laboratory tools to molecular medicines. *Mol. Biotechnol.* 5, 139 (1996).
- [7] Pack, D. W., Hoffman, A. S., Pun, S., and Stayton, P. S. Design and development of polymers for gene delivery. *Nature Reviews* 4, 581 (2005).
- [8] Putnam, D. Polymers for gene delivery across length scales. *Nature Materials.* 5, 439 (2006).
- [9] Duncan, R. The dawning era of polymer therapeutics. *Nature Reviews.* 2, 347 (2003).
- [10] He, E., Ravi, P. and Tam, K. C. Synthesis and self-assembly behavior of four-arm poly(ethylene oxide)-b-poly(2-(diethylamino)ethyl methacrylate) star block copolymer in salt solutions. *Langmuir* 23 (5), 2382 (2007).
- [11] Wang, C., Ravi, P., Tam, K. C. and Gan, L. H. Self-assembly behavior of poly(methacrylic acid-block-ethyl acrylate) polymer in aqueous medium: Potentiometric titration and laser light scattering studies. *J Phys. Chem. B* 108, 5, 1621 (2004).
- [12] Finsy, R. Particle sizing by quasi-elastic light scattering. *Adv. in Colloid and Interface Sci.* 52, 79 (1994).
- [13] Hiemenz, P. C. and Rajagopalan, R. Principles of colloids and surface chemistry. CRC Press, Taylor & Francis, 3<sup>rd</sup> edition, (1994).
- [14] Gohy, J. F., Creutz, S. Garcia, M., Mahltig, B., Stamm, M., Jérôme, R. Aggregates formed by amphoteric diblock copolymers in water. *Macromolecules.* 33, 17, 6378 (2000).